2 Add.
P5.

FORMULATIONS FOR INCREMENTAL ELASTIC-PLASTIC ANALYSIS AND THE CONSOLIDATION OF POROUS MEDIA

by

W. W. Bird.

a thesis submitted for the degree of Doctor of Philosophy in Engineering

March 1987

Department of Civil Engineering

University of Cape Town.

DECLARATION

I, Wyndham Wadham Bird, declare that this thesis is essentially my own work and has not been submitted for a degree at another university.

Signed by candidate

W. W. Bird.

March 1987.

Acknowledgements

I would like to express my gratitude to the following:

My supervisor, Professor J.B.Martin, for his encouragement and interest during my postgraduate studies

The Council for Scientific and Industrial Research for their financial assistance

My AMRU colleagues past and present, especially those who were involved in the development of NOSTRUM Version 3.0, for many helpful discussions.

Umberto Perego for his assistance with the backward difference algorithm, with the consistent tangent predictor and for providing the rather elegant way of writing the consistent predictor which facilitated the programming

Mrs Shirley Breedt for the typing of the manuscript

Mrs Cheryl Wright for the labelling of the diagrams

My wife, Lois, for smoothing out several discontinuities in the text, for helping with the diagrams, and for her patience and support

CONTENTS

NOMENCLATURE

This is a list of symbols used in the main text of this thesis.

Special Symbol

$\dot{}$	the differential with respect to a time scale
$\sim$	a vector or matrix
[ ]	a matrix
$\lvert\ \rvert$	the absolute value of
$\lVert\ \rVert$	the norm of
T (superscript)	the transpose of a vector or matrix
-1 (superscript)	the inverse of a matrix
d	differentiation with respect to
∂	the partial differentiation with respect to
Δ	the increment in
O	of the order of

Lower Case Characters

a_{ij}, b_{ij}, b_i	constants used for evaluating the consistent constitutive matrix
c_i	constants used to evaluate the plane stress constitutive matrix
d	a constant used for evaluating the consistent constitutive matrix
dV	the increment in volumetric strain
dV_w	the volume of the migrated fluid
dW	the incremental work density
e	the voids ratio
e_o	the initial void ratio
$\underset{\sim}{e}$	the deviator strain vector

e_{ij} the deviator strain tensor

e^{*} the radius of a strain point in deviator strain space

e^{**} the radius of a strain point for a kinematically hardening material

$\underset{\sim}{f}$ the vector of nodal values for imposed fluid flow

$\underset{\sim}{g}$ the 'load' vector resulting from the migration water strain

k a yield parameter

k_{ij} the permeability tensor

n the porosity

n_o the initial porosity

p the excess pore pressure

$\underset{\sim}{p}$ the vector of nodal values for excess pore pressure

$\underset{\sim}{r}$ the out of balance residual force vector

s the second invariant of the deviator stress tensor

$\underset{\sim}{s}$ the deviator stress vector

s_{ij} the deviator stress tensor

t time

t_c a critical time parameter

$\underset{\sim}{u}$ the global displacement vector

u_i the local displacement vector

$\bar{u}_i$ the local prescribed displacement vector

x_i the position vector

Upper Case Characters

A the shear modulus multiplier

B the bulk modulus multiplier

$[B]$ the strain displacement matrix

C a constant used for evaluating the consistent constitutive matrix

C_{v1} one-dimensional coefficient of consolidation

C_{v2} two-dimensional coefficient of consolidation

D a material constant (when referring to the cap model)

D the dissipation function (when refering to the internal variable formulation)

$[D]$ the elastic constitutive matrix

$[D^{ep}]$ the elastic-plastic constitutive matrix

D_{ijkl} the elastic stiffness modulus

D^{ep}_{ijkl} the elastic-plastic stiffness modulus

E Young's modulus

E_{ij} the predicted elastic deviator strain

F the strain energy

F_i the body force vector

G the shear modulus

G_T the tangent shear modulus

H a linear hardening parameter

$\underline{H}$ a submatrix defined in the text

$[H]$ the compatibility matrix (imposes the incompressibility constraint)

I the improvement during minimisation of the in the potential energy

$[K]$ the global stiffness matrix

$[K^s]$ the global stiffness of the soil skeleton

$\underline{K}$ the contribution to the stiffness matrix from an integration point

$\underline{K}^*$ the contribution to the predictor stiffness from an integration point

$\underline{K}_T$ the contribution to the tangent stiffness from an integration point

K_s the bulk modulus of the soil skeleton

K_v the bulk modulus of the pore fluid

$[K^w]$ a matrix relating excess pore pressure to flow rate

L a constant used for evaluating the consistent constitutive matrix

$\underline{L}$ a submatrix defined in the text

$[L]$ a transformation matrix used for the consolidation formulation

M a constant used for evaluating the consistent constitutive matrix

$[N^p]$ a matrix of shape functions

$[N]$ a matrix of shape functions

P a constant used for evaluating the consistent constitutive matrix

$\underset{\sim}{P}$ the global load vector evaluated at the nodes

$\underset{\sim}{P}'$ the imposed strain load vector

Q a constant used for evaluating the consistent constitutive matrix

R the cap yield surface shape factor

$\underset{\sim}{R}$ the nodal force vector

S a constant used for evaluating the consistent constitutive matrix

T the tension cut-off value

T_i the local surface traction vector

U the potential energy functional

U_p^A the augmented potential energy functional

U^{SE} the strain energy density of the body

U^* the potential energy functional

V the volume of the body

V_v the volume of voids

V_s the volume of solids

V_o the initial volume of the body

V_{vo} the initial volume of voids

V_{so} the initial volume of solids

W the limiting value of volumetric strain for the cap yield surface

W the strain energy functional

W^* the deviator part of the strain energy functional

W^v the volumetric part of the strain energy functional

$\underset{\sim}{X}$ the internal forces acting on the slips

$\underset{\sim}{X}^*$ a vector of internal forces acting on the slips and satisfying yield

Y a constant used for evaluating the consistent constitutive matrix

Z a constant used for evaluating the consistent constitutive matrix

Greek

α a material constant

β the time integration constant

δ_{ij} the Kronecker delta

$\underset{\sim}{\epsilon}$ the total strain vector

$\underset{\sim}{\epsilon}_i$ the imposed strain vector

$\underset{\sim}{\epsilon}^e$ the elastic part of the strain vector

ϵ_{ij} the total strain tensor

ϵ_v^e the elastic volumetric strain

ϵ_v^p the inelastic/plastic volume strain

$\bar{\epsilon}_v^p$ the total inelastic/plastic volume strain

$\bar{\epsilon}_{vo}^p$ the initial total inelastic/plastic volume strain

ϵ_v the volumetric strain

ϵ_{vv} the volumetric strain in the pore fluid

ϵ_w the migration water strain

$\underset{\sim}{\epsilon}_w$ the vector of nodal values of migration water strain

ϵ^* the difference between the total and inelastic volumetric strain

γ_w the specific weight of the pore fluid

∞ infinity

$\underset{\sim}{\lambda}$ the internal slip vector

λ_η non-negative plastic multipliers associated with plastic strain rate

Λ a non-negative scalar plastic multiplier

Λ_η non-negative plastic multipliers associated with increments in plastic strain

μ defined in equation (4.46)

ν Poissons's ratio

ν_i the outward normal to the surface

ϕ the yield function

ψ the specified fluid flow across a boundary

Ψ the product of the yield function and non-negative scalar multiplier

θ a time increment multiplier

$\underset{\sim}{\sigma}$ the stress vector

σ'_{ij} the effective stress tensor

σ_{ij} the stress tensor

σ'_{kk} the effective volumetric stress

σ_{kk} the total volumetric stress

σ_m the mean hydrostatic stress

σ_m^c the cap yield surface hardening parameter

σ_y the uniaxial yield stress

ζ a Lagrange multiplier

Subscripts

SE the strain energy density

e element

i the iteration number

j the iteration number

n the time increment number

Right Superscripts

T the transpose of a matrix or vector

e the elastic part of

i the iteration number

j the iteration number

n the time increment number

p the plastic part of

SE the strain energy density

Left Superscripts

(i) the iteration number

(j) the iteration number

CHAPTER 1

INTRODUCTION

The formulation and solution of the problem of an elastic-plastic body subject to successive increments of loading is a fundamental problem in plasticity. A variety of powerful iterative techniques are available for the solution of the problem [1-4], mostly based on Newton-Raphson methods using an explicit scheme for the integration of the constitutive relations.

The procedures in current use can be criticised [5] in that they are essentially heuristic, and they are not fully linked to the governing mechanical principles of the incremental plasticity problem. Recent work aimed at the improvement of the accuracy and stability of the numerical algorithms in plasticity explores the fundamental relationship between the nature of the forward integration algorithm and the mechanical principles of the problem [6].

In this thesis we attempt to advance this understanding. Through the use of an internal variable formulation of the problem, we are able to explore links between a consistent mathematical programming formulation of the incremental problem in plasticity [5 & 7] and the conventional Newton-Raphson iterative solution procedures.

The internal variable formulation is closely linked to initial strain or imposed inelastic strain formulations of problems in plasticity, and provides considerable insight into the nature of the problems. The imposed inelastic strain concept is used to extend the formulation discussed in the thesis to

consolidation problems, adopting the concept of a *migration water strain* which traces the diffusion of the pore fluid in a porous medium.

The organisation of the thesis is as follows. In Chapter 2 imposed inelastic strains are introduced, and a finite element formulation which incorporates the strains as a load vector is presented . A porous medium is considered as a two phase material and the concept of a *migration water strain* which traces the flow of pore fluid in the medium is introduced . The principle of effective stress is used, and various methods of approaching the solution to the mechanical problem are explored.

In Chapter 3 the structural formulation of the incremental elastic-plastic problem is presented using an internal variable approach. Successive minimum principles are used to arrive at a Newton-Raphson scheme. For the case of a von Mises yield criterion various predictors are considered, and their performance evaluated with regard to efficiency and robustness. A simple numerical example is used for this purpose. Special attention is drawn to two of the predictors investigated : the one utilises a secant shear modulus, and the other (the "consistent" tangent predictor) is derived from a Taylor's series expansion about the increment in plastic strain. In the latter case second and higher order terms are neglected.

An algorithm for the numerical solution of static incremental problems which uses imposed inelastic strains and iterates on the secant shear modulus is dealt with in Chapter 4. Initially only elastic-plastic materials with a von Mises yield condition are considered. The algorithm involves the minimisation of a series of quadratic functionals, and a proof for convergence is given. The relationship between this approach and the Newton-Raphson scheme which uses the secant shear modulus is shown. The application of the algorithm is then extended to a material with a Drucker-Prager yield condition. Numerical

examples illustrating the robustness of the algorithm are presented. They however also show that the rate of convergence is relatively slow when compared to a commercial finite element code.

In Chapter 5 a formulation is proposed for the backward difference integration of three plastic constitutive materials namely, a von Mises, a Drucker-Prager, and a Drucker-Prager with a nonlinearly hardening parabolic cap and tension cut-off. The corresponding consistent tangent predictors are derived and presented in a form which can easily be implemented into a finite element code. A special numerical approach is required to solve plane stress problems and this method, common to all the predictors considered, is shown. Examples which validate the theory and show that the algorithm converges quadratically are analysed numerically. The results are compared to results obtained with ABAQUS [8] and a code using the forward integration method.

Finally, Chapter 6 deals with a formulation for the consolidation of a porous medium. The formulation makes use of the previously defined *migration water strain*. The mechanical and seepage problems considered separately are then linked by means of this *migration water strain* and a backward difference integration scheme. A series of examples which are compared with analytical solutions and solutions obtained with ABAQUS are analysed. These examples aim at highlighting certain practical issues involved in solving consolidation problems as well as at showing the effectiveness of the algorithm.

CHAPTER 2

IMPOSED INELASTIC STRAINS

2.1 CAUSES OF IMPOSED STRAINS

Imposed inelastic strains occur in bodies due to influences such as shrinkage, creep, temperature changes, crystal growth, and various in situ conditions. Further imposed strains could be induced by manufacturing and assembly processes or by the body's previous loading history. The sum of all these effects can be viewed as constituting the total imposed strain field.

The use of inelastic strains for solving elastic-plastic and consolidation problems is of major interest. Various methods have been proposed for solving problems with nonlinear material behaviour, and many of these methods make use of imposed strains, either directly or indirectly. In the former case these are generally refered to as initial strain methods [2].

2.2 FINITE ELEMENT FORMULATION FOR IMPOSED STRAINS

Let the total imposed strain field be represented by the vector $\underset{\sim}{\epsilon}_i$. To obtain a finite element formulation for small initial strains, the stresses are related to the elastic strains $\underset{\sim}{\epsilon}^e$ as follows:

$$\underset{\sim}{\sigma} = [D]\,\underset{\sim}{\epsilon}^e \quad , \tag{2.1}$$

where $\underset{\sim}{\epsilon}^e = \underset{\sim}{\epsilon} - \underset{\sim}{\epsilon}_i$,

and $\underset{\sim}{\epsilon}$ is the total strain vector.

The stresses and strains contribute to the strain energy density of the potential energy functional only, and subsequently it is the only term that needs to be considered. The strain energy density term can be written as

$$U^{SE} = \tfrac{1}{2} \int_V \underset{\sim}{\epsilon}^{eT} [D] \underset{\sim}{\epsilon}^{e} \, dV \quad . \tag{2.2a}$$

By substituting (2.1) into the above, we obtain

$$U^{SE} = \tfrac{1}{2}\int_V \underset{\sim}{\epsilon}^{T} [D] \underset{\sim}{\epsilon} \, dV - \tfrac{1}{2}\int_V \underset{\sim}{\epsilon}_i^{T} [D] \underset{\sim}{\epsilon} \, dV - \tfrac{1}{2}\int_V \underset{\sim}{\epsilon}^{T} [D] \underset{\sim}{\epsilon}_i \, dV + \tfrac{1}{2}\int_V \underset{\sim}{\epsilon}_i^{T} [D] \underset{\sim}{\epsilon}_i \, dV \quad . \tag{2.2b}$$

When differentiating the resultant potential energy functional to obtain the equilibrium equations, the contribution from the imposed strains is in the form of an additional load vector $\underset{\sim}{P}'$. The final equilibrium equations can be written as

$$[K]\underset{\sim}{u} = \underset{\sim}{P} + \underset{\sim}{P}' \quad , \tag{2.3}$$

where

$$\underset{\sim}{P}' = \int_V [B]^T [D] \underset{\sim}{\epsilon}_i dV \quad ,$$

$$[K] = \int_V [B]^T [D] [B] dV \quad ,$$

$\underset{\sim}{u}$ is the vector of nodal displacements,

$\underset{\sim}{P}$ is the vector of applied nodal loads,

and $[B]$ is the matrix relating the strains to the displacements.

The load term $\underset{\sim}{P}'$ essentially brings about a displacement field which is compatible with the imposed inelastic strain and the boundary conditions. In a statically determinate case the displacement field resulting from $\underset{\sim}{P}'$ will have no internal stresses associated with it as $(\underset{\sim}{\epsilon} - \underset{\sim}{\epsilon}_i) = \underset{\sim}{\epsilon}^{e} = 0$, whereas this will not necessarily be so in a statically indeterminate case.

2.3 IMPOSED STRAINS IN CONSOLIDATION PROBLEMS

In consolidation problems we are concerned with multiphase soils. The phases are essentially a mineral skeleton containing a pore fluid which could be either air, or water, or a mixture of the two. When the pore fluid is air only, the contribution to the stiffness of the whole is negligible. From a mechanical point of view the soil can be considered as a single phase material and modelled as such. When the soil is saturated or partially saturated some of the load is carried by the pore fluid.

We will assume that the material is saturated, and therefore a two phase material. The soil skeleton and the pore fluid may be considered as separate elements which occupy the same physical space. Considering an instant in time Δt, in the limiting case where $\Delta t \to 0$, there is no movement of the pore fluid relative to the soil skeleton, and we essentially have quasi-static conditions.

Consider an infinitesimal element where

i) the current volume is V,

ii) the current volume of the skeleton frame is V_s,

and iii) the current volume of voids is V_v.

In the initial state these volumes are V_o, V_{so}, and V_{vo} respectively. In general the change in V_s is due to the volume strain of the skeleton only, whereas the change in V_v is due to both volume strain in the pore fluid as well as migration of pore fluid.

The void ratio is defined as

$$e = \frac{V_v}{V_s} \quad , \tag{2.4}$$

the porosity as

$$n = \frac{V_v}{V} \quad , \tag{2.5}$$

the volume strain as

$$\epsilon_v = \frac{dV}{V_o} \quad , \tag{2.6}$$

and the volume strain in the pore fluid as

$$\epsilon_{vv} = \frac{dV_v}{V_{vo}} \quad . \tag{2.7}$$

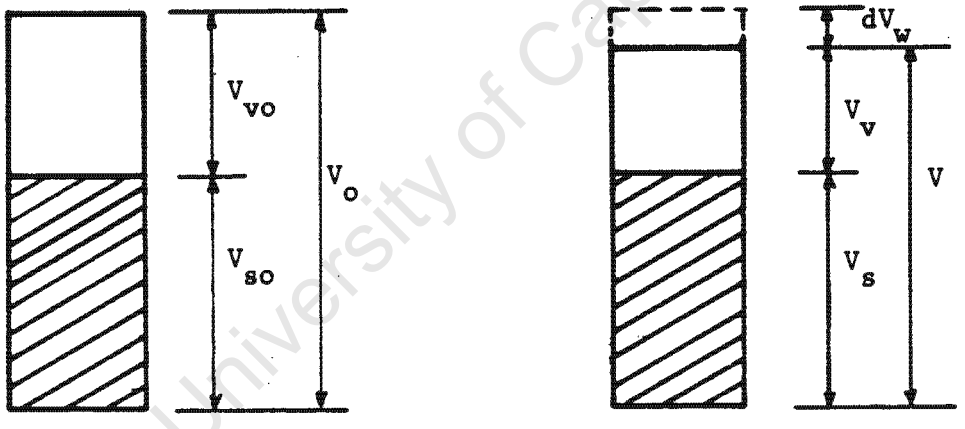

(a) Initial configuration (b) Current configuration

Figure 2.1 : Infinitesimal element of soil.

From Fig. 2.1 it is evident that $V = V_v + V_s$, and this can be rewritten as

$$V = V_s(1 + e) \quad . \tag{2.8}$$

Since the pore fluid can sustain hydrostatic stress only, we concentrate on the hydrostatic stress in the soil skeleton. Generally, soil subjected to hydrostatic stress will have a stress strain relationship of the form depicted in Fig. 2.2 with

$$\sigma'_{kk} = 3K_s \epsilon_v^e \quad , \tag{2.9}$$

where

σ'_{kk} is the hydrostatic stress in the soil skeleton,

K_s is the bulk modulus of the soil skeleton,

and ϵ_v^e is the elastic volumetric strain.

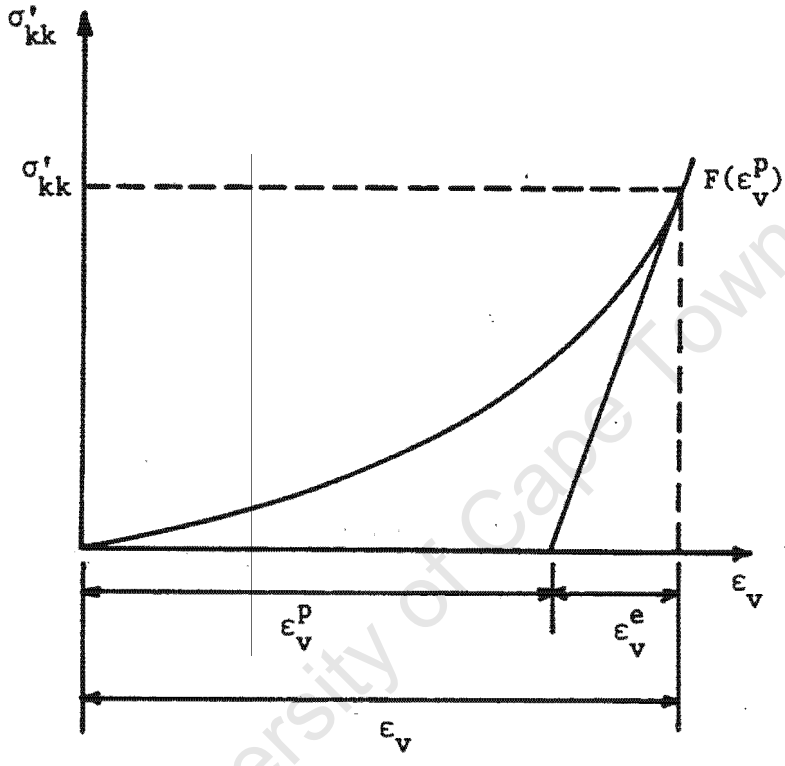

Figure 2.2 : Nonlinear volumetric behaviour of soil.

The volumetric strain ϵ_v has an elastic component ϵ_v^e which involves the deformation of soil grains, and an inelastic component ϵ_v^p which occurs as the result of the crushing of asperities etc., without change in volume of the soil grains.

The hydrostatic stress in the pore fluid is related elastically to ϵ_{vv} by

$$p = 3K_v \epsilon_{vv} \quad , \tag{2.10}$$

where

p is the excess pore pressure,

and K_v is the bulk modulus of the pore fluid.

The total hydrostatic stress sustained by the two phase mixture is given by the sum of the contributions from the skeleton and the pore fluid as

$$\sigma_{kk} = \sigma'_{kk} + p \quad . \tag{2.11}$$

This is known as Terzaghi's principle of effective stress.

From equation (2.6) we have

$$\epsilon_v = \frac{dV_s}{V_o} + \frac{dV_v}{dV_{vo}} \cdot \frac{dV_{vo}}{V_o} \quad , \tag{2.12}$$

and it is easy to verify that

$$\epsilon_v = \frac{\sigma'_{kk}}{3K_s} + n_o \epsilon_{vv} \tag{2.13a}$$

and that

$$\epsilon_{vv} = \frac{1}{n_o} \epsilon_v - \frac{\sigma'_{kk}}{3n_o K_s} \quad . \tag{2.13b}$$

It was mentioned earlier that the change in volume V_v has two components, namely the volume strain in the pore fluid and the migration of the pore fluid. Supposing that a volume of fluid dV_w has migrated to or from an element, the migration volume strain is defined as

$$\epsilon_w = \frac{dV_w}{V_o} \quad . \tag{2.14}$$

The quantity dV_v denotes the change in original volume of voids and hence

$$dV = dV_s + dV_v + dV_w \quad . \tag{2.15}$$

It thus follows from equation (2.6) that

$$\epsilon_v = \frac{\sigma'_{kk}}{3K_s} + n_o \epsilon_{vv} + \epsilon_w \quad , \tag{2.16}$$

and hence

$$p = \frac{3K_v}{n_o} \epsilon_v - \frac{K_v}{n_o K_s} \sigma'_{kk} - \frac{3K_v}{n_o} \epsilon_w \tag{2.17a}$$

with

$$\sigma_{kk} = \sigma'_{kk}(1 - \frac{K_v}{n_o K_s}) + \frac{3K_v}{n_o} \epsilon_v - \frac{3K_v}{n_o} \epsilon_w \quad . \tag{2.17b}$$

The solution to the instantaneous problem can easily be found by treating ϵ_w as an imposed strain. It should be noted that when $\epsilon_v^p = \epsilon_w$, the term $\epsilon_{vv} = 0$ and hence $p = 0$. This is equivalent to the fully drained case in consolidation analyses, and the fully undrained case can be recovered by setting $\epsilon_w = 0$.

We have discussed the more general case where the pore fluid is considered to be compressible. Problems are often encountered when trying to obtain numerical solutions for this general case, and special techniques are required to obtain acceptable solutions. One method of solving this is to treat the pore fluid as incompressible and in this case $K_v \to \infty$ with $\epsilon_{vv} \to 0$. Starting again at equation (2.16), it is apparent that

$$\epsilon_v = \frac{\sigma'_{kk}}{3K_s} + \epsilon_w \quad . \qquad (2.18a)$$

Since $\epsilon_{vv} = 0$, we know that $\epsilon_w = \epsilon_v^p$, and hence

$$\sigma'_{kk} = 3K_s(\epsilon_v - \epsilon_w) \quad . \qquad (2.18b)$$

The total hydrostatic stress is given by equation (2.11) with the excess pore pressure p not related to the strains, but included in the formulation as Lagrange multipliers. This topic will be addressed in some detail in Chapter 6.

CHAPTER 3

A FORMULATION FOR ELASTIC-PLASTIC ANALYSIS

3.1 OBJECTIVES AND ASSUMPTIONS

The aim of this Chapter will be to use the insights gained from the application of mathematical programming concepts to plasticity to provide a formulation for the incremental elastic-plastic problem. This permits the efficient heuristic methods to be compared more clearly with the framework of mathematical programming applications.

Discussion will be limited to the classical stable time-independent elastic-plastic problem. Phenomena which lead to strain softening and non-associated flow rules will not be considered. A simple formulation of the elastic-plastic problem is presented in discrete terms, and evolves naturally as an incremental deformation theory (or holonomic) problem. The appropriate minimum principle, or mathematical programming problem for this formulation can then be easily established.

3.2 FORMULATION OF THE ELASTIC-PLASTIC PROBLEM

The structural formulation used in this Chapter is based on the form given by Martin [9]. The formulation will be presented in discrete terms in a manner which can readily be identified with finite element approximations.

Consider a structure discretised by a finite element mesh where the nodal displacements can be represented by the components of a displacement vector $\underset{\sim}{u}$. The continuous displacement field can be approximated as closely as necessary by increasing the components of $\underset{\sim}{u}$. Similarly, the internal slips in the structure can be represented by the vector $\underset{\sim}{\lambda}$. Strain quantities do not appear directly in the formulation, but will be brought in later when various constitutive relations are discussed.

The strain energy F of the structure is assumed to be a homogeneous quadratic function of the components of $\underset{\sim}{u}$ and $\underset{\sim}{\lambda}$. Small changes in the kinematic variables yield

$$dF = \frac{\partial F}{\partial \underset{\sim}{u}} d\underset{\sim}{u} + \frac{\partial F}{\partial \underset{\sim}{\lambda}} d\underset{\sim}{\lambda}$$

$$= \underset{\sim}{R}\, d\underset{\sim}{u} \; - \underset{\sim}{X}\, d\underset{\sim}{\lambda} \quad , \tag{3.1}$$

where the nodal forces $\underset{\sim}{R}$ and the internal forces $\underset{\sim}{X}$ acting on the slips are identified as

$$\underset{\sim}{R} = \frac{\partial F}{\partial \underset{\sim}{u}} \tag{3.2a}$$

and

$$\underset{\sim}{X} = - \frac{\partial F}{\partial \underset{\sim}{\lambda}} \quad . \tag{3.2b}$$

The minus sign is chosen in equation (3.2b) to represent the forces applied by the structure to the slips. Both $\underset{\sim}{R}$ and $\underset{\sim}{X}$ are homogeneous linear functions of $\underset{\sim}{u}$ and $\underset{\sim}{\lambda}$.

Note that since $\frac{\partial^2 F}{\partial \underline{\lambda}\ \partial \underline{u}} = \frac{\partial^2 F}{\partial \underline{u}\ \partial \underline{\lambda}}$, the nodal and internal forces are

$$\underline{R} = \underline{K}\ \underline{u} + \underline{L}\ \underline{\lambda}$$

and

$$-\underline{X} = \underline{L}^T\ \underline{u} + \underline{H}\ \underline{\lambda} \quad ; \tag{3.3}$$

the expression for strain energy thus becomes

$$F = \tfrac{1}{2}\ \underline{u}^T\ \underline{K}\ \underline{u} + \tfrac{1}{2}\ \underline{u}^T\ \underline{L}\ \underline{\lambda} + \tfrac{1}{2}\ \underline{\lambda}^T\ \underline{L}\ \ \underline{u} + \tfrac{1}{2}\ \underline{\lambda}^T\ \underline{H}\ \underline{\lambda}$$

$$= \tfrac{1}{2} \begin{Bmatrix} \underline{u} \\ \underline{\lambda} \end{Bmatrix}^T \begin{bmatrix} \underline{K} & \underline{L} \\ \underline{L}^T & \underline{H} \end{bmatrix} \begin{Bmatrix} \underline{u} \\ \underline{\lambda} \end{Bmatrix} . \tag{3.4}$$

The rate of change of the internal slip vector is governed by a rigid perfectly plastic relation. The existence of a dissipation function D which is homogeneous and of degree one in $\dot{\underline{\lambda}}$ is assumed. It is further assumed to be related to the internal force vector as follows:

$$\underline{X} = \frac{\partial D}{\partial \dot{\underline{\lambda}}} \quad . \tag{3.5}$$

It is assumed that D is convex, and that $D \geq 0$ with $D = 0$ if and only if $\partial \dot{\underline{\lambda}} = 0$. It follows that the derivatives of D are discontinuous at the origin, and that since $\partial D / \partial \dot{\underline{\lambda}}$ is homogeneous and of degree zero in $\dot{\underline{\lambda}}$, derivatives of D may be discontinuous along lines which are radial in the $\dot{\underline{\lambda}}$ space. This is so because D will generally be the sum of independent dissipation functions associated with individual components of $\dot{\underline{\lambda}}$, or groups

of components of $\dot{\underline{\lambda}}$. At a point on the surface D, where $\partial D/\partial \dot{\underline{\lambda}}$ is not continuous, equation (3.5) is interpreted as requiring $\underline{X}$ to assume some value within the domain bounded by adjacent values of $\partial D/\partial \dot{\underline{\lambda}}$.

Equations (3.3) and (3.5) completely define the mechanical behaviour of the structure. If the external forces at the nodes are defined by $\underline{P}$, equilibrium requires that

$$\underline{R} = \underline{P} \quad , \tag{3.6}$$

and that the governing equations can be conveniently written as

$$\underline{K}\,\underline{u} + \underline{L}\,\underline{\lambda} = \underline{P} \quad , \tag{3.7a}$$

$$\underline{L}^{T}\,\underline{u} + \underline{H}\,\underline{\lambda} = -\frac{\partial D}{\partial \dot{\underline{\lambda}}} \quad . \tag{3.7b}$$

Equation (3.7a) represents the equilibrium condition of the structure, whereas (3.7b) represents the yield condition.

In elastic-plastic problems, the loading $\underline{P}$ is regarded as a function of time and hence

$$\underline{P} = \underline{P}(t) \quad ,$$

$$\underline{u} = \underline{u}(t) \quad ,$$

$$\underline{\lambda} = \underline{\lambda}(t) \quad , \tag{3.8}$$

and $$\dot{\underline{\lambda}} = \frac{d\underline{\lambda}}{dt} \quad .$$

The problems are rate independent, and the parameter t measures the order of events, rather than real time. Equations (3.7) must hold at each instant of the loading history.

The initial conditions are given by

$$\underset{\sim}{P}(o) = P_o \quad ,$$

$$\underset{\sim}{u}(o) = u_o \quad , \tag{3.9}$$

and $$\underset{\sim}{\lambda}(o) = \lambda_o \quad ,$$

which could easily be accommodated in the formulation, but will be taken to be zero for the sake of convenience. This is done without loss of generality. These equations describe a broad class of stable, quasi-static, time independent, elastic-plastic problems.

3.3 INCREMENTAL ELASTIC-PLASTIC SOLUTIONS

In order to set up a numerical procedure which determines the response of the structure to a certain loading program $P(t)$, the time as well as the spatial domain is discretised. The time is divided into discrete intervals Δt which are not necessarily equal. We seek to satisfy equations (3.7) only at the end of these intervals. Thus at time t_n , after the passage of n intervals, the equations (3.7) are written as

$$\underset{\sim}{K}\,\underset{\sim}{u}_n + \underset{\sim}{L}\,\underset{\sim}{\lambda}_n = \underset{\sim}{P}_n \quad , \tag{3.10a}$$

$$\underset{\sim}{L}^T\,\underset{\sim}{u}_n + \underset{\sim}{H}\,\underset{\sim}{\lambda}_n = -\left[\frac{\partial D}{\partial \dot{\underset{\sim}{\lambda}}}\right]_{\dot{\underset{\sim}{\lambda}}_n} \quad . \tag{3.10b}$$

The only difficulty in this problem is posed by the term on the right hand side of equation (3.10b), which is a function of $\dot{\underset{\sim}{\lambda}}_n$. This indicates that the only further assumptions that we need to make, relate to the way in which $\underset{\sim}{\lambda}$ varies with time.

Firstly, we note that since $\partial D/\partial \dot{\underset{\sim}{\lambda}}$ is homogeneous and of degree zero in the components of $\dot{\underset{\sim}{\lambda}}$, we are concerned only with the direction of $\dot{\underset{\sim}{\lambda}}$ in the $\dot{\underset{\sim}{\lambda}}$ space, rather than with its magnitude. Secondly, we note that the direction $\dot{\underset{\sim}{\lambda}}(t)$ can be expected to be discontinuous, in as far as yielding or unloading can take place on any slip system at any time in the loading history.

Clearly, in the discretized scheme, $\dot{\underset{\sim}{\lambda}}_n$ must be written in terms of $\underset{\sim}{\lambda}_{n-i+1}$ and $\dot{\underset{\sim}{\lambda}}_{n-i}$ where $i = 1,2,3, \ldots$. In view of the possible discontinuities in $\dot{\underset{\sim}{\lambda}}(t)$, caution must be exercised in using information at previous time intervals $t_{n-1}, t_{n-2}, \ldots$. The most evident choice is thus one in which $\dot{\underset{\sim}{\lambda}}_n$ is written as terms of $\underset{\sim}{\lambda}_n$ and $\underset{\sim}{\lambda}_{n-1}$, and the discussion will therefore be limited to this case.

In addition to the decision that $\dot{\underset{\sim}{\lambda}}_n$ depends only on the values $\underset{\sim}{\lambda}_n$ and $\underset{\sim}{\lambda}_{n-1}$, we need an assumption on the path in $\underset{\sim}{\lambda}$ space between $\underset{\sim}{\lambda}_{n-1}$ and $\underset{\sim}{\lambda}_n$ as shown diagrammatically in Figure 3.1. In many finite element applications it is assumed implicitly that the total strain $\underset{\sim}{\epsilon}$ follows a straight line path from $\underset{\sim}{\epsilon}_{n-1}$ to $\underset{\sim}{\epsilon}_n$; a recent review of some commonly used algorithms has been given by Marques [10]. In general, this implies a relatively complicated path in the $\underset{\sim}{\lambda}$ space, and the direction of $\dot{\underset{\sim}{\lambda}}_n$ is effectively taken as tangential to the path at $\underset{\sim}{\lambda}_n$. The calculations are carried out in terms of stress $\underset{\sim}{\sigma}$ and the total strain $\underset{\sim}{\epsilon}$, frequently using a subincrementation procedure.

A more direct choice would be to adopt a simple backward difference scheme, assuming that $\underset{\sim}{\lambda}$ follows a straight line path in the $\underset{\sim}{\lambda}$ space between $\underset{\sim}{\lambda}_{n-1}$ and $\underset{\sim}{\lambda}_n$, as shown by the dotted line in Figure 3.1. This is achieved by putting

$$\dot{\underset{\sim}{\lambda}}_{n-1} = \frac{1}{\Delta t}\,(\underset{\sim}{\lambda}_n - \underset{\sim}{\lambda}_{n-1}) = \frac{\Delta \underset{\sim}{\lambda}_n}{\Delta t} \quad . \tag{3.11}$$

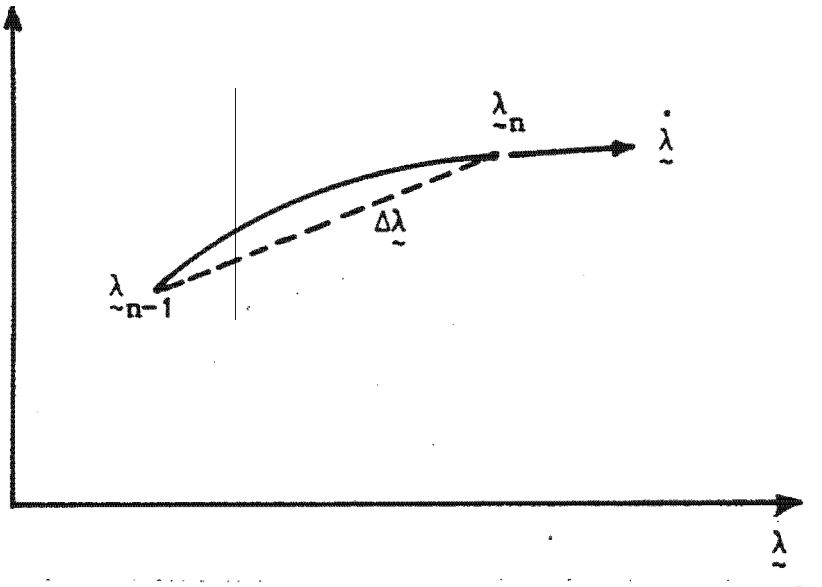

Figure 3.1 : Path followed between $\underset{\sim}{\lambda}_{n-1}$ and $\underset{\sim}{\lambda}_n$.

Because $\partial D/\partial\dot{\underset{\sim}{\lambda}}$ is homogeneous and of degree zero, it is not necessary to distinguish between $\dot{\underset{\sim}{\lambda}}_n$ and $\Delta\underset{\sim}{\lambda}_n$. We write

$$D = D(\Delta\underset{\sim}{\lambda}) \quad ,$$

and this may be interpreted as the dissipated work associated with $\Delta\underset{\sim}{\lambda}_n$. Equations (3.10) become

$$\underset{=}{K}\,\underset{\sim}{u}_n + \underset{=}{L}\,\underset{\sim}{\lambda}_n = \underset{\sim}{P}_n \quad , \tag{3.12a}$$

$$\underset{=}{L}^T\,\underset{\sim}{u}_n + \underset{=}{H}\,\underset{\sim}{\lambda}_n = -\left[\frac{\partial D}{\partial \Delta\underset{\sim}{\lambda}}\right]_{\Delta\underset{\sim}{\lambda}_n} \quad . \tag{3.12b}$$

The advantage now is that $\underset{\sim}{X}_n$ can be written as a potential function, which is not necessarily true if $\Delta\underset{\sim}{\lambda}$ is based on a straight line path in total strain space. Following the concepts discussed by Ponter and Martin [11] and Carter and Martin [12], the assumption of a straight line path in $\underset{\sim}{\lambda}$ space implies that the total strain $\underset{\sim}{\epsilon}$ follows a minimum work path from $\underset{\sim}{\epsilon}_{n-1}$ to $\underset{\sim}{\epsilon}_n$.

3.4 MINIMUM PRINCIPLE FOR THE INCREMENTAL PROBLEM

Equations (3.12) imply a minimum principle for the incremental problem. This will be indicated at this stage without attempting to be rigorous in the argument. Putting

$$\begin{aligned} \underset{\sim}{u}_n &= \underset{\sim}{u}_{n-1} + \Delta\underset{\sim}{u}_n \quad , \\ \underset{\sim}{\lambda}_n &= \underset{\sim}{\lambda}_{n-1} + \Delta\underset{\sim}{\lambda}_n \quad , \end{aligned} \tag{3.13}$$

equations (3.12) can be written in incremental form :

$$\underset{\sim}{K}\Delta\underset{\sim}{u}_n + \underset{\sim}{L}\Delta\underset{\sim}{\lambda}_n = \underset{\sim}{P}_n - \underset{\sim}{K}\,\underset{\sim}{u}_{n-1} - \underset{\sim}{L}\,\underset{\sim}{\lambda}_{n-1} \quad , \tag{3.14a}$$

$$\underset{\sim}{L}^T\Delta\underset{\sim}{u}_n + \underset{\sim}{H}\Delta\underset{\sim}{\lambda}_n + \left[\frac{\partial D}{\partial \Delta\underset{\sim}{\lambda}}\right]_{\Delta\underset{\sim}{\lambda}_n} = - \underset{\sim}{L}^T\,\underset{\sim}{u}_{n-1} - \underset{\sim}{H}\,\underset{\sim}{\lambda}_{n-1} \quad . \tag{3.14b}$$

If the solution at t_{n-1} is exact,

$$\begin{aligned} \underset{\sim}{K}\,\underset{\sim}{u}_{n-1} + \underset{\sim}{L}\,\underset{\sim}{\lambda}_{n-1} &= \underset{\sim}{P}_{n-1} \quad , \\ \underset{\sim}{L}^T\underset{\sim}{u}_{n-1} + \underset{\sim}{H}\,\underset{\sim}{\lambda}_{n-1} &= - \underset{\sim}{X}_{n-1} \quad . \end{aligned} \tag{3.15}$$

It then follows that equations (3.14) express the condition that the convex function $U_p(\Delta\underset{\sim}{u}_n \, , \, \Delta\underset{\sim}{\lambda}_n)$ should assume its least value, where

$$\begin{aligned} U_p = \tfrac{1}{2} &\begin{Bmatrix} \Delta\underset{\sim}{u}_n \\ \Delta\underset{\sim}{\lambda}_n \end{Bmatrix}^T \begin{bmatrix} \underset{\sim}{K} & \underset{\sim}{L} \\ \underset{\sim}{L}^T & \underset{\sim}{H} \end{bmatrix} \begin{Bmatrix} \Delta\underset{\sim}{u}_n \\ \Delta\underset{\sim}{\lambda}_n \end{Bmatrix} + D(\Delta\underset{\sim}{\lambda}_n) \\ &- \Delta\underset{\sim}{u}_n^T\,\Delta\underset{\sim}{P}_n - \Delta\underset{\sim}{\lambda}_n^T\,\underset{\sim}{X}_{n-1} \quad . \end{aligned} \tag{3.16}$$

Note also that if the solution at t_{n-1} is not exact, due to the use of an iterative scheme with some specified tolerance, we may use equations (3.14) directly and define

$$\hat{U}_p = \tfrac{1}{2} \begin{Bmatrix} \Delta u_n \\ \Delta \lambda_n \end{Bmatrix}^T \begin{bmatrix} K & L \\ L^T & H \end{bmatrix} \begin{Bmatrix} \Delta u_n \\ \Delta \lambda_n \end{Bmatrix} + D(\Delta \lambda_n) - \Delta u_n^T (P_n - K u_{n-1} - L \lambda_{n-1})$$

$$+ \Delta \lambda_n (L^T u_{n-1} + H \lambda_{n-1}) \quad . \qquad (3.17)$$

Equations (3.12) express the condition that $\hat{U}_p$ should take its least value.

Framed in this way, the minimum principle does not limit the choice of the step size in any way. The load may be applied in a single step (n=1), in which case $u_{n-1} = \lambda_{n-1} = 0$, and the principle reduces to that for the minimum work path deformation theory given by Ponter and Martin [11]. As the number of steps over which a given load P is applied is increased, the sequence of solutions at t_1, t_2, ..., will converge towards the continuous analytical solution.

3.5 NUMERICAL ALGORITHMS FOR THE INCREMENTAL PROBLEM

Solution strategies for equations (3.14), or minimisation of the functions given in equations (3.16) and (3.17) can be based on what have been referred to as heuristic Newton-Raphson iterative approaches [5]. In such iterative approaches we seek algorithms which permit us to replace estimates Δu_n^i , $\Delta \lambda_n^i$ by improved estimates Δu_n^{i+1} , $\Delta \lambda_n^{i+1}$. One strategy is to iterate between equations (3.14a) and (3.14b), using one equation to improve Δu_n and the other to improve $\Delta \lambda_n$. This follows the general thrust of the algorithms which are in common use in elastic-plastic finite element analysis [1-3]. We show how this strategy can be evaluated in terms of the minimisation of $\hat{U}_p$ in

equation (3.17). We assume that we have estimates $\Delta\underset{\sim}{u}_n^i$, $\Delta\underset{\sim}{\lambda}_n^i$ which satisfy equation (3.14), so that

$$\underline{L}^T\Delta\underset{\sim}{u}_n^i + \underline{H}\Delta\underset{\sim}{\lambda}_n^i + \left[\frac{\partial D}{\partial \Delta\underset{\sim}{\lambda}}\right]_{\Delta\underset{\sim}{\lambda}_n^i} = -\underline{L}^T\underset{\sim}{u}_{n-1} - \underline{H}\,\underset{\sim}{\lambda}_{n-1} \quad . \tag{3.18}$$

Put

$$\Delta\underset{\sim}{u}_n^{i+1} = \Delta\underset{\sim}{u}_n^i + \Delta\hat{\underset{\sim}{u}} \tag{3.19a}$$

and

$$\Delta\underset{\sim}{\lambda}_n^{i+1} = \Delta\underset{\sim}{\lambda}_n^i + \Delta\hat{\underset{\sim}{\lambda}} \quad . \tag{3.19b}$$

Substituting equations (3.19a) and (3.19b) into equation (3.14a), we find that

$$\underline{K}\Delta\hat{\underset{\sim}{u}} + \underline{L}\Delta\hat{\underset{\sim}{\lambda}} = \underset{\sim}{P}_n - \underline{K}(\underset{\sim}{u}_{n-1} + \Delta\underset{\sim}{u}_n^i) - \underline{L}(\underset{\sim}{\lambda}_{n-1} + \Delta\underset{\sim}{\lambda}_n^i) \quad . \tag{3.20}$$

We write equation (3.14b) without updating the $(\partial D/\partial\Delta\underset{\sim}{\lambda})$ term as

$$\underline{L}^T\Delta\underset{\sim}{u}_n^{i+1} + \underline{H}\Delta\underset{\sim}{\lambda}_n^{i+1} + \left[\frac{\partial D}{\partial \Delta\underset{\sim}{\lambda}}\right]_{\Delta\underset{\sim}{\lambda}_n^i} = -\underline{L}^T\underset{\sim}{u}_{n-1} - \underline{H}\,\underset{\sim}{\lambda}_{n-1} \quad . \tag{3.21}$$

On substituting from equations (3.18) and (3.19), this becomes

$$\underline{L}^T\Delta\hat{\underset{\sim}{u}} + \underline{H}\Delta\hat{\underset{\sim}{\lambda}} = 0 \quad . \tag{3.22}$$

We eliminate $\Delta\hat{\underset{\sim}{\lambda}}$ from equations (3.20) and (3.22) : note that $\Delta\hat{\underset{\sim}{\lambda}}$ will be non-zero only at integration points where the material is at yield and where it can be expected from the previous iteration to be yielding. We set $\Delta\hat{\underset{\sim}{\lambda}} = 0$ at other integration points, and introduce $\hat{\underline{L}}$, $\hat{\underline{H}}$ as matrices which contain only those parts of $\underline{L}$, $\underline{H}$ which refer to the integration points where yield is expected. Elimination of $\Delta\hat{\underset{\sim}{\lambda}}$ from equations (3.20) and (3.22) leads to

$$(\underset{\sim}{K} - \hat{\underset{\sim}{L}}\,\hat{\underset{\sim}{H}}^{-1}\,\hat{\underset{\sim}{L}}^{T})\hat{\Delta\underset{\sim}{u}} = \underset{\sim}{K}_T\hat{\Delta\underset{\sim}{u}} = \underset{\sim}{R}_i \quad , \tag{3.23}$$

where

$$\underset{\sim}{R}^i = \underset{\sim}{P}_n - \underset{\sim}{K}(\underset{\sim}{u}_{n-1} + \Delta\underset{\sim}{u}_n^i) - \underset{\sim}{L}(\underset{\sim}{\lambda}_{n-1} + \Delta\underset{\sim}{\lambda}_n^i) \tag{3.24}$$

is the residual force vector and $\underset{\sim}{K}_T$ is the tangent stiffness matrix.

Equation (3.23) is solved for $\hat{\Delta\underset{\sim}{u}}$ and the revised estimate for the internal variable increment is obtained from equation (3.14b); $\Delta\underset{\sim}{\lambda}_n^{i+1}$ satisfies the equation

$$\underset{\sim}{L}^T\Delta\underset{\sim}{u}_n^{i+1} + \underset{\sim}{H}\Delta\underset{\sim}{\lambda}_n^{i+1} + \left[\frac{\partial D}{\partial\Delta\underset{\sim}{\lambda}}\right]_{\Delta\underset{\sim}{\lambda}_n^{i+1}} = -\underset{\sim}{L}^T\underset{\sim}{u}_{n-1} - \underset{\sim}{H}\underset{\sim}{\lambda}_{n-1} \quad . \tag{3.25}$$

We now have "improved" estimates $\Delta\underset{\sim}{u}^{i+1}$, $\Delta\underset{\sim}{\lambda}^{i+1}$. The iteration is started with the assumption that both $\Delta\underset{\sim}{u}_n^o$ and $\Delta\underset{\sim}{\lambda}_n^o$ are zero, and proceeds until a tolerance on some norm or norms of $\underset{\sim}{R}_i$ and $\Delta\underset{\sim}{u}_n^i$ is satisfied.

Assessment of whether the revised estimates provided by the iteration loop are indeed improvements should be based on whether the value of $\hat{U}_p$ in equation (3.17) is decreased in the step. We thus consider

$$I = \hat{U}_p(\Delta\underset{\sim}{u}_n^{i+1} , \Delta\underset{\sim}{\lambda}_n^{i+1}) - \hat{U}_p(\Delta\underset{\sim}{u}_n^i , \Delta\underset{\sim}{\lambda}_n^i) \quad . \tag{3.26}$$

It follows from equation (3.17) that

$$I = \tfrac{1}{2} \begin{Bmatrix} \Delta u_{\sim n}^{i+1} \\ \Delta \lambda_{\sim n}^{i+1} \end{Bmatrix}^T \begin{bmatrix} K & L \\ L^T & H \end{bmatrix} \begin{Bmatrix} \Delta u_{\sim n}^{i+1} \\ \Delta \lambda_{\sim n}^{i+1} \end{Bmatrix}$$

$$- \tfrac{1}{2} \begin{Bmatrix} \Delta u_{\sim n}^{i} \\ \Delta \lambda_{\sim n}^{i} \end{Bmatrix}^T \begin{bmatrix} K & L \\ L^T & H \end{bmatrix} \begin{Bmatrix} \Delta u_{\sim n}^{i} \\ \Delta \lambda_{\sim n}^{i} \end{Bmatrix}$$

$$+ D(\Delta \lambda_{\sim n}^{i+1}) - D(\Delta \lambda_{\sim n}^{i})$$

$$- \hat{\Delta u}^T (P_{\sim n} - K\, u_{\sim n-1} - L\, \lambda_{\sim n-1}) + \hat{\Delta \lambda}^T (L^T\, u_{\sim n-1} - H\, \lambda_{\sim n-1}) \quad . \qquad (3.27)$$

With some straightforward manipulation we can rewrite equation (3.27) in the form

$$I = I_1 + I_2 + I_3 \quad , \qquad (3.28a)$$

where

$$I_1 = - \tfrac{1}{2} \begin{Bmatrix} \hat{\Delta u} \\ \hat{\Delta \lambda} \end{Bmatrix}^T \begin{bmatrix} K & L \\ L^T & H \end{bmatrix} \begin{Bmatrix} \hat{\Delta u} \\ \hat{\Delta \lambda} \end{Bmatrix} \quad , \qquad (3.28b)$$

$$I_2 = - \hat{\Delta u}^T R^{i+1} \quad , \qquad (3.28c)$$

$$I_3 = - D(\lambda_{\sim n}^{i}) + D(\Delta \lambda_{\sim n}^{i+1}) + (\Delta \lambda_{\sim n}^{i} - \Delta \lambda_{\sim n}^{i+1})^T X_{\sim n}^{i+1} \quad , \qquad (3.28d)$$

and where

$$\underset{\sim}{R}^{i+1} = \underset{\sim}{P}_n - \underset{\sim}{K}(\underset{\sim}{u}_{n-1} + \Delta\underset{\sim}{u}_n^{i+1}) - \underset{\sim}{L}(\underset{\sim}{\lambda}_{n-1} + \Delta\underset{\sim}{\lambda}_n^{i+1}) \quad , \tag{3.28e}$$

$$-\underset{\sim}{X}_n^{i+1} = \underset{\sim}{L}^T(\underset{\sim}{u}_{n-1} + \Delta\underset{\sim}{u}_n^{i+1}) + \underset{\sim}{H}(\underset{\sim}{\lambda}_{n-1} + \Delta\underset{\sim}{\lambda}_n^{i+1}) \quad . \tag{3.28f}$$

The terms I_1 and I_3 are negative definite and non-positive respectively, from the convexity of the strain energy F and the dissipation function D . The sign of I_2 however, could be either positive or negative. Clearly, if

$$\Delta\hat{\underset{\sim}{u}}^T \underset{\sim}{R}^{i+1} > 0 \quad , \tag{3.29}$$

we have a sufficient condition that $\hat{U}_p$ decreases in the iteration. The sign of I_2 will depend on the calculation of $\underset{\sim}{K}_T$. The predictor step (equation 3.23) is often replaced by a modified Newton-Raphson procedure involving less frequent updates of $\underset{\sim}{K}_T$, or by matrix updating techniques. The condition given in equation (3.29) can potentially provide a test for the appropriateness of the choice $\underset{\sim}{K}_T$ in a particular iteration, permitting the iteration to be scrapped and redone if the sign constraint is not met. The procedure described above is not identical to that used in conventional finite element codes. Nevertheless, the general thrust remains the same, and it would appear that the general class of Newton-Raphson methods follow the requirements of the solution of a mathematical programming problem quite closely.

3.6 PLASTIC CONSTITUTIVE EQUATIONS

At this point it is necessary for us to take a closer look at the material behaviour. The internal variable framework adopted in this Chapter makes it possible to represent conventional perfect plasticity, kinematic and isotropic hardening, as well as simple combinations of these without

difficulty. Uniaxial models for these cases are discussed by Martin [13]. Multiaxial constitutive equations can be generated through piecewise linear yield surfaces, or more directly through appropriate forms of the free energy and dissipation functions.

The global dissipation function D will in general be the sum of dissipation functions associated with elements, or with integration points within elements. The local dissipation functions will each be convex functions of degree one in the local components of $\dot{\underline{\lambda}}$. The convexity permits us to define convex yield functions on the local and global level. On the global level we introduce the yield function $\phi(\underline{X})$. The forces $\underline{X}$ acting on the slips are restricted by the condition that

$$\phi(\underline{X}) \leq 0 \quad . \tag{3.30}$$

Equation (3.5) can be written as

$$\partial \dot{\underline{\lambda}}^T \underline{X} = \partial D \quad ,$$

and noting that

$$\begin{aligned} \partial \underline{X}^T \dot{\underline{\lambda}} &= \partial \underline{X}^T \dot{\underline{\lambda}} + \partial \dot{\underline{\lambda}}^T \underline{X} - \partial D \\ &= \partial (\underline{X}^T \dot{\underline{\lambda}} - D) = \partial \Psi \end{aligned}$$

with $\Psi = \Lambda.\phi(\underline{X})$ and Λ being a scalar multiplier we obtain the equation

$$\dot{\underline{\lambda}} = \Lambda \frac{\partial \phi}{\partial \underline{X}} \quad , \tag{3.31a}$$

with

$$\begin{aligned} &\Lambda \geq 0 \quad \text{if} \quad \phi(\underline{X}) = 0 \quad , \\ &\Lambda \not\geq 0 \quad \text{if} \quad \phi(\underline{X}) < 0 \quad . \end{aligned} \tag{3.31b}$$

As a result of the convexity of D , the principle of maximum plastic work holds in its conventional form. If the relationship between $\underset{\sim}{X}$ and $\dot{\underset{\sim}{\lambda}}$ are given by equation (3.5) or (3.31), and $\underset{\sim}{X}^*$ is a set of slip forces such that $\phi(\underset{\sim}{X}^*) \leq 0$, then

$$\dot{\underset{\sim}{\lambda}}^T(\underset{\sim}{X} - \underset{\sim}{X}^*) \geq 0 \quad .$$

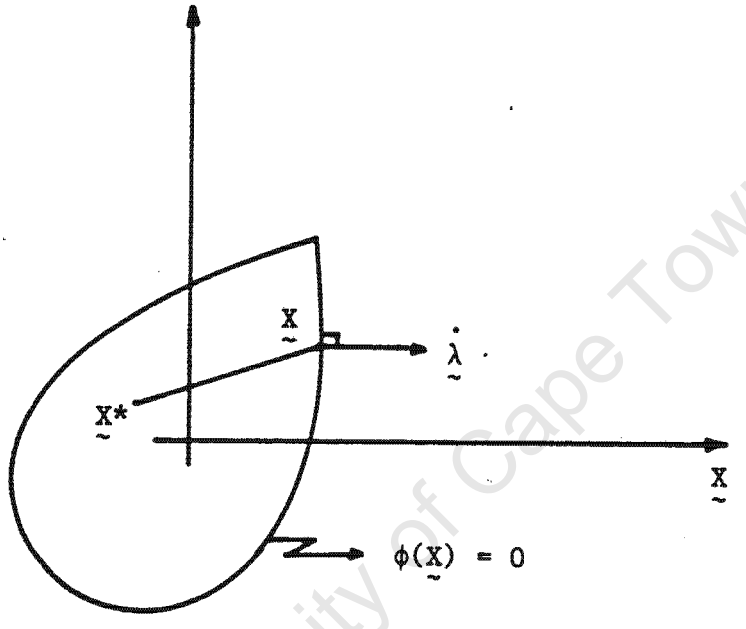

Figure 3.2 : Principle of maximum plastic work.

3.7 INCREMENTAL ANALYSIS WITH A VON MISES YIELD CONDITION

In order to gain insight into how the method relates to multiaxial constitutive equations, we will consider a von Mises yield condition. Let us assume that we have an elastic, perfectly plastic material. The strain tensor ϵ_{ij} is divided into its hydrostatic and deviator components, ϵ_{kk} and e_{ij} respectively, where

$$\epsilon_{ij} = e_{ij} + \frac{1}{3}\epsilon_{kk}\delta_{ij} \quad . \qquad (3.32a)$$

The stress tensor σ_{ij} is similarly divided into its hydrostatic and deviator parts, σ_{kk} and s_{ij}, with

$$\sigma_{ij} = s_{ij} + \frac{1}{3}\sigma_{kk}\delta_{ij} \quad . \tag{3.32b}$$

Plastic behaviour is confined to the deviator part of the strain which can further be split up into elastic and plastic components as

$$e_{ij} = e^{e}_{ij} + e^{p}_{ij} \quad .$$

The e^{p}_{ij} term is equivalent to the internal variable $\underset{\sim}{\lambda}$. The volumetric behaviour is always elastic and is governed by

$$\sigma_{kk} = 3K\,\epsilon_{kk} \tag{3.33}$$

where K is the bulk modulus.

The von Mises yield condition is given by

$$\phi = \tfrac{1}{2}\, s_{ij}\, s_{ij} - k^2 \quad , \tag{3.34}$$

and since we can write

$$s_{ij} = 2G(e_{ij} - e^{p}_{ij}) \quad , \tag{3.35}$$

where G is the shear modulus, the yield condition can also be written as

$$\phi = 2G^2(e_{ij} - e^{p}_{ij})(e_{ij} - e^{p}_{ij}) - k^2 \quad . \tag{3.36}$$

In a generic problem the strain deviator changes over a load increment from a value e_{ij}^{n-1} to a value e_{ij}^{n} . The deviator strain increment is Δe_{ij}^{n} where

$$\Delta e_{ij}^{n} = e_{ij}^{n} - e_{ij}^{n-1} \quad . \tag{3.37}$$

We assume that the plastic strain at the beginning and end of the increment is given by $e_{ij}^{p(n-1)}$ and e_{ij}^{pn} respectively, and that the plastic strain increment Δe_{ij}^{pn} is

$$\Delta e_{ij}^{pn} = e_{ij}^{pn} - e_{ij}^{p(n-1)} \quad . \tag{3.38}$$

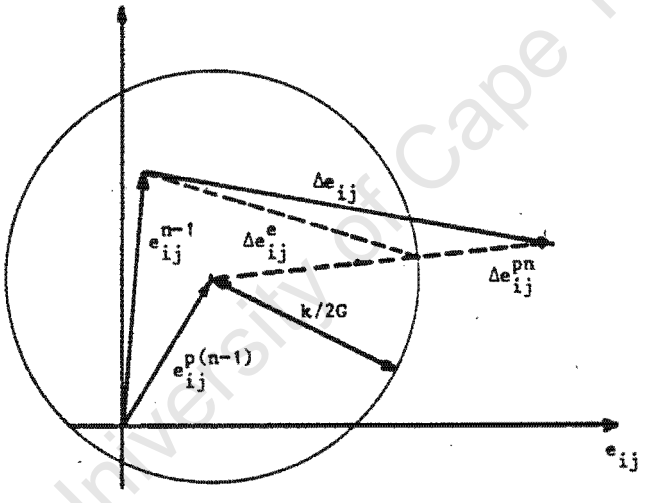

Figure 3.3 : Von Mises yield at t_{n-1} .

Fig. 3.3 shows diagrammatically the yield condition at the beginning of the load increment. In strain space the yield condition is a hypersphere with its centre at $e_{ij}^{p(n-1)}$. The current strain is indicated, and

$$s_{ij}^{n-1} = 2G(e_{ij}^{n-1} - e_{ij}^{p(n-1)}) \quad . \tag{3.39}$$

It is clear that $\phi(s_{ij}^{n-1}) \leq 0$.

Also indicated in Fig. 3.3 are the deviator strain increment Δe_{ij} and the plastic strain increment Δe^{p}_{ij} which follows a straight line path in deviator strain space. For a perfectly plastic material, the deviator strain change Δe_{ij} can be divided into two sequential parts : an elastic change Δe^{e}_{ij} given by

$$\Delta e^{e}_{ij} = \frac{1}{2G} \Delta s_{ij} = \frac{1}{2G} (s^{n}_{ij} - s^{n-1}_{ij}) \quad , \tag{3.40}$$

and a plastic change Δe^{p}_{ij} which takes place at a constant deviator stress s^{n}_{ij}. This is essentially the method commonly known as the radial return algorithm, and the strain path between e^{n-1}_{ij} and e^{n}_{ij} is a <u>minimum work path</u> (i.e. the incremental work density

$$dW = \int_{e^{n-1}_{ij}}^{e^{n}_{ij}} s_{ij} \, de_{ij} \tag{3.41}$$

takes its least value) .

The constitutive relations follow directly from geometric considerations. Let us define

$$e^{*} = (\tfrac{1}{2} (e^{n}_{ij} - e^{p(n-1)}_{ij})(e^{n}_{ij} - e^{p(n-1)}_{ij}))^{\frac{1}{2}} \quad , \tag{3.42}$$

then we will have either

$$s^{n}_{ij} = 2G(e^{n}_{ij} - e^{p(n-1)}_{ij}) \tag{3.43a}$$

$$\Delta e^{pn}_{ij} = 0 \qquad \text{for } e^{*} \leq \frac{k}{2G} \quad ,$$

or

$$s_{ij}^{n} = \left(\frac{k}{2Ge^{*}}\right) 2G(e_{ij}^{n} - e_{ij}^{p(n-1)})$$

$$\Delta e_{ij}^{pn} = \left(1 - \frac{k}{2Ge^{*}}\right) (e_{ij}^{n} - e_{ij}^{p(n-1)}) \text{ for } e^{*} > \frac{k}{2G} \quad . \qquad (3.43b)$$

These relations are supplemented by the volumetric relations of equation (3.33), which we now write in the form

$$\sigma_{kk}^{n} = 3K\ \epsilon_{kk}^{n} \quad , \qquad (3.44)$$

and hence

$$\sigma_{ij}^{n} = s_{ij}^{n} + \frac{1}{3}\ \sigma_{kk}^{n}\ \delta_{ij} \quad . \qquad (3.45)$$

As mentioned earlier, the internal slips $\underset{\sim}{\lambda}$ are simply the plastic strain tensor e_{ij}^{p} written in vector form. Similarly, the internal forces $\underset{\sim}{X}$ acting on the slips are the deviator stresses s_{ij} . For the meaning of the matrices $\underset{=}{K}$, $\underset{=}{L}$, and $\underset{=}{H}$ we need to refer to the equations (3.10) and (2.3) and see that the contribution from each integration point to these is respectively, $[B]^{T}[D][B]$, $-[B]^{T}[D]$, and $[D]$. The dissipation function $D(\Delta e_{ij}^{p})$ can be obtained from equations (3.5), (3.31), and (3.36) and is

$$D(\Delta e_{ij}^{p}) = k \sqrt{2\ \Delta e_{ij}^{p}\ \Delta e_{ij}^{p}} \quad . \qquad (3.46)$$

Note that the tensors e_{ij} and s_{ij} may also be written in vector form as $\underset{\sim}{e}$ and $\underset{\sim}{s}$ respectively. Using this notation the incremental problem described by equation (3.14) can be rewritten as :

$$\underline{K}\Delta\underline{u}_n + \underline{L}\Delta\underline{e}^p_n = \underline{P}_n - \underline{K}\,\underline{u}_{n-1} - \underline{L}\,\underline{e}^{p(n-1)} \qquad (3.47a)$$

$$\underline{L}^T\Delta\underline{u}_n + \underline{H}\Delta\underline{e}^p_n + \left(\frac{\partial D}{\partial \Delta \underline{e}^p}\right)\Bigg|_{\Delta\underline{e}^{pn}} = -\underline{L}^T\,\underline{u}_{n-1} - \underline{H}\,\underline{e}^{p(n-1)} \quad . \qquad (3.47b)$$

3.8 EVALUATION OF PREDICTORS

In this section we wish to investigate certain aspects of four different predictors in the Newton-Raphson procedure described earlier. We are concerned mainly with the term $I_2 = -\hat{\Delta\underline{u}}\,\underline{R}^{i+1}$ for evaluating the performance of each predictor. In every case, for the first iteration $i = 1$ of an increment n, the elastic stiffness will be used. We write

$$e^{*(i)} = (\tfrac{1}{2}\,(e_{ij}^{n(i)} - e_{ij}^{p(n-1)})(e_{ij}^{n(i)} - e_{ij}^{p(n-1)}))^{\frac{1}{2}} \quad ,$$

and hence we define

$$A^{(i)} = \frac{k}{2Ge^{*(i)}} \quad . \qquad (3.48)$$

Equation (3.43b) can now be rewritten as

$$s_{ij}^{n(i)} = A^{(i)}\,2G(e_{ij}^{n(i)} - e_{ij}^{p(n-1)}) \qquad (3.49a)$$

$$\Delta e_{ij}^{pn} = (1 - A^{(i)})(e_{ij}^{\hat{p}(i)} - e_{ij}^{p(n-1)}) \qquad (3.49b)$$

We also define the strain displacement matrices $\underline{B}^D$ and $\underline{B}^V$ as

$$\underline{e} = \underline{B}^D\,\underline{u} \qquad (3.50a)$$

and $$\epsilon_V = \underline{B}^V\,\underline{u} \quad . \qquad (3.50b)$$

We note that

$$\underline{K} = \underline{B}^T \underline{D} \underline{B} = \underline{B}^{D^T} \underline{D} \underline{B}^D + \underline{B}^{V^T} \underline{D} \underline{B}^V \quad . \tag{3.51}$$

The change in plastic strain within each iteration is

$$\begin{aligned} \Delta\hat{\underline{e}}^p &= \Delta\underline{e}^{p(i+1)} - \Delta\underline{e}^{p(i)} \qquad (3.52) \\ &= (1 - A^{(i+1)})\, \underline{B}^D\, \Delta\hat{\underline{u}} + (A^{(i)} - A^{(i+1)})(\underline{B}^D\, \underline{u}^{(i)} - \underline{e}^{p(n-1)}) \\ &= (1 - A^{(i)})\, \underline{B}^D\, \Delta\hat{\underline{u}} + (A^{(i)} - A^{(i+1)})(\underline{B}^D\, \underline{u}^{(i+1)} - \underline{e}^{p(n-1)}) \quad , \end{aligned}$$

and these relations are independent of the predictor used.

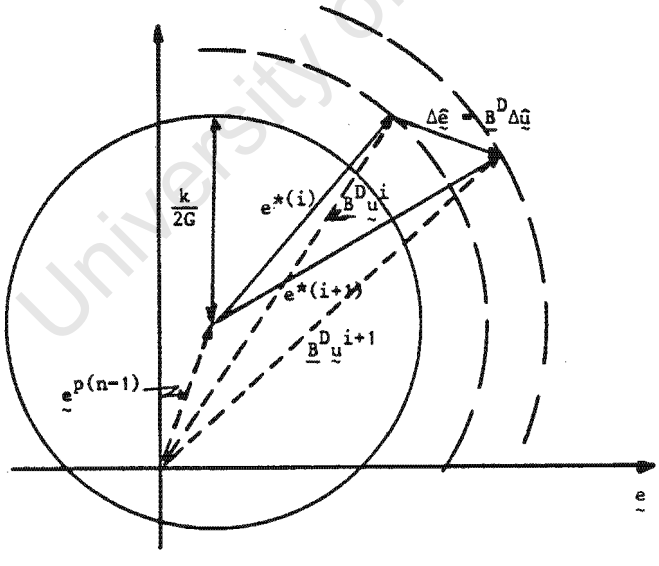

Figure 3.4 : Typical strain quantities for two sucessive iterations.

The terms of equation (3.52), geometrically represented in deviator strain space, are shown in Fig. 3.4.

Consider the arbitrary predictor $\underset{\sim}{K}^*$, and let the displacement increment for the iteration be related to the residual at the end of the previous iteration by

$$\underset{\sim}{K}^* \, \Delta\hat{\underset{\sim}{u}} = \underset{\sim}{R}^i \quad . \tag{3.53}$$

It follows from equation (3.24) that

$$\underset{\sim}{R}^{i+1} = \underset{\sim}{R}^i - \underset{\sim}{K} \, \Delta\hat{\underset{\sim}{u}} - \underset{\sim}{L} \, \Delta\hat{\underset{\sim}{e}}^p \quad , \tag{3.54}$$

and by substituting in equation (3.53),

$$\underset{\sim}{R}^{i+1} = (\underset{\sim}{K}^* - \underset{\sim}{K})\Delta\hat{\underset{\sim}{u}} - \underset{\sim}{L} \, \Delta\hat{\underset{\sim}{e}}^p \quad . \tag{3.55}$$

The above relations are diagramatically presented in Fig. 3.5 .

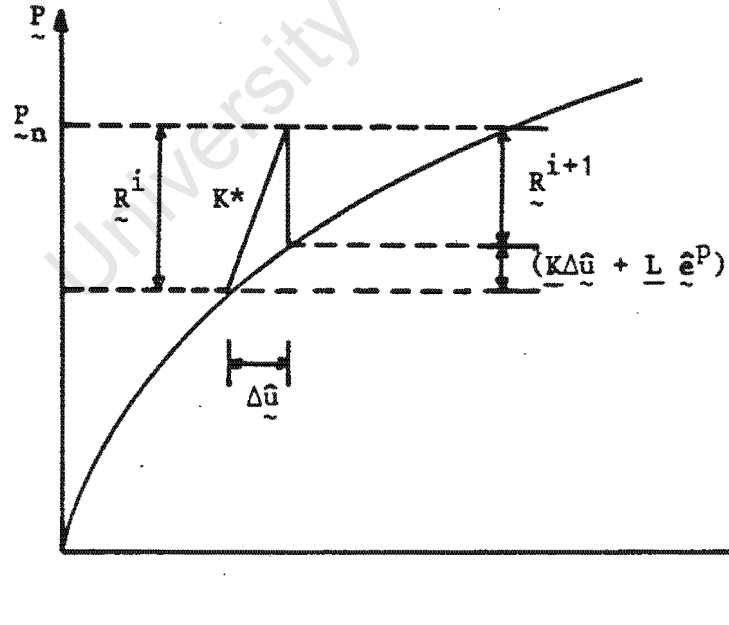

Figure 3.5 : Load vs displacement for a typical iteration.

We will now discuss various predictors. In each case, the predictor at the beginning of the first iteration will be the elastic predictor $\underset{\sim}{K}$. For the

second and third iterations $\underline{K}^*$ may depend on the stress or strain state at the end of the previous iteration. The tangent stiffness as described in equation (3.23) will not be considered here.

3.8.1 The Elastic Stiffness Predictor (Initial Stiffness Method)

For this method we set $\underline{K}^* = \underline{K}$. It follows that

$$\underline{R}^{i+1} = (- \underline{L}\, \Delta\hat{\underline{e}}^p) \quad , \tag{3.56}$$

and equation (3.23) becomes

$$I_2 = - \Delta\hat{\underline{u}}\, \underline{R}^{i+1} = \Delta\hat{\underline{u}}^T(\underline{L}\, \Delta\hat{\underline{e}}^p) \quad , \tag{3.57}$$

which in expanded form is

$$I_2 = \Delta\hat{\underline{u}}^T \underline{B}^{D^T} \underline{D}\left[(1 - A^{(i+1)})\underline{B}^D \Delta\hat{\underline{u}} + (A^{(i)} - A^{(i+1)})(\underline{B}^D \underline{u}^i - \underline{e}^{p(n-1)})\right] \tag{3.58a}$$

$$= \Delta\hat{\underline{u}}^T \underline{B}^{D^T} \underline{D}\left[(1 - A^{(i)})\underline{B}^D \Delta\hat{\underline{u}} + (A^{(i)} - A^{(i+1)})(\underline{B}^D \underline{u}^{i+1} - \underline{e}^{p(n-1)})\right] . \tag{3.58b}$$

When referring to Fig. 3.4 in conjunction with equations (3.58), it becomes obvious that

$$I_2 < 0$$

irrespective of the sign of

$$(A^{(i+1)} - A^{(i)}) \quad .$$

It therefore follows from the argument presented in section (3.5) that by means of an elastic predictor one is guaranteed of improving the estimate of $\hat{U}^p$ in each iteration. A typical sequence of solutions is shown in Fig. 3.6.

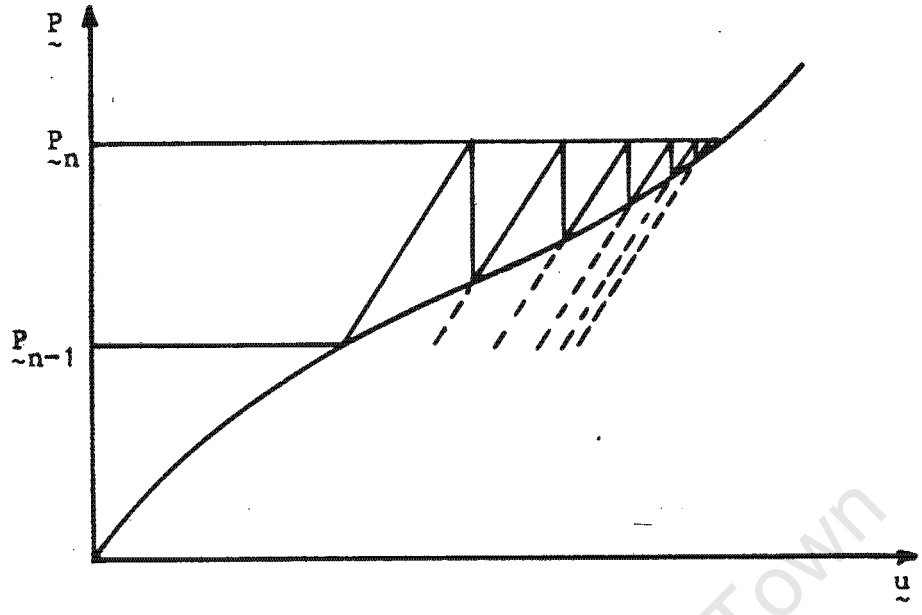

Figure 3.6 : Elastic stiffness predictor.

3.8.2 The Secant Stiffness Predictor

Under this heading we wish to discuss two separate secant predictors.

3.8.2.1 The "Total" Secant Stiffness For a problem with a single load increment this method corresponds to the direct iteration method [2]. The predictor is obtained by multiplying the shear modulus G at each integration point by the value $A^{(i)}$ from the previous iteration. We therefore set

$$\underset{\sim}{K}^{*} = A^{(i)} \underset{\sim}{B}^{D^T} \underset{\sim}{D} \underset{\sim}{B}^{D} + \underset{\sim}{B}^{V^T} \underset{\sim}{D} \underset{\sim}{B}^{V} \quad , \tag{3.59}$$

and equation (3.55) becomes

$$\begin{aligned} \underset{\sim}{R}^{i+1} &= \left[-(1 - A^{(i)}) \underset{\sim}{B}^{D^T} \underset{\sim}{D} \underset{\sim}{B}^{D} + (1 - A^{(i)}) \underset{\sim}{B}^{D^T} \underset{\sim}{D} \underset{\sim}{B}^{D}\right] \hat{\Delta \underset{\sim}{u}} \\ &\quad + (A^{(i)} - A^{(i+1)}) \underset{\sim}{B}^{D^T} \underset{\sim}{D} (\underset{\sim}{B}^{D} \underset{\sim}{u}^{i+1} - \hat{\underset{\sim}{e}}^{p(n-1)}) \\ &= (A^{(i)} - A^{(i+1)}) \underset{\sim}{B}^{D^T} \underset{\sim}{D} (\underset{\sim}{B}^{D} \underset{\sim}{u}^{i+1} - \hat{\underset{\sim}{e}}^{p(n-1)}) \quad . \end{aligned} \tag{3.60}$$

The result of substituting equation (3.60) into equation (3.23) is:

$$I_2 = - \Delta\hat{\underset{\sim}{u}}^T \underset{\sim}{B}^{D^T} (A^{(i)} - A^{(i+1)}) \underset{\sim}{D} (\underset{\sim}{B}^D \underset{\sim}{u}^{i+1} - \hat{\underset{\sim}{e}}^{p(n-1)}) \quad , \quad (3.61)$$

and it becomes evident from Fig. 3.4 that when

$$(A^{(i)} - A^{(i+1)}) > 0 \quad ,$$

I_2 is negative for all values of $\Delta\hat{\underset{\sim}{e}}^p$. However, when

$$(A^{(i+1)} - A^{(i)}) > 0 \quad ,$$

I_2 is negative only if the condition that the line between $\underset{\sim}{e}^{p(i)}$ and $\underset{\sim}{e}^{p(i+1)}$ does not cross the surface of radius $\frac{k}{2GA^{(i+1)}}$, holds. It is required that this condition be satisfied at each integration point.

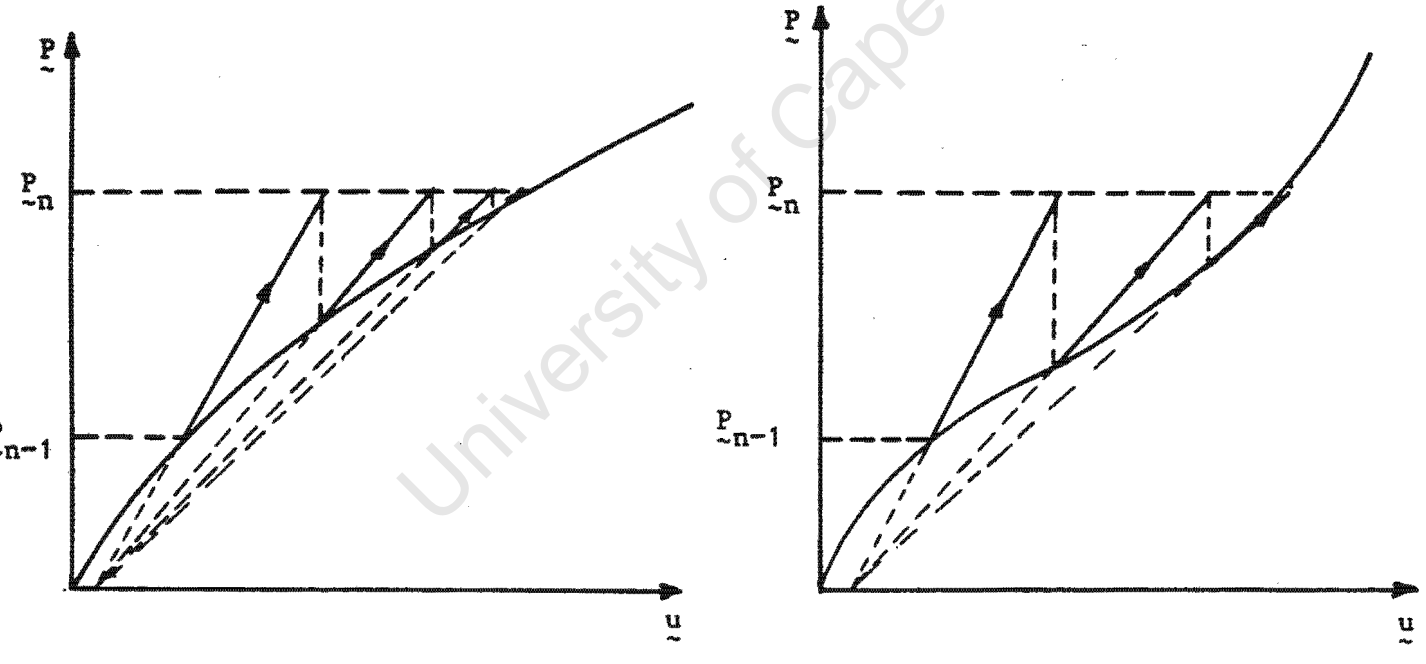

a) convergent b) possibly divergent

Figure 3.7 : The "total" secant stiffness.

A global condition for the negativity of I_2 is that if stiffening occurs in a structure, the degree of this stiffening remains below the calculated secant stiffness. This statement can be appreciated by referring to Fig. 3.7(b).

3.8.2.2 The "Incremental" Secant Stiffness In this case, the predictor is calculated by replacing $2G\,\delta_{ij}\delta_{kl}$ by $2G\left(\frac{\Delta s^i_{ij}}{\Delta e_{kl}}\right)$ in the construction of the $\underset{\sim}{D}$ matrix.

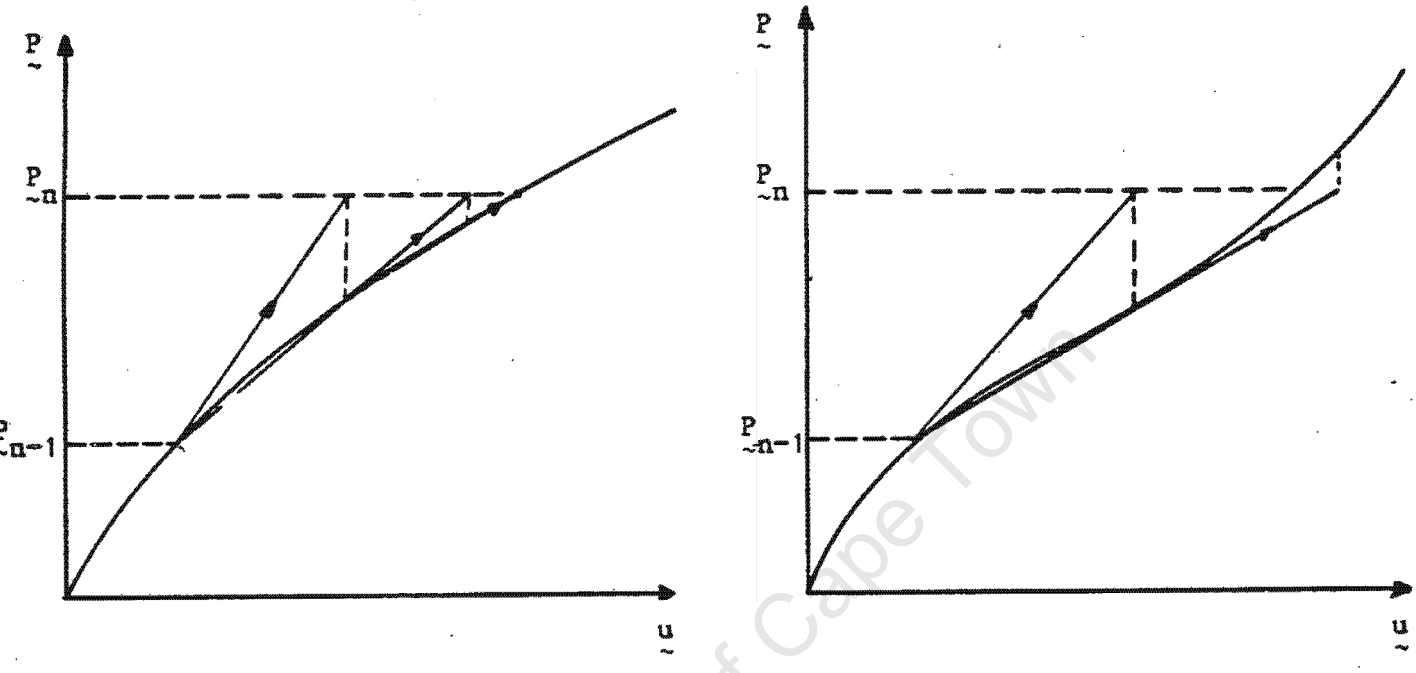

a) convergent b) possibly divergent

Figure 3.8 : The "incremental" secant stiffness.

For this predictor it is not possible to set up conditions for which contributions to I_2 from the individual integration points will be negative. It is evident from Fig. 3.8(b) however, that I_2 may well be non-negative if stiffening of the structure occurs within a time increment.

3.8.3 The "Consistent" Tangent Stiffness Predictor

In order to develop this predictor we refer to equations (3.18) and (3.21). Instead of writing equations (3.21) without updating the $\left(\frac{\partial D}{\partial \Delta \underset{\sim}{e}^p}\right)$ term, we write it in its updated form

$$\underline{L}^T \Delta \underline{u}_n^{i+1} + \underline{H} \Delta \underline{e}^{p(i+1)} + \left(\frac{\partial D}{\partial \Delta \underline{e}^p}\right)\Bigg|_{\Delta \underline{e}^{p(i+1)}} = - \underline{L}^T \underline{u}_{n-1} - \underline{H}\, \underline{e}^{p(n-1)} \quad . \tag{3.62}$$

By subtracting equation (3.18) from (3.62) we obtain

$$\underline{L}^T \Delta \hat{\underline{u}} + \underline{H} \Delta \hat{\underline{e}}^p = \left(\frac{\partial D}{\partial \Delta \underline{e}^p}\right)\Bigg|_{\Delta \underline{e}^{p(i)}} - \left(\frac{\partial D}{\partial \Delta \underline{e}^p}\right)\Bigg|_{\Delta \underline{e}^{p(i+1)}} , \tag{3.63}$$

and by expanding $\left(\frac{\partial D}{\partial \Delta \underline{e}^p}\right)\Big|_{\Delta \underline{e}^{p(i+1)}}$ as a Taylor's series about $\Delta e^{p(i)}$, we obtain

$$\left(\frac{\partial D}{\partial \Delta \underline{e}^p}\right)\Bigg|_{\Delta \underline{e}^{p(i+1)}} = \left(\frac{\partial D}{\partial \Delta e^p}\right)\Bigg|_{(\Delta \underline{e}^{p(i)} + \Delta \hat{\underline{e}}^p)}$$

$$= \left(\frac{\partial D}{\partial \Delta \underline{e}^p}\right)\Bigg|_{\Delta \underline{e}^{p(i)}} + \Delta \hat{\underline{e}}^p \frac{\partial}{\partial \Delta \underline{e}^p} \left(\frac{\partial D}{\partial \Delta \underline{e}^p}\right)\Bigg|_{\Delta \underline{e}^{p(i)}} \quad \ldots$$

$$\ldots + \sum_{m=2}^{\infty} \frac{1}{m} (\Delta \hat{\underline{e}}^p)^m \frac{\partial^m}{(\partial \Delta \underline{e}^p)^m} \left(\frac{\partial D}{\partial \Delta \underline{e}^p}\right)\Bigg|_{\Delta \underline{e}^{p(i)}} , \tag{3.64}$$

and hence equation (3.62) becomes

$$\underline{L}^T \Delta \hat{\underline{u}} + \underline{H} \Delta \hat{\underline{e}}^p = - \Delta \hat{\underline{e}}^p \frac{\partial}{\partial \Delta \underline{e}^p} \left(\frac{\partial D}{\partial \Delta \underline{e}^p}\right)\Bigg|_{\Delta \underline{e}^{p(i)}} - O\left[(\Delta \hat{\underline{e}}^p)^2\right] \quad . \tag{3.65}$$

Neglecting the terms $O\left[(\Delta \hat{\underline{e}}^p)^2\right]$, the change in plastic strains is

$$\Delta \hat{\underline{e}}^p = \left[\hat{\underline{H}} + \frac{\partial}{\partial \Delta \underline{e}^p} \left(\frac{\partial D}{\partial \Delta \underline{e}^p}\right)\Bigg|_{\Delta \underline{e}^{p(i)}}\right]^{-1} \hat{\underline{L}}^T \Delta \hat{\underline{u}} \quad . \tag{3.66}$$

Substituting equation (3.66) into equation (3.20) results in

$$\left\{\underset{\sim}{K} - \hat{\underset{\sim}{L}}\left[\hat{\underset{\sim}{H}} + \frac{\partial}{\partial \Delta \underset{\sim}{e}^{p}}\left(\frac{\partial D}{\partial \Delta \underset{\sim}{e}^{p}}\right)\Bigg|_{\Delta \underset{\sim}{e}^{p(i)}}\right]^{-1} \hat{\underset{\sim}{L}}^{T}\right\} \Delta \hat{\underset{\sim}{u}} = \underset{\sim}{R}^{i} \quad . \tag{3.67}$$

The carets indicate contributions from integration points where it is expected from the previous iteration that yield will occur. This matrix can easily be evaluated.

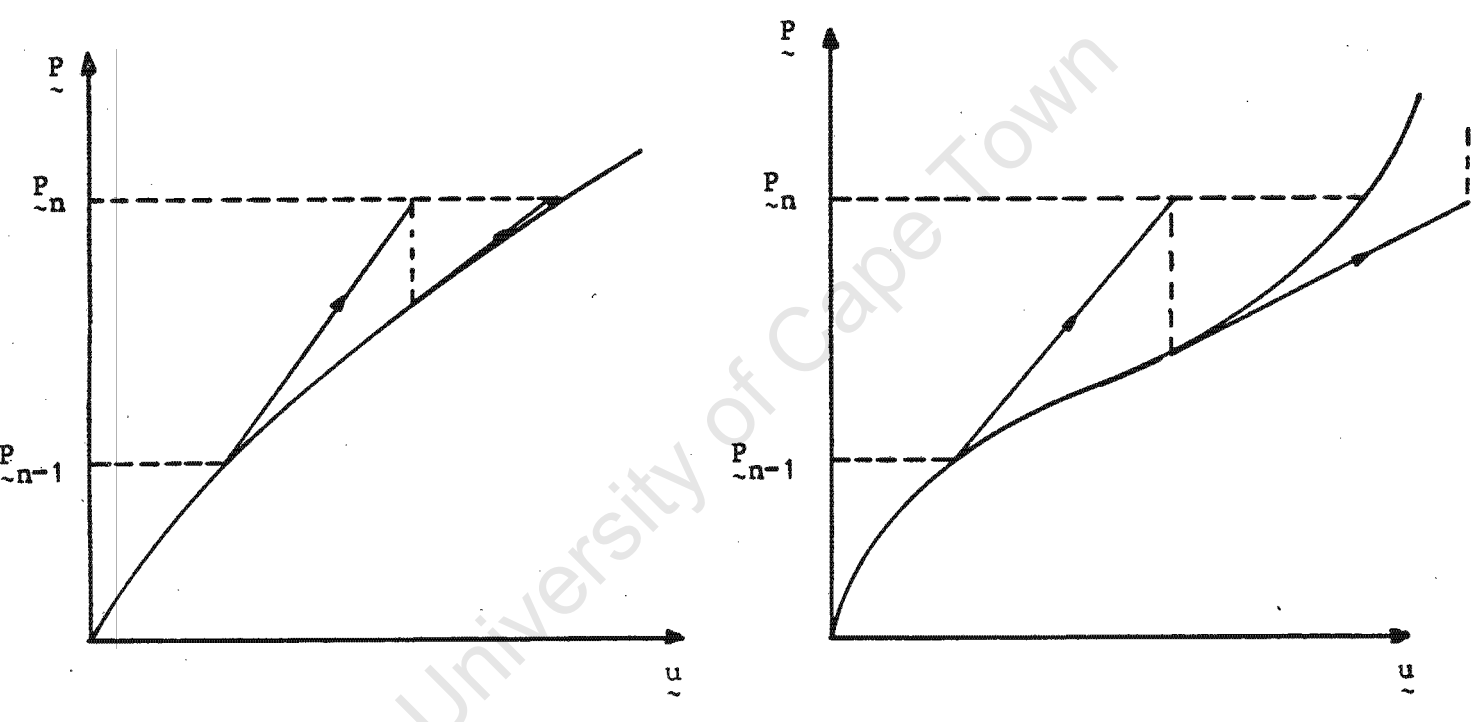

(a) Convergent (b) Possibly divergent

Figure 3.9 : The "Consistent" Tangent Predictor.

As in the case of the "incremental" secant predictor, the "consistent" tangent predictor will be used essentially for comparative purposes at this stage. It is evident from Fig. 3.9b that I_2 may be non-negative if stiffening of the structure occurs within a time increment.

3.8.4 NUMERICAL EXAMPLE

The above predictors have all been implemented in NOSTRUM [14], a general purpose finite element package for solving plane and axisymmetric problems. For the purpose of comparing convergence characteristics of the predictors described, we shall consider a simple example.

3.8.4.1 Thin plate made up of two materials The structure used for this illustration is depicted by Fig. 3.10. The inner core consists of an elastic, perfectly plastic material with a von Mises yield criterion, whereas the outer material is elastic. The material constants used for the problem are Young's modulus E = 1.0, Poisson's ratio ν = 0.3, and the uniaxial yield stress σ_y = 10.0 . The thickness of the plate is 0.1, and due to the symmetry of the problem only a quarter of the structure needs to be considered.

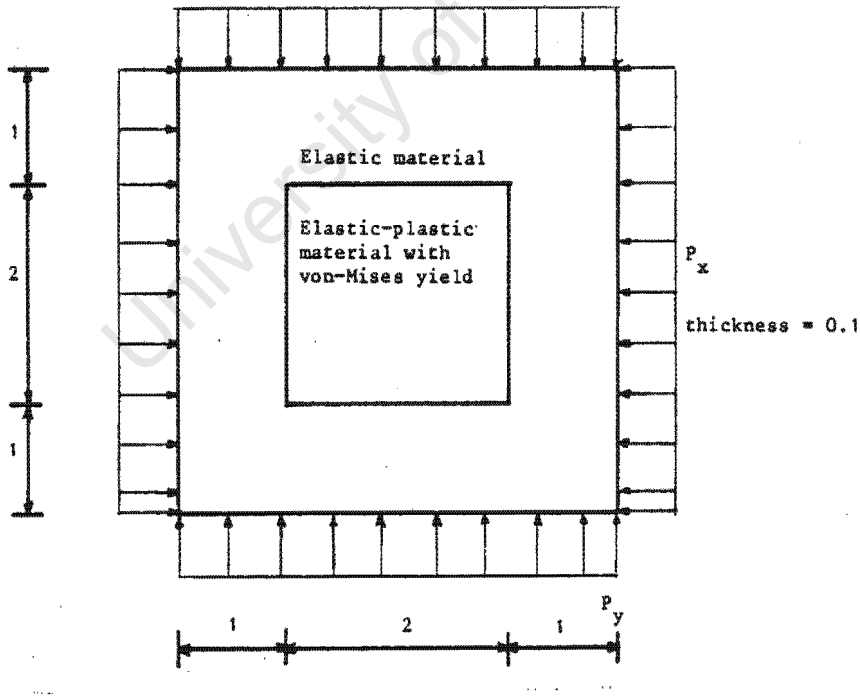

Figure 3.10 : Thin Plate with two materials.

The loads are applied in such a way that the initial yielding is uniaxial. These are then varied so that the stress point moves around the yield surface.

Fig. 3.11a and Fig 3.11b respectively, show the finite element model used in this example and the applied load path.

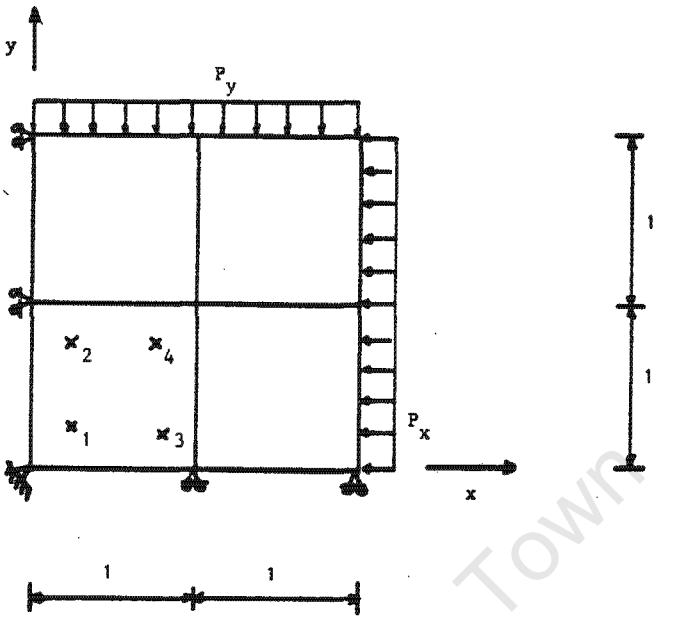

a: Finite element mesh.

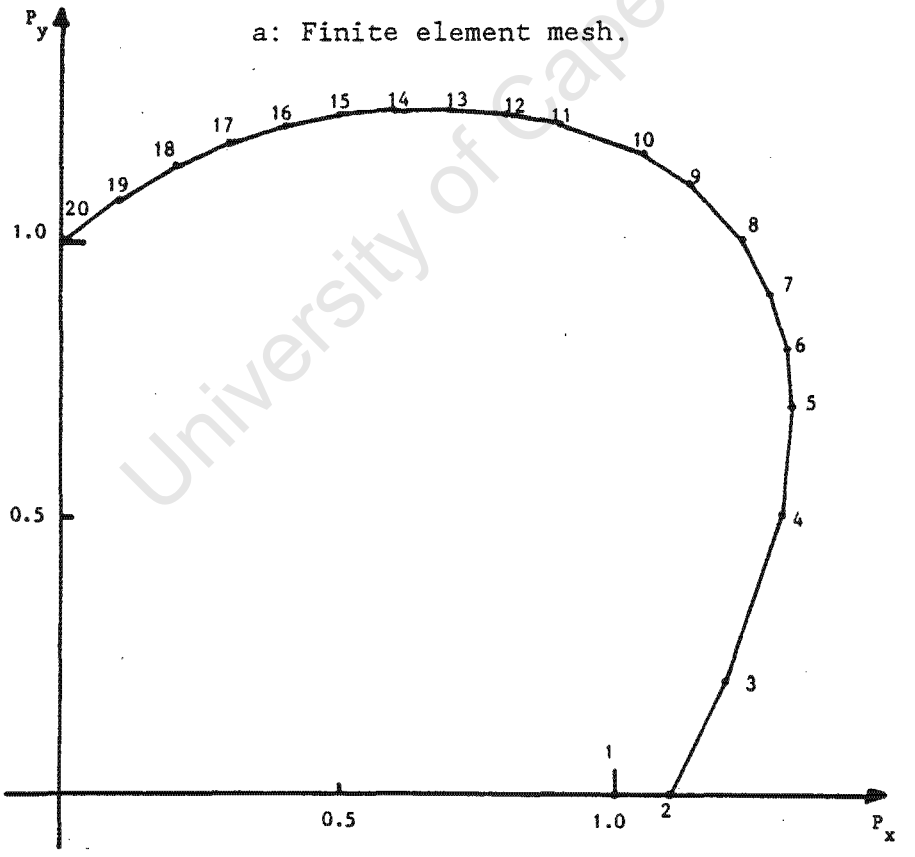

b: Load path.

Figure 3.11 :

Four noded plane stress elements are used with 2 X 2 Gaussian integration. The resulting stresses at integration point 1 (Fig 3.11a) are shown in Fig 3.12 .

These are superimposed on the locus of points given by the von Mises yield condition in plane stress space

$$\phi = \sigma_{11}^2 - \sigma_{11}\sigma_{22} + \sigma_{22}^2 + 3\sigma_{12}^2 - \sigma_y^2 = 0 \qquad (3.68)$$

with $\sigma_{12} = 0$. The calculated values of σ_{12} are not precisely zero, but the differences are so small that the points all appear to be on this yield surface.

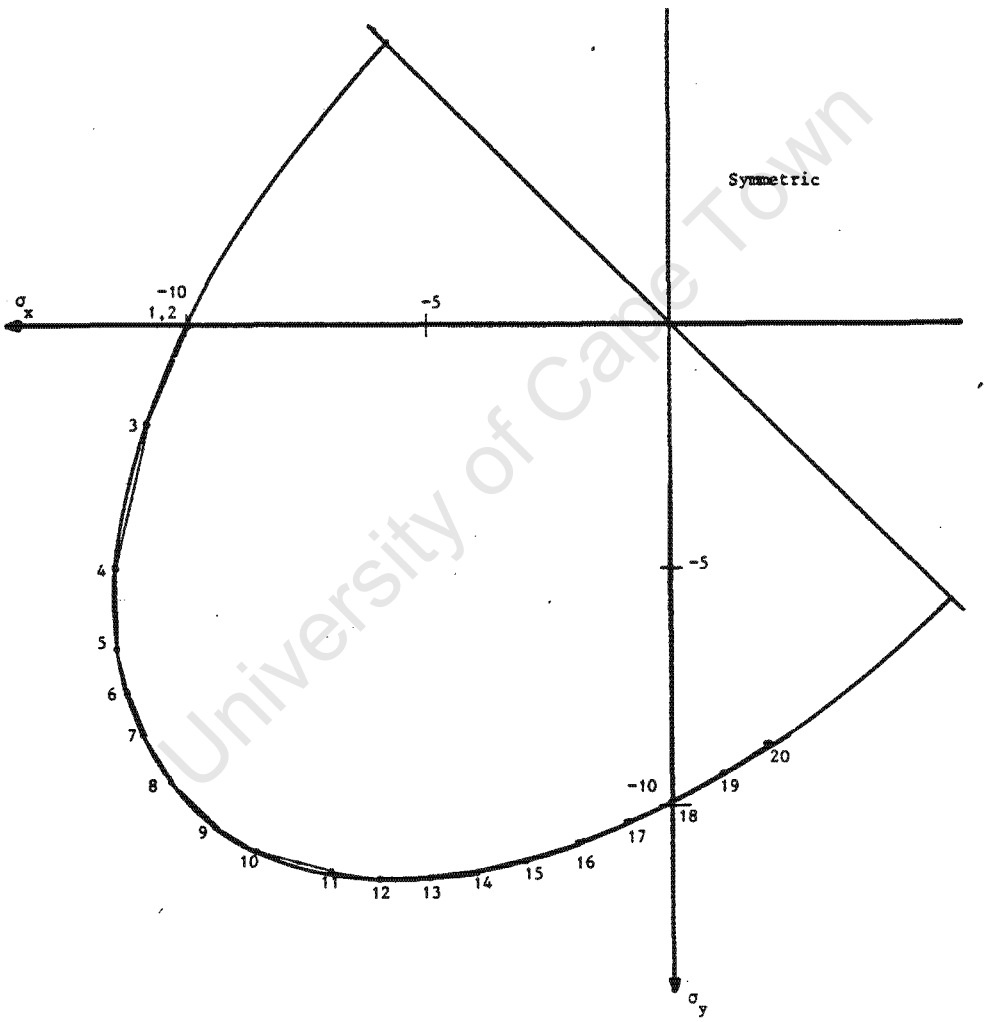

Figure 3.12: Stress history.

The results obtained with all four predictors are almost identical ; what does however vary is the number of iterations required to reach convergence. The value of I_2 and the convergence ratio (C.R.) at each iteration of the eighth

time increment (i.e. where P_x changes from 12.8 to 12.3 and P_y changes from 9.0 to 10.0) are tabulated below. The convergence ratio referred to is the ratio of the norm of the out of balance forces (residual forces) to the norm of the applied loads [3], and is given by

$$TOL = \frac{\| \underline{R}^{i+1} \|}{\| \underline{P}_n \|} \quad . \tag{3.69}$$

	Elastic		Total Secant		Incremental Secant		Consistent Tangent	
i	I_2	C.R.	I_2	C.R.	I_2	C.R.	I_2	C.R.
1	-0.00190	0.379	-0.00190	0.379	-0.00190	0.379	-0.00190	0.379
2	-0.00038	0.264	-0.00038	0.263	-0.00041	0.257	-0.00039	0.147
3	-0.00020	0.191	-0.00020	0.191	-0.00019	0.159	-0.00001	0.011
4	-0.00010	0.139	-0.00010	0.138	-0.00008	0.095	0	0.001
5	-0.00006	0.101	-0.00005	0.100	-0.00002	0.062		
6	-0.00002	0.074	-0.00003	0.072	-0.00001	0.041		
7	-0.00002	0.053	-0.00001	0.052	0	0.026		
8	-0.00001	0.039	-0.00001	0.038				
9	0	0.028	0	0.027				

Table 3.1: Values of I_2 and the convergence ratio for different predictors.

	Elastic		Total Secant		Incremental Secant		Consistent Tangent	
i	I_1	I	I_1	I	I_1	I	I_1	I
1	-0.30862	-0.31052	-0.30862	-0.31052	-0.30861	-0.31051	-0.30863	-0.31052
2	-0.00009	-0.00047	-0.00009	-0.00047	-0.00041	-0.00055	-0.00045	-0.00084
3	-0.00004	-0.00024	-0.00004	-0.00024	-0.00007	-0.00026	-0.00012	-0.00013
4	-0.00002	-0.00012	-0.00002	-0.00012	-0.00002	-0.00010	0	0
5	-0.00001	-0.00007	-0.00001	-0.00007	-0.00001	-0.00004		
6	-0.00001	-0.00003	-0.00001	-0.00004	-0.00001	-0.00002		
7	0	-0.00002	0	-0.00002	0	-0.00001		
8	0	-0.00001	0	-0.00001	0	0		
9	0	-0.00001	0	0				
10	0	0						
	$\Sigma I = -0.31149$		$\Sigma I = -0.31149$		$\Sigma I = -0.31149$		$\Sigma I = -0.31149$	

Table 3.2: Values of I_1 and I for the different predictors.

These results tabulated above show that the value of I_2 is generally negative. It is not evident from these tables that there is any difference between the results of the elastic predictor and the total secant predictor. This however,

is not normally the case and in general the number of iterations required to reach convergence is about 20% more when using an elastic predictor. Note that the total improvement (i.e. ΣI) is the same for all four the predictors. This is to be expected since the same functional is essentially being minimised in each case.

3.9 CONCLUSION

In this Chapter we have discussed the application of mathematical programming techniques to incremental elastic-plastic analysis. We have considered four different Newton-Raphson predictors in order to gain insight into the performance of these with respect to the convergence and the minimisation of the potential energy.

It is clear that when the elastic predictor is used throughout a time step, the algorithm is guaranteed to converge onto an existing solution. For the global secant predictor we have only managed to show conditional convergence at the integration point level, but in the following Chapter we will show that the convergence is unconditional.

For the "incremental" secant and the "consistent" tangent predictors we cannot show that the algorithms will converge. It does however appear that convergence is guaranteed if there is no local stiffening of the structure within an increment. These methods are more efficient, and the "consistent" predictor method in particular, yields a quadratic rate of convergence.

CHAPTER 4

THE SECANT APPROXIMATION FOR HOLONOMIC ELASTIC-PLASTIC INCREMENTAL ANALYSIS

4.1 INTRODUCTION

In this Chapter our objective is to develop an algorithm for the numerical solution of static incremental problems for elastic, perfectly plastic materials with a von Mises yield condition. The algorithm iterates on the secant shear modulus, and at the end of each iteration equilibrium is satisfied, but the yield condition may be violated. The algorithm is closely related to the Newton-Raphson method with the "total" secant predictor ; this relationship will be shown.

It is assumed that the strain follows a minimum work path which can be associated with a potential function. In the previous Chapter it was assumed that the internal variable followed a straight line path which is, by implication, a minimum work path in internal variable space. Another important feature of the algorithm is that it is guaranteed to converge, and proof of this will be given. The algorithm is also extended to include both linear isotropic and linear kinematic hardening. A potential function for the Drucker-Prager yield condition is set up, and proof of the convergence for the resulting algorithm is presented.

Although the algorithm may not be very efficient, it does have several advantages which may make it attractive as a means of finding comparison solutions for general purpose packages. Convergence does not depend on the

size of load increment, or on the degree of unloading which takes place. The algorithm can easily be implemented in a program capable of performing elastic analyses with arbitrarily imposed inelastic strains.

4.2 CONSTITUTIVE MODEL FOR THE ELASTIC, PERFECTLY PLASTIC VON MISES MATERIAL

We will consider the constitutive relations developed in Section 3.7. It is assumed that the strain follows a minimum work path in strain deviator space, and can thus be associated with a potential function. This is evident from the fact that equations (3.43) can be written in the form

$$s_{ij}^{n} = \left(\frac{\partial W^{*}}{\partial e_{ij}^{n}}\right) , \tag{4.1a}$$

where

$$W^{*} = G(e_{ij}^{n} - e_{ij}^{p(n-1)})(e_{ij}^{n} - e_{ij}^{p(n-1)}) \qquad \text{for } e^{*} \leq \frac{k}{2G} , \tag{4.1b}$$

$$W^{*} = 2k\,(\tfrac{1}{2}\,(e_{ij}^{n} - e_{ij}^{p(n-1)})(e_{ij}^{n} - e_{ij}^{p(n-1)}))^{\frac{1}{2}} - \frac{k^{2}}{2G} \qquad \text{for } e^{*} > \frac{k}{2G} . \tag{4.1c}$$

A question concerning the convergence of a sequence of minimum work paths onto a continuous solution now arises. Let us consider a strain history $\epsilon_{ij}(t)$, $0 \leq t \leq T$. If we were to solve the rate equations for the perfectly plastic material exactly, we would compute the associated stress history $\sigma_{ij}(t)$ and the plastic strain history $e_{ij}^{p}(t)$. We may subdivide the time interval into m steps as shown in Fig. 4.1 below, and compute the stress and plastic strain at the end of each increment by means of equations (3.43) - (3.45). It becomes clear that as $m \to \infty$, the sequence of stress and plastic strain computed will converge onto $\sigma_{ij}(t)$ and $e_{ij}^{p}(t)$.

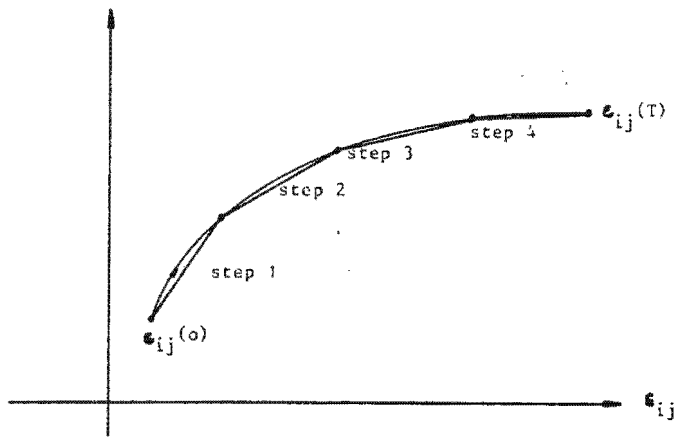

Figure 4.1 : Piecewise approximation to a continuous strain path.

4.3 MINIMUM PRINCIPLE FOR THE INCREMENTAL PROBLEM

We will formulate the incremental problem in continuum terms. Let us consider a body of volume V and surface S and assume, for the sake of simplicity, that the displacements are zero on part of the surface S_u . The body is subjected to a history of surface tractions $T_i(x_i,t)$, $0 \leq t \leq T$, on the remainder of the surface S_T . The material is assumed to be elastic, perfectly plastic with a von Mises yield condition. Our aim is to compute the history of displacements $u_i(x_i,t)$, stresses $\sigma_{ij}(x_i,t)$, and strains $\epsilon_{ij}(x_i,t)$. The problem is taken to be static and hence independent of time. The parameter t simply measures the order of events.

We treat the problem as incremental and divide the interval [0,T] into m sub-intervals. The n-th interval extends from t_{n-1} to t_n and the tractions change from $T_i^{n-1}(x_i)$ to $T_i^n(x_i)$. We assume that the solution is known at t_{n-1} so that $u_i^{n-1}(x_i)$, $T_i^{n-1}(x_i)$, $\sigma_i^{n-1}(x_i)$, $\epsilon_{ij}^{n-1}(x_i)$, and $e_{ij}^{p(n-1)}(x_i)$ are given. The solution at t_n is denoted by $u_i^n(x_i)$, $\sigma_{ij}^n(x_i)$, and $\epsilon_{ij}^n(x_i)$. The plastic strain increment $\Delta e_{ij}^p(x_i)$ must also be computed in order to update $e_{ij}^{p(n-1)}(x_i)$ for the next increment. The constitutive relations which govern at time t_n are given by equations (3.43) - (3.45). The equilibrium and compatibility equations which must be satisfied at t_n are

$$\frac{\partial \sigma_{ij}^{n}}{\partial x_j} = 0 \quad \text{on } V \quad , \tag{4.2a}$$

$$\sigma_{ij}^{n} \nu_i = T_j^{n} \quad \text{on } S_T \quad , \tag{4.2b}$$

$$\epsilon_{ij}^{n} = \tfrac{1}{2}\left[\frac{\partial u_i^{n}}{\partial x_j} + \frac{\partial u_j^{n}}{\partial x_i}\right] \quad , \tag{4.2c}$$

where ν_i is the outward normal vector on S. In the case where $m = 1$ this problem becomes the classical deformation theory problem. The more general case where $m > 1$ leads to a generic problem in each increment which has the same characteristics as the deformation theory problem. It is effectively equivalent to a problem of nonlinear elasticity, the solution of which can be written in terms of a minimum principle. The solution is given by the least value of

$$U^{*} = \int_V W(\epsilon_{ij}^{n})\, dV - \int_{S_T} T_i^{n} u_i^{n}\, dS \tag{4.3}$$

subject to equation (4.2c) and the condition that $u_i^{n} = 0$ on S_u. The strain energy function W consists of a volumetric component

$$W^{v} = \tfrac{1}{2} K(\epsilon_{kk}^{n})^2 \quad , \tag{4.4}$$

and the deviatoric component W^{*} (given in equation (4.1)). These components are related by the expression

$$W = W^{v} + W^{*} \quad . \tag{4.5}$$

It is evident that W , and hence U^* is convex and the condition that $\delta U^* = 0$ (i.e. U^*_{min}) yields equations (4.2a) and (4.2b). This general formulation does not place any restrictions upon the spacial variation of the potential function W .

4.4 SECANT ALGORITHM AND PROOF OF CONVERGENCE

We propose an iterative solution algorithm as a sequence of approximations to the deviatoric potential function W^*. The function W^* can be plotted against e^* (equation (3.42)) as shown in Fig. 4.2.

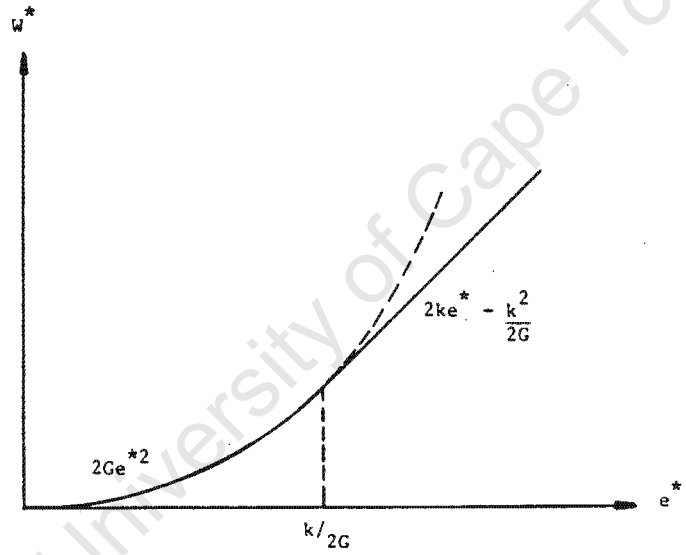

Figure 4.2 : Deviator potential function.

The potential has a parabolic central region bounded by $e^* = k/2G$ and is linear for $e^* > k/2G$. The derivative $\frac{dW^*}{\partial e^*}$ is continuous at $e^* = k/2G$.

For the first iteration we replace W^* by

$$W_1^* = G(e_{ij}^n - e_{ij}^{p(n-1)})(e_{ij}^n - e_{ij}^{p(n-1)}) \quad . \qquad (4.6)$$

This is identical to equation (4.1b), and implies that we use linear elastic relations. Putting

$$W_1 = W_1^* + W_1^v \quad , \tag{4.7}$$

we minimise

$$U_1 = \int_V W_1(\epsilon_{ij}^n)\, dV - \int_{S_T} u_i^n\, T_i^n\, dS \tag{4.8}$$

subject to equation (4.2c) and the condition that $u_i^n = 0$ on S_u. If we let the solution field be denoted by ${}^{(1)}\epsilon_{ij}^n$, ${}^{(1)}u_i^n$, we can define

$$U_1^{(1)} = \int_V W_1({}^{(1)}\epsilon_{ij}^n)\, dV - \int_{S_T} {}^{(1)}u_i^n\, T_i^n\, dS \tag{4.9a}$$

and

$$U^{*(1)} = \int_V W({}^{(1)}\epsilon_{ij}^n)\, dV - \int_{S_T} {}^{(1)}u_i^n\, T_i^n\, dS \quad , \tag{4.9b}$$

where U^* is previously given in equation (4.3). From the strict convexity of W^* it is evident that

$$W({}^{(1)}\epsilon_{ij}^n) \leq W_1({}^{(1)}\epsilon_{ij}^n) \quad , \tag{4.10a}$$

and hence that

$$U^{*(1)} \leq U_1^{(1)} \quad . \tag{4.10b}$$

In the second iteration we examine each material point in the body, and define a new deviatoric potential function W_2^* at each of these points.

If

$$e^{(1)} = e^*({}^{(1)}e^n_{ij}) \leq k/2G \quad ,$$

we put

$$W_2^* = G(e^n_{ij} - e^{p(n-1)}_{ij})(e^n_{ij} - e^{p(n-1)}_{ij}) \quad ; \qquad (4.11a)$$

whereas if

$$e^{(1)} = e^*({}^{(1)}e^n_{ij}) > k/2G \quad , \qquad (4.11b)$$

we put

$$W_2^* = \frac{k}{2e^{(1)}}(e^n_{ij} - e^{p(n-1)}_{ij})(e^n_{ij} - e^{p(n-1)}_{ij}) + (k\,e^{(1)} - \frac{k^2}{2G}) \quad .$$

In this process we fit a parabola W_2^* into the potential function W^* for material points where $e^{(1)} > k/2G$ as shown below in Fig. 4.3 .

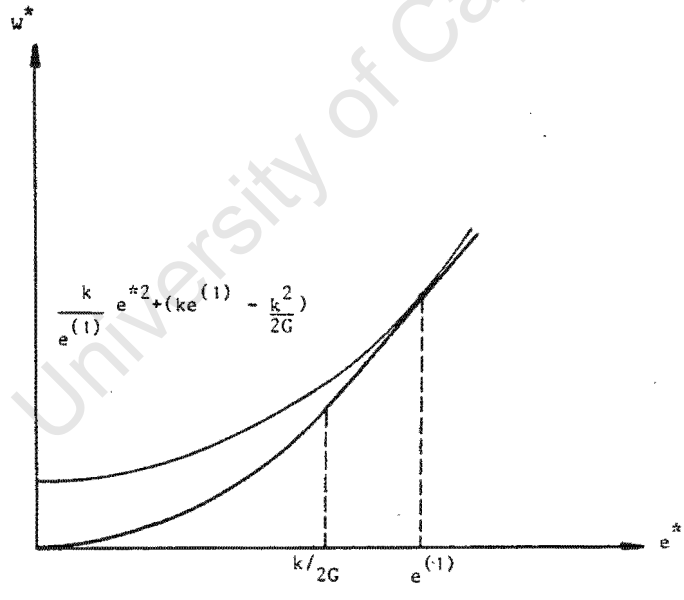

Figure 4.3 : Fit of a parabolic potential functional.

The parabola W_2^* touches W^* at $e^{(1)}$ with a common slope. It is evident from the diagram that in general

$$W^*(e_{ij}^n) \leq W_2^*(e_{ij}^n) \quad , \tag{4.12a}$$

and that in particular

$$W^*(^{(1)}e_{ij}^n) = W_2^*(^{(1)}e_{ij}^n) \quad . \tag{4.12b}$$

Putting

$$W_2 = W^v + W_2^* \quad , \tag{4.13}$$

we now minimise the quadratic functional

$$U_2 = \int_V W_2(\epsilon_{ij}^n)\, dV - \int_{S_T} u_i^n\, T_i^n\, dS \tag{4.14}$$

subject to equation (4.2c) and the condition that $u_i^n = 0$ on S_u . Let the solution be denoted by the fields $^{(2)}u_i^n$, $^{(2)}e_{ij}^n$. Given these fields, we can define

$$U_2^{(2)} = \int_V W_2(^{(2)}\epsilon_{ij}^n)\, dV - \int_{S_T} u_i^n\, T_i^n\, dS \tag{4.15a}$$

and

$$U^{*(2)} = \int_V W(^{(2)}\epsilon_{ij}^n)\, dV - \int_{S_T} u_i^n\, T_i^n\, dS \quad . \tag{4.15b}$$

From equation (4.12b) we know that

$$U_2(^{(1)}u_i^n\ ,\ ^{(1)}\epsilon_{ij}^n) = U^{*(1)} \quad , \tag{4.16a}$$

where $U^{*(1)}$ is given in equation (4.9b). Because we minimise the functional U_2 in order to find fields $^{(2)}u_i^n$, $^{(2)}\epsilon_{ij}^n$, we also know that

$$U_2^{(2)} \leq U_2(^{(1)}u_i^n\ ,\ ^{(1)}\epsilon_{ij}^n) \quad . \tag{4.16b}$$

Further, from equation (4.12a)

$$U^{*(2)} \leq U_2^{(2)} \quad . \tag{4.16c}$$

It then follows that

$$U^{*(2)} \leq U^{*(1)} \quad , \tag{4.17}$$

and hence the functional which we seek to minimise (equation (4.3)), decreases in the iteration. It can be seen from the strict convexity of the approximating potential functions W_2^* that the equality sign in equation (4.17) holds only if the least value of U^* has been achieved.

The third and subsequent iterations are carried out in the same way as the second iteration. At each iteration U^* is decreased and hence, since U^* is a convex function, the algorithm decreases onto the least value of U^* .

Each iteration in the algorithm involves the minimisation of a quadratic functional with equality constraints, and hence is equivalent to the solution of a linear problem. The deviator constitutive equations for any material point in the (j+1)-th iteration reduce very simply to

$$s_{ij}^n = 2G(e_{ij}^n - e_{ij}^{p(n-1)}) \qquad \text{for } e^{(j)} \leq k/2G \quad , \tag{4.18a}$$

$$s_{ij}^n = \frac{k}{e^{(1)}} (e_{ij}^n - e_{ij}^{p(n-1)}) \qquad \text{for } e^{(j)} > k/2G \quad , \tag{4.18b}$$

where

$$e^{(j)} = (\tfrac{1}{2} ({}^{(j)}e_{ij}^n - e_{ij}^{p(n-1)}) ({}^{(j)}e_{ij}^n - e_{ij}^{p(n-1)}))^{\frac{1}{2}} \quad . \tag{4.18c}$$

A comparison of equations (4.18) and (3.43) clearly shows the basis of the algorithm. The parameter

$$A^{(j)} = \frac{k}{2G\ e^{(j)}} \tag{4.19}$$

is set to unity for the first iteration and the iteration process continues until the improvement in the solution becomes less than some predetermined tolerance. Once this convergence criterion is satisfied, the plastic strain increments

$$\Delta e_{ij}^{n} = (1 - A)(e_{ij}^{n} - e_{ij}^{p(n-1)}) \tag{4.20}$$

are computed in readiness for the next load increment.

The convergence proof does not depend on the load step size, and is not affected by the direction of the load increment in the load space. In terms of the incremental elastic-plastic solution techniques presented in Chapter 3, the procedure described above is as follows : at the beginning of step n we know the value of the plastic strain from the previous increment $e_{ij}^{p(n-1)}$. Our aim is to determine Δe_{ij}^{p} and u_i^n and we do this by replacing $\underset{\sim}{\lambda}_n$ by $e_{ij}^{p(n-1)}$ in equation (3.12a). The term $e_{ij}^{p(n-1)}$ is treated as an imposed strain, and we solve for equation (3.12a) which is rewritten as

$$\begin{aligned} \underset{\sim}{K}\ \underset{\sim}{u}_n &= \underset{\sim}{P}_n - \underset{\sim}{L}\ \underset{\sim}{e}^{p(n-1)} \\ &= \underset{\sim}{P}_n - \underset{\sim}{P}^1 \quad , \end{aligned} \tag{4.21a}$$

where $\underset{\sim}{e}$ is the deviator strain tensor in vector notation.

Equilibrium will be satisfied, but the yield condition of equation (3.12b) may be violated. We substitute into this equation as follows :

$$\underline{L}^T \underline{u}_n + \underline{H}\, \underline{e}^{p(n-1)} = - \left(\frac{\partial D}{\partial \Delta \underline{e}^p}\right)\Bigg|_{\Delta \underline{e}^p} \qquad (4.21b)$$

thus obtaining the parameter $A^{(j)}$ described in equation (4.19). We multiply the shear modulus G by the value of $A^{(j)}$ obtained at each iteration point, and hence recompute $\underline{K}$, $\underline{L}$ and $\underline{H}$ in readiness for the next iteration. This iterative procedure continues until equation (4.21b) is satisfied. Note that the stiffness $\underline{K}$, evaluated for the "total" secant method in Chapter 3 is the same as $\underline{K}$ in equation (4.21a).

4.5 EXTENSION TO LINEAR ISOTROPIC AND KINEMATIC HARDENING

Up to now we have considered only an elastic, perfectly plastic material. The extension to isotropic and kinematic hardening materials for the case of a von Mises yield condition is straightforward. Without going into detail we will present the equivalent of equations (3.43) for the case of a linear isotropic and a linear kinematic hardening material. The tangent shear modulus is denoted by G_T during simple plastic shearing.

4.5.1 Linear isotropic hardening

The yield condition is given by

$$\phi = \tfrac{1}{2}\, s_{ij}\, s_{ij} - k^2 \quad , \quad k = k(\tfrac{1}{2}\, e^p_{ij}\, e^p_{ij}) \quad . \qquad (4.22)$$

In strain space the yield surface at the beginning of an increment is shown in Fig. 4.4 . The minimum work path from e^{n-1}_{ij} to e^n_{ij} is again sequential : the first part is purely elastic, the second part is in a direction normal to the yield surface. The second part in this case involves both elastic and plastic strain.

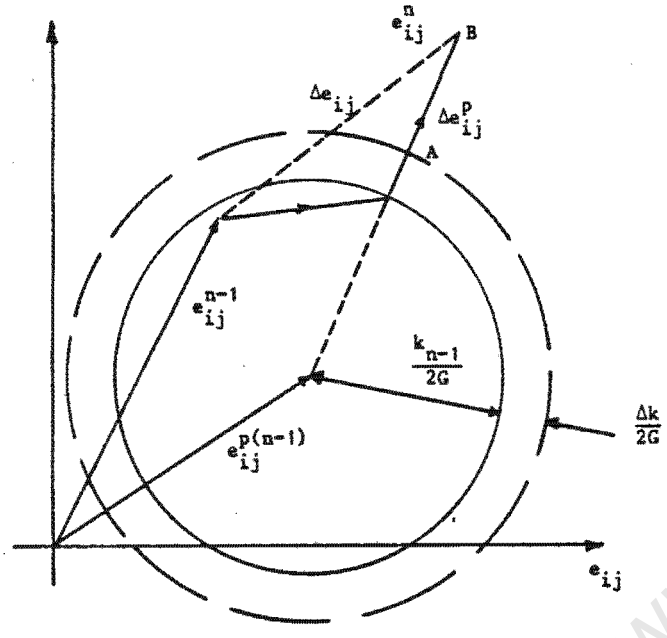

Figure 4.4 : Strain path for linear isotropic hardening.

The radius of the yield surface changes from $\frac{k_{n-1}}{2G}$ to $\frac{(k_{n-1} + \Delta k)}{2G}$. Plotting both yield surfaces with their centres at $e^{p(n-1)}_{ij}$, we can see from the diagram that the stress can be computed elastically from the strain point at A , while the change in plastic strain is represented by AB .

Conventional arguments show that

$$\frac{\Delta k}{2G} = \frac{G_T}{G} (e^* - \frac{k_{n-1}}{2G}) \quad , \qquad (4.23)$$

where e^* is defined by equation (3.42). The stress and plastic strain increment is either

$$\begin{aligned} s^n_{ij} &= 2G(e^n_{ij} - e^{p(n-1)}_{ij}) \\ \Delta e^p_{ij} &= 0 \\ \Delta k &= 0 \\ k_n &= k_{n-1} \qquad \text{for } e^* \leq \frac{k_{n-1}}{2G} \quad , \end{aligned} \qquad (4.24a)$$

or

$$s_{ij}^{n} = \frac{(k_{n-1} + \Delta k)}{2G\ e^{*}} \cdot 2G(e_{ij}^{n} - e_{ij}^{p(n-1)})$$

$$\Delta e_{ij}^{p} = \left[1 - \frac{(k_{n-1} + \Delta k)}{2G\ e^{*}}\right] \cdot (e_{ij}^{n} - e_{ij}^{p(n-1)})$$

$$\Delta k = 2G_{T}(e^{*} - \frac{k_{n-1}}{2G})$$

$$k_{n} = k_{n-1} + \Delta k \qquad \text{for } e^{*} > \frac{k_{n-1}}{2G} \quad . \qquad (4.24b)$$

The first two equations of (4.24b) can alternatively be written in terms of the shear moduli :

$$s_{ij}^{n} = \left\{\frac{G_{T}}{G} + \frac{k_{n-1}}{2G\ e^{*}}\left[1 - \frac{G_{T}}{G}\right]\right\} 2G\ (e_{ij}^{n} - e_{ij}^{p(n-1)})$$

$$\Delta e_{ij}^{p} = \left\{1 - \frac{k_{n-1}}{2G\ e^{*}}\left[1 - \frac{G_{T}}{G}\right]\right\} (e_{ij}^{n} - e_{ij}^{p(n-1)}) \quad . \qquad (4.25)$$

It can readily be seen that these equations reduce to equation (3.43) when $G_{T} = 0$. The deviator stresses can also be written in terms of the deviator potential as

$$s_{ij}^{n} = \frac{\partial W^{*}}{\partial e_{ij}^{n}} \quad , \qquad (4.26a)$$

where

$$W^{*} = G(e_{ij}^{n} - e_{ij}^{p(n-1)})(e_{ij}^{n} - e_{ij}^{p(n-1)}) \qquad \text{for } e^{*} \leq \frac{k_{n-1}}{2G} \quad , \qquad (4.26b)$$

$$W^{*} = 2k\left[1 - \frac{G_{T}}{G}\right]e^{*} + 2G_{T}\ e^{*2} - \frac{k^{2}}{2G}\left[1 - \frac{G_{T}}{G}\right] \qquad \text{for } e^{*} > \frac{k_{n-1}}{2G} \quad . \qquad (4.26c)$$

For implementing the algorithm we simply set

$$A^{(j)} = \frac{k_{n-1}}{2G\ e^{(j)}} + \frac{G_T}{G}\left[1 - \frac{k}{2G\ e^{(j)}}\right] \quad , \tag{4.27}$$

and equation (4.20) is replaced by

$$\Delta e^{p}_{ij} = (1 + \frac{G_T}{G} - A)(e^{n}_{ij} - e^{p(n-1)}_{ij}) \quad . \tag{4.28}$$

4.5.2 Linear Kinematic Hardening

For linear kinematic hardening, the radius of the yield surface remains fixed, but the centre does not coincide with $e^{p(n-1)}_{ij}$. We define the strain e^{o}_{ij} which defines the centre of the yield surface in strain space. It is also convenient to introduce a stress s^{o}_{ij}, given by

$$s^{o}_{ij} = 2G_T\ e^{o}_{ij} \quad . \tag{4.29}$$

From Fig. 4.5a we see that

$$s^{o}_{ij} = 2G(e^{o}_{ij} - e^{p(n-1)}_{ij}) \quad , \tag{4.30}$$

and hence it follows that

$$e^{o}_{ij} = \frac{G}{G - G_T}\ e^{p(n-1)}_{ij} \quad ,$$

$$s^{o}_{ij} = \frac{2G\ G_T}{G - G_T}\ e^{p(n-1)}_{ij} \quad . \tag{4.31}$$

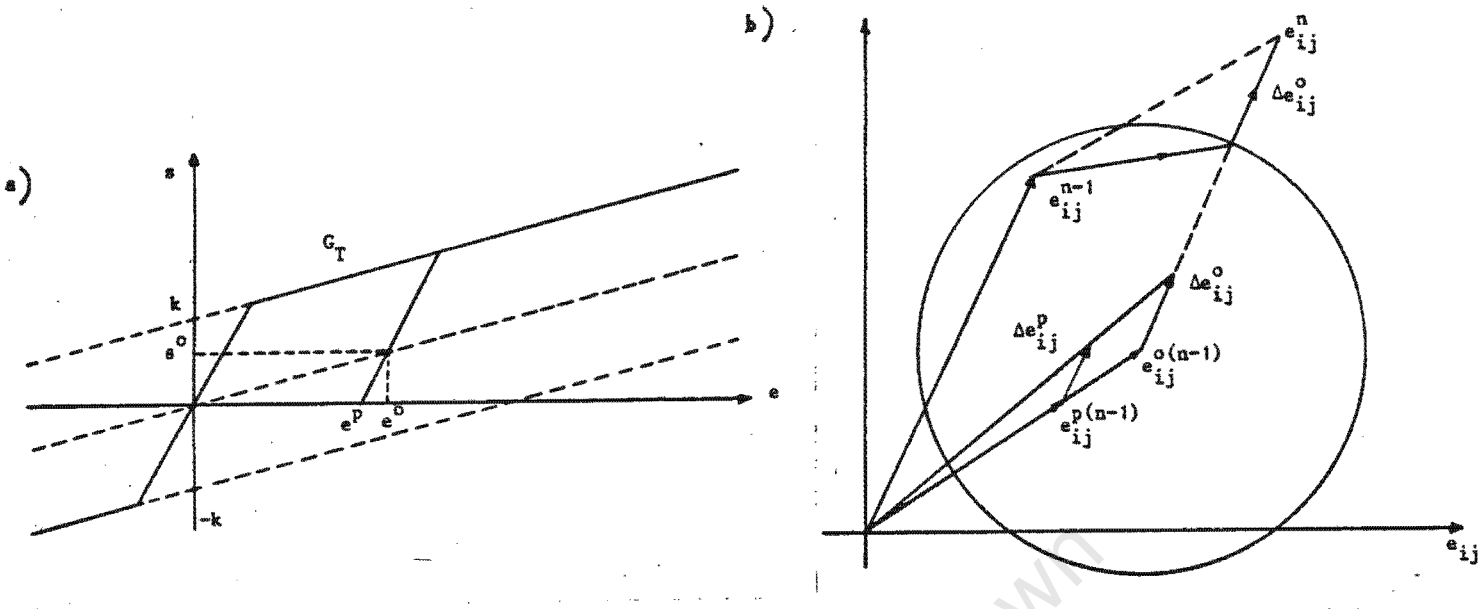

Figure 4.5 : Strain path for linear kinematic hardening.

The incremental work path is illustrated by Fig. 4.5b. At first the path is elastic; it is then normal to the yield surface, moving out along a line which is radial from $e^{o(n-1)}_{ij}$. We can see that

$$s^n_{ij} = s^{o(n-1)}_{ij} + 2G(e^n_{ij} - e^{o(n-1)}_{ij})$$
$$\Delta e^o_{ij} = 0 \qquad \text{for } e^{**} \leq \frac{k}{2G} \quad , \quad (4.32a)$$

and

$$s^n_{ij} = s^{o(n-1)}_{ij} + \frac{k}{2G\, e^{**}} = 2G(e^n_{ij} - e^{o(n-1)}_{ij})$$
$$\Delta e^o_{ij} = \left[1 - \frac{k}{2G\, e^{**}}\right](e^n_{ij} - e^{o(n-1)}_{ij}) \qquad \text{for } e^{**} > \frac{k}{2G} \quad , \quad (4.32b)$$

where

$$e^{**} = (\tfrac{1}{2}\,(e^n_{ij} - e^{o(n-1)}_{ij})(e^n_{ij} - e^{o(n-1)}_{ij}))^{\frac{1}{2}} \quad . \qquad (4.33)$$

The relationship between equations (4.32) and (4.33), and equations (3.42) and (3.43) can clearly be seen. Equations (4.32) reduce to equations (3.43) if $G_T = 0$.

A more convenient form of equations (4.32) may be achieved by using equations (4.31) to eliminate $e_{ij}^{o(n-1)}$ and $s_{ij}^{o(n-1)}$. Here we obtain

$$s_{ij}^{n} = 2G(e_{ij}^{n} - e_{ij}^{p(n-1)})$$
$$\Delta e_{ij}^{p} = 0 \qquad \text{for } e^{**} \leq \frac{k}{2G} \quad , \qquad (4.34a)$$

and

$$s_{ij}^{n} = \frac{k}{2G\, e^{**}} 2G \left[e_{ij}^{n} - \frac{G}{G - G_T} e_{ij}^{p(n-1)} \right] + \frac{2G\, G_T}{G - G_T} e_{ij}^{p(n-1)}$$
$$\Delta e_{ij}^{p} = \left[1 - \frac{k}{2G\, e^{**}} \right] \left[e_{ij}^{n} - \frac{G}{G - G_T} e_{ij}^{p(n-1)} \right]$$
$$\text{for } e^{**} > \frac{k}{2G} \quad . \qquad (4.34b)$$

Here we put

$$e^{**} = \tfrac{1}{2} \left\{ \left[e_{ij}^{n} - \frac{G}{G - G_T} e_{ij}^{p(n-1)} \right] \left[e_{ij}^{n} - \frac{G}{G - G_T} e_{ij}^{p(n-1)} \right] \right\}^{\frac{1}{2}} \quad . \qquad (4.35)$$

In implementing these relationships, we see that $A^{(j)}$ can be defined in the same way as in the perfectly plastic case with e^{**} replacing e^{*} . When $e^{**} > \frac{k}{2G}$ however, we must add a further term to the load vector to accommodate the "initial stress", $\frac{2G\, G_T}{G - G_T} e_{ij}^{p(n-1)}$.

4.6 CONVERSION TO A NEWTON-RAPHSON METHOD

We have briefly discussed the Newton-Raphson method which uses a "total" secant predictor and noted that the stiffness matrix is the same as the stiffness matrix used in the secant approximation method described above. In the latter case we are able to prove that the algorithm will always converge if a solution exists. We will now show how these algorithms are related.

We start by minimising the potential energy functional of equation (4.3), written loosely here as

$$U^* = \int_V W(\underline{\epsilon}^n)\, dV - \int_{S_T} \underline{T}^{n^T}\, \underline{u}^n\, dS \qquad (4.36)$$

in order to obtain the solution fields ${}^{(1)}\underline{u}^n$, ${}^{(1)}\underline{\epsilon}^n$. Using the constitutive and kinematic relations we can compute the corresponding stress field ${}^{(1)}\underline{\sigma}^n$, and internal force vector ${}^{(1)}\underline{X}^n$.

We write

$$\underline{T}^n = {}^{(1)}\underline{X} + {}^{(1)}\underline{r} \quad , \qquad (4.37a)$$

where $\underline{r}$ is the residual force vector, and we rewrite

$$\underline{\epsilon}^n = {}^{(1)}\underline{\epsilon} + \Delta\underline{\epsilon} \qquad (4.37b)$$

and

$$\underline{u}^n = {}^{(1)}\underline{u}^n + \Delta\underline{u} \quad . \qquad (4.37c)$$

Substituting these relations into equation (4.36), we obtain

$$\begin{aligned} U^* &= \int_V W({}^{(1)}\underline{\epsilon} + \Delta\underline{\epsilon})\, dV - \int_{S_T} ({}^{(1)}\underline{X} + {}^{(1)}\underline{r})^T({}^{(1)}\underline{u}^n + \Delta\underline{u})\, dS \\ &= \int_V W({}^{(1)}\underline{\epsilon} + \Delta\underline{\epsilon})\, dV - \int_{S_T} \underline{T}^T\, {}^{(1)}\underline{u}^n\, dS - \int_{S_T} {}^{(1)}\underline{X}^T\, \Delta\underline{u}\, dS \\ &\qquad - \int_{S_T} {}^{(1)}\underline{r}^T\, \Delta\underline{u}\, dS \end{aligned} \qquad (4.38)$$

If we write the first term in this expression as a Taylor's series expansion about $^{(1)}\underline{\epsilon}$, the result is

$$U^* = \int_V W(^{(1)}\underline{\epsilon})\, dV + \int_V \Delta\underline{\epsilon}\, \frac{\partial W(\underline{\epsilon})}{\partial \underline{\epsilon}}\bigg|_{(1)\underline{\epsilon}} dV + \int_V \tfrac{1}{2}\, \Delta\underline{\epsilon}^T \Delta\underline{\epsilon}\, \frac{\partial^2 W(\underline{\epsilon})}{\partial \underline{\epsilon}^T \partial \underline{\epsilon}}\bigg|_{(1)\underline{\epsilon}} dV \quad \ldots$$

$$\ldots + \int_V \sum_{m=3}^{\infty} \frac{1}{m!}\, \Delta\underline{\epsilon}^m\, \frac{\partial^m W(\underline{\epsilon})}{\partial \underline{\epsilon}^m}\bigg|_{(1)\underline{\epsilon}} dV - \int_{S_T} \underline{T}^{n^T}\, {}^{(1)}\underline{u}^n\, dS - \int_{S_T} {}^{(1)}\underline{X}^T\, \Delta\underline{u}\, dS$$

$$- \int_{S_T} {}^{(1)}\underline{r}^T\, \Delta\underline{u}\, dS \quad . \tag{4.39}$$

We write this expression as

$$U^* = U_a^* + U_b^* + U_c^* + U_d^* \tag{4.40}$$

where

$$U_a^* = \int_V W(^{(1)}\underline{\epsilon})\, dV - \int_{S_T} {}^{(1)}\underline{T}^{n^T}\, {}^{(1)}\underline{u}^n\, dS \quad ,$$

$$U_b^* = \int_V \Delta\underline{\epsilon}\, \frac{\partial W(\underline{\epsilon})}{\partial \underline{\epsilon}}\bigg|_{(1)\epsilon} dV - \int_{S_T} {}^{(1)}\underline{X}^T\, \Delta\underline{u}\, dS \quad ,$$

$$U_c^* = \int_V \tfrac{1}{2}\, \Delta\underline{\epsilon}^T \Delta\underline{\epsilon}\, \frac{\partial^2 W(\underline{\epsilon})}{\partial \underline{\epsilon}^T \partial \underline{\epsilon}}\bigg|_{(1)\underline{\epsilon}} dV - \int_{S_T} {}^{(1)}\underline{r}^T\, \Delta\underline{u}\, dS \quad ,$$

and

$$U_d^* = \int_V \sum_{m=3}^{\infty} \frac{1}{m!}\, \Delta\underline{\epsilon}^m\, \frac{\partial^m W(\underline{\epsilon})}{\partial \underline{\epsilon}^m}\bigg|_{(1)\underline{\epsilon}} dV \quad .$$

The term U_a^* is a constant, and it follows from the principle of virtual work that $U_b^* = 0$.

Let us consider the secant approximation in this context. At the beginning of the second iteration we are replacing $W^*(e_{ij})$ (equation (4.1)) with a parabola $W_2^*(e_{ij})$ (equation (4.11b)) so that

$$W^*(^{(1)}e_{ij}) = W_2^*(^{(1)}e_{ij})$$

and

$$\left.\frac{\partial W^*}{\partial e_{ij}}\right|_{(1)e_{ij}} = \left.\frac{\partial W_2^*}{\partial e_{ij}}\right|_{(1)e_{ij}} \quad . \tag{4.41}$$

It follows that

$$\left.\frac{\partial W\ (\underset{\sim}{\epsilon})}{\partial \underset{\sim}{\epsilon}}\right|_{(1)\underset{\sim}{\epsilon}} = \left.\frac{\partial W_2(\underset{\sim}{\epsilon})}{\partial \underset{\sim}{\epsilon}}\right|_{(1)\underset{\sim}{\epsilon}} ,$$

and hence $U_b^* = 0$ for this case as well. With $W_2(\underset{\sim}{\epsilon})$ being quadratic in $\underset{\sim}{\epsilon}$,

$$\frac{\partial^m W_2(\underset{\sim}{\epsilon})}{\partial \underset{\sim}{\epsilon}^m} = 0 \qquad \text{for } m \geq 3 \quad ,$$

and hence

$$U^* = U_a^* + \int \tfrac{1}{2}\, \Delta\underset{\sim}{\epsilon}^T \Delta\underset{\sim}{\epsilon}\, \left.\frac{\partial^2 W_2(\underset{\sim}{\epsilon})}{\partial \underset{\sim}{\epsilon}^T \partial \underset{\sim}{\epsilon}}\right|_{(1)\underset{\sim}{\epsilon}} dV - \int_{S_T} {}^{(1)}\underset{\sim}{r}^T\, \Delta\underset{\sim}{u}\, dS \quad .$$

For the minimisation of U^* , U_a^* may be neglected since it is a constant. It can thus readily be shown that the resulting equation for the iteration is

$$\underset{\sim}{K}^* \Delta\underset{\sim}{u} = \underset{\sim}{R}^i \quad , \tag{4.42}$$

where $\underset{\sim}{K}^*$ is the "total" secant stiffness matrix and $\underset{\sim}{R}^i$ is the residual out-of-balance load vector. The procedure is the same for subsequent iterations and is identical to the Newton-Raphson method with the "total" secant predictor as described in Section 3.8.2.1. Since proof exists for the convergence of the secant algorithm, it follows from the relationship above that the Newton-Raphson method is also guaranteed to converge.

4.7 NUMERICAL EXAMPLES FOR THE VON MISES YIELD CONDITION

In this section our first objective is to illustrate what happens when the number of subdivisions of the time interval under consideration is varied. Hereafter we proceed to solve a more practical problem.

4.7.1 Single Element Problem

Consider the single 8-noded plane stress element (Fig. 4.6a) subjected to the applied displacements Δx and Δy as shown in Fig. 4.6b . The analysis is done with 10, 20, and 40 subdivisions of the time domain. In each case 3x3 integration is used, and the results obtained for both stress and strain are compared to results obtained with ABAQUS [8] in Fig. 4.8(a-f). The strain histories for the three different numbers of subdivisions are compared in Fig. 4.7.

The difference between our results and those obtained with ABAQUS is due to the difference in integration algorithms ; this phenomenon has been discussed in some detail by Krieg and Krieg [15]. It can be seen that as the number of subdivisions increase the solution converges, and in the limiting case the exact solution would be obtained.

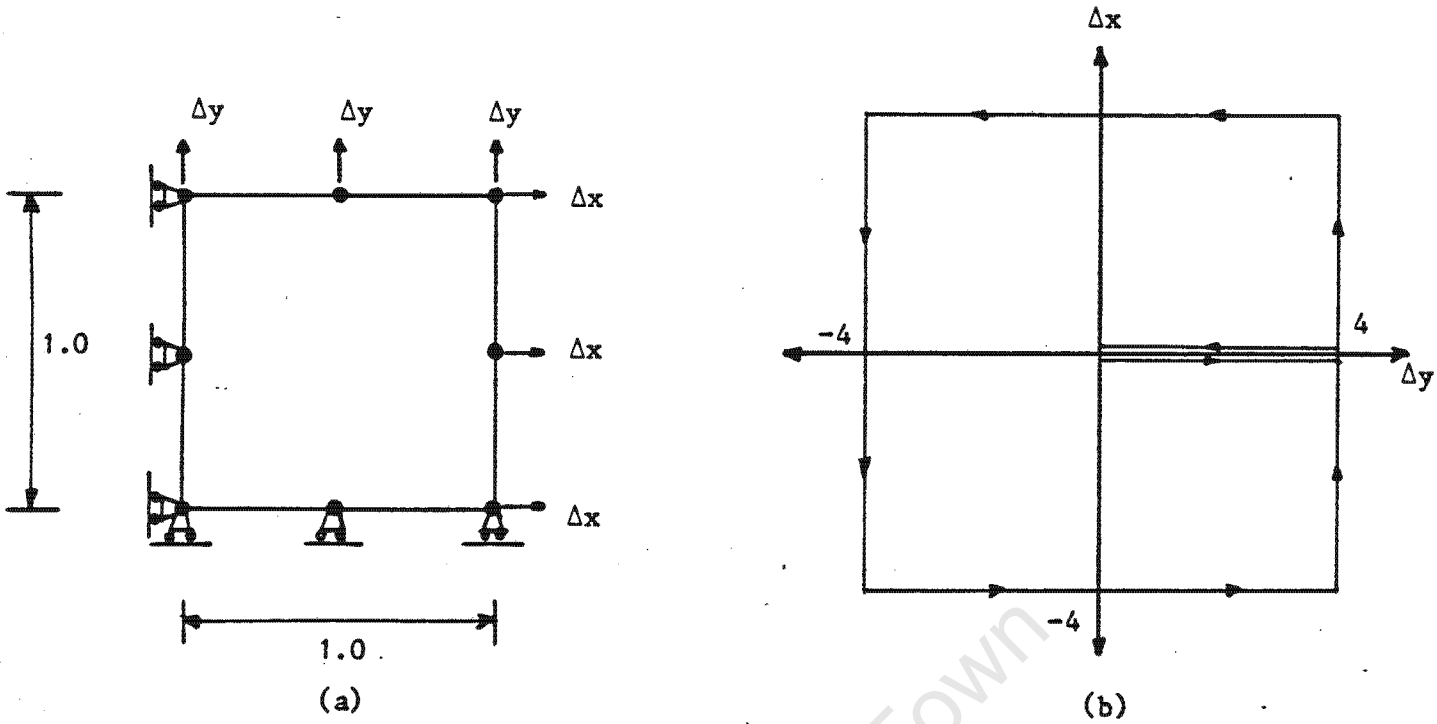

$E = 1.0$; $\nu = 0.3$; $H = 0.0$; $\sigma_y = 1.0$; $t = 1.0$

Figure 4.6 : Single element example.

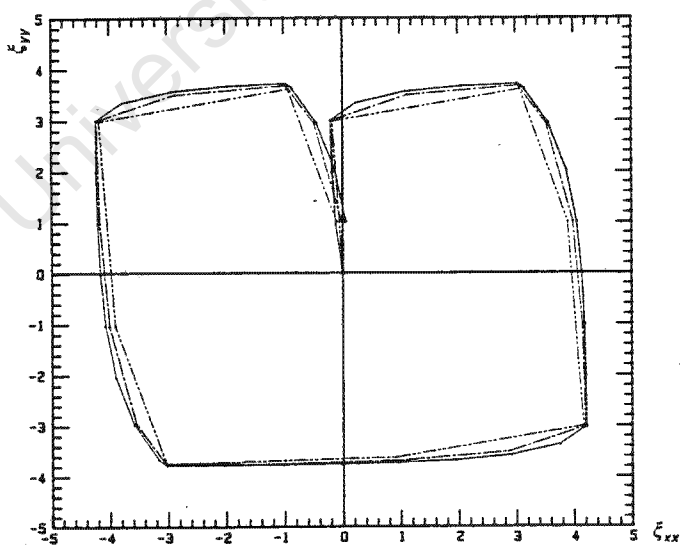

Figure 4.7 : Plastic strain histories for 10,20, and 40 increments.

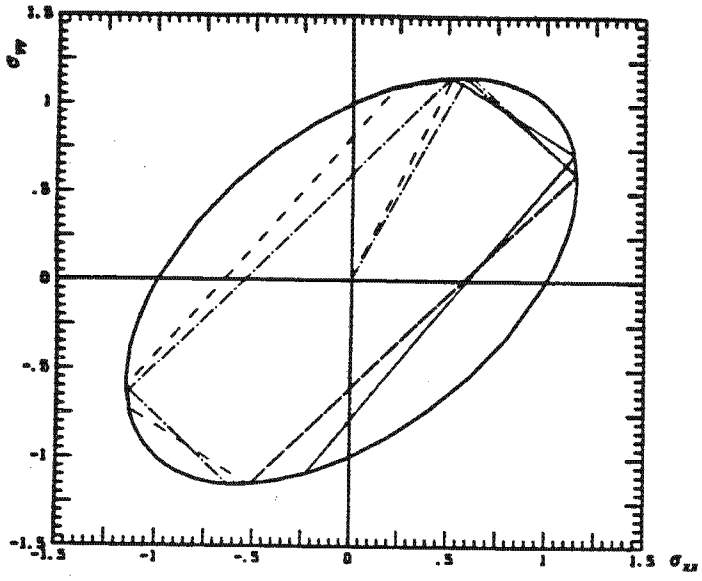

(a) Stress histories for 10 increments. ——, Yield surface; ——, secant; – – – –, ABAQUS

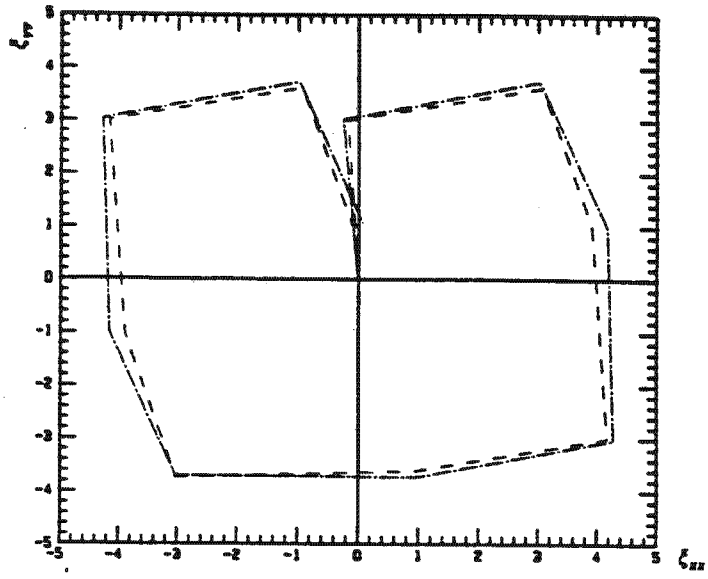

(b) Plastic strain histories for 10 increments. ——, Secant; – – – –, ABAQUS

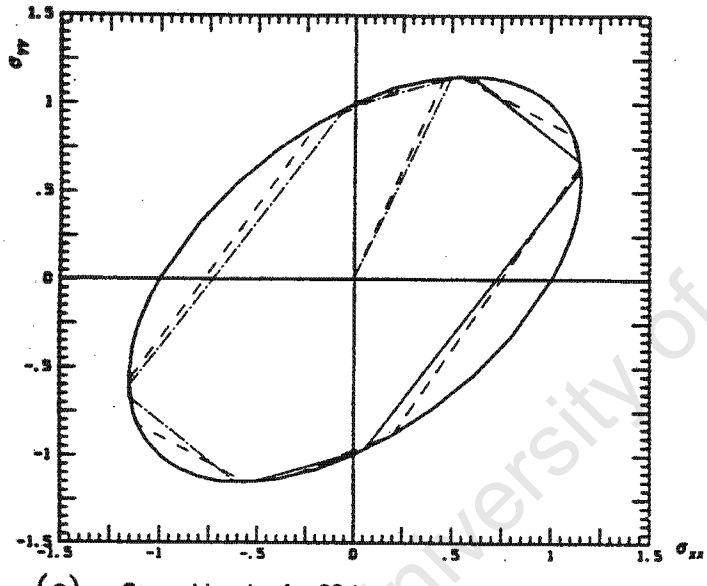

(c) Stress histories for 20 increments. ——, Yield surface;

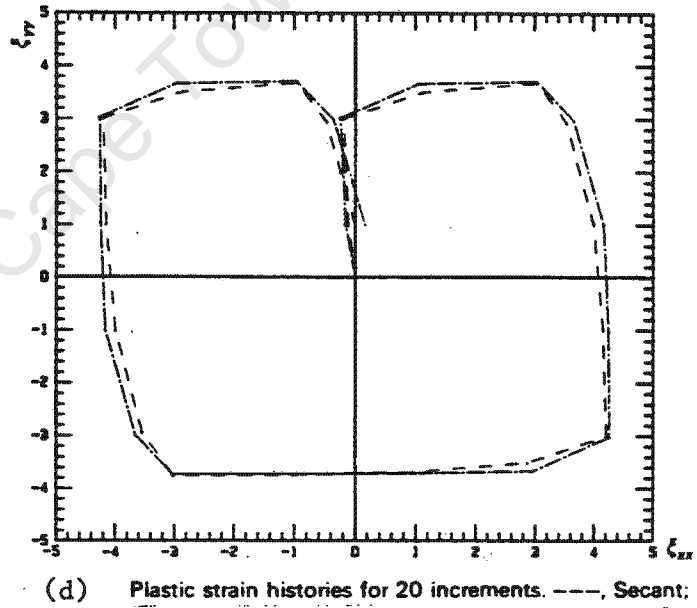

(d) Plastic strain histories for 20 increments. – – –, Secant;

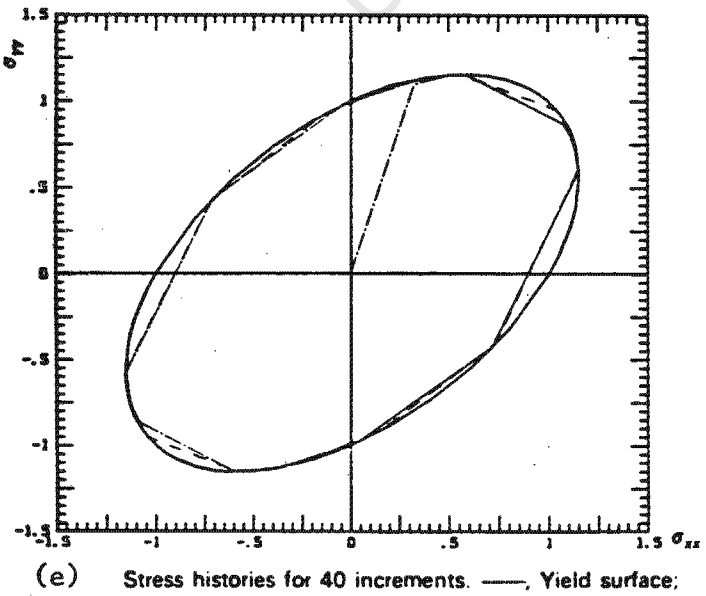

(e) Stress histories for 40 increments. ——, Yield surface;

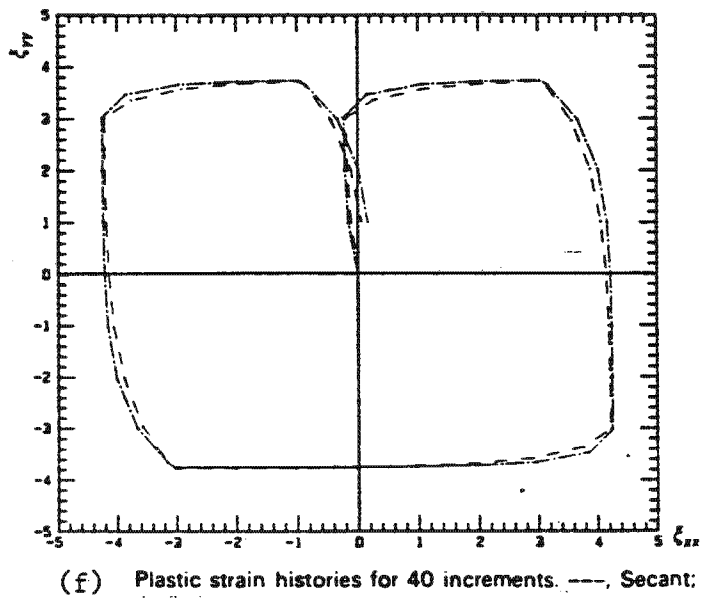

(f) Plastic strain histories for 40 increments. – – –, Secant;

Figure 4.8 : Stress and strain histories for single element problem.

4.7.2 Solution of Rachet Rates

In the nuclear industry, the walls of the pressure vessels are subjected to an extreme cyclic variation in temperature. Problems have been encountered in the past with the numerical modelling of this feature. We are concerned here essentially with the nature of the numerical problem and not with physical details. For illustration purposes we have considered a single (plane stress/strain) element problem where tractions are first applied and then held fixed to simulate the loading applied by the pressure. The thermal cycling is modelled by applying displacements in a cyclic manner. Details of the loading can be seen in Fig. 4.9a. Three ranges of behaviour depending on the applied stress and the applied displacment amplitude are possible :

(i) elastic behaviour with no plastic strain,

(ii) elastic shakedown where plastic strain occurs, but the element converges on a steady state where no further plastic strain occurs,

(ii) ratchetting, or plastic shakedown, where the steady state involves incremental creep in the direction of the applied displacement.

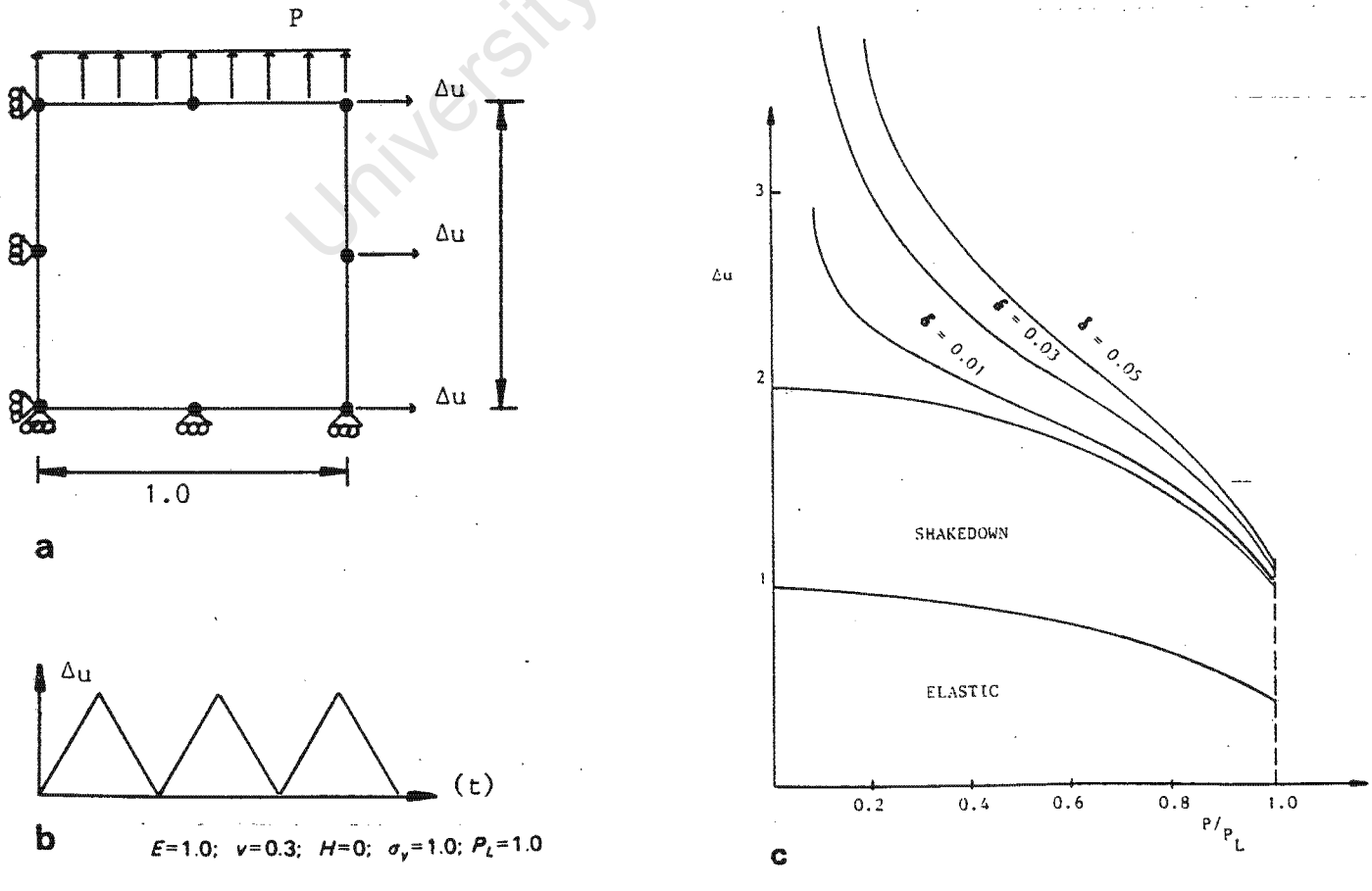

Figure 4.9 : Ratchetting example.

The object of the analysis is to predict the elastic limit, the elastic shakedown limit, and the contours of constant rachet rate. This is done by conducting a series of analyses at different load levels and different cyclic displacement amplitudes. In each analysis the displacement is imposed or removed in one step (giving two steps per cycle), and the analysis continued until a steady state is reached. The contours of constant ratchet rate are interpolated from these results.

The contours are compared to an analytical solution provided by Ponter [16]. Agreement is very good and within the resolution of the diagram.

4.8 SECANT APPROXIMATION FOR THE DRUCKER-PRAGER YIELD CONDITION

In the case of a Drucker-Prager yield surface, the radius of the yield surface in the stress and strain deviator space depends on the hydrostatic stress and volumetric strain. The yield condition is defined by

$$\phi = s - k + 3\alpha\sigma_m \quad , \tag{4.43}$$

where $s = \sqrt{\tfrac{1}{2}\, s_{ij}\, s_{ij}}$ is the second invariant of the deviator stress

and $\sigma_m = \frac{1}{3}\,\sigma_{kk}$.

By writing the stresses at the end of the load increment explicitly in terms of total strains, plastic strains from the previous time increment, and the plastic strain increment, we have

$$s_{ij}^n = 2G(e_{ij}^n - e_{ij}^{p(n-1)})$$

$$\sigma_m^n = 3\,K\,\epsilon^* \qquad \text{for } e^* \le \frac{k - 3\alpha K\epsilon^*}{2G} \quad , \tag{4.44a}$$

$$s_{ij}^{n} = \frac{18\alpha^2 K\, e^{*} - 3\alpha\, K\, \epsilon^{*} + k}{(G + 9\alpha^2\, K)\, e^{*}}\, G(e_{ij}^{n} - e_{ij}^{p(n-1)})$$

$$\sigma_{m}^{n} = \frac{G\, K\, \epsilon^{*} - 6\alpha\, K\, Ge^{*} + 3\alpha\, Kk}{(G + 9\alpha^2\, K)} \quad \text{for } e^{*} > \frac{k - 3\alpha\, K\epsilon^{*}}{2G}\ , \qquad (4.44b)$$

and

$$s_{ij}^{n} = 0$$

$$\sigma_{m}^{n} = \frac{k}{3\alpha} \qquad \text{for } \epsilon^{*} - 6\alpha\, e^{*} \leq \frac{k}{3\alpha\, K}\ ,$$

where

$$\epsilon^{*} = (\epsilon_{v}^{n} - \epsilon_{v}^{p(n-1)})\ . \qquad (4.44c)$$

We need to construct a function $W(\epsilon_{ij}, \epsilon_{ij}^{p})$ so that

$$W(\epsilon_{ij}\ \epsilon_{ij}^{p}) = W(e^{*}, \epsilon^{*}) = W^{e}(e^{*}, \epsilon^{*}) = 2G\, e^{*2} + \tfrac{1}{2} K\epsilon^{*2}\ ,$$

$$\left.\frac{\partial W}{\partial e_{ij}}\right|_{(e^{*}, \epsilon^{*})} = s_{ij}^{n}\ , \qquad (4.45)$$

and

$$\left.\frac{\partial W}{\partial \epsilon_{v}}\right|_{(e^{*}, \epsilon^{*})} = \sigma_{m}^{n} \quad \text{when } e^{*} = \frac{k - 3\alpha\, K\epsilon^{*}}{2G}\ .$$

If we set

$$W = 2G\, e^{*2} + \tfrac{1}{2} K\epsilon^{*2} \quad \text{for } e^{*} = \frac{k - 3\alpha\, K\epsilon^{*}}{2G}\ , \qquad (4.46a)$$

$$W = \frac{1}{\mu}\left(18\alpha^2\, K\, Ge^{*2} - 6\alpha\, K\, Ge^{*}\epsilon^{*} + 2k\, Ge^{*} + 3\alpha\, K\, k\epsilon^{*} + \frac{GK}{2}\,\epsilon^{*2} - \frac{k^2}{2}\right)$$

$$\text{for } e^{*} > \frac{k - 3\alpha\, K\epsilon^{*}}{2G} \qquad (4.46b)$$

and $$W = \frac{k}{3\alpha}\,\epsilon^{*} - \frac{1}{2K}\left(\frac{k}{3\alpha}\right)^2 \quad \text{for } \epsilon^{*} - 6\alpha\, e^{*} \leq \frac{k}{3\alpha\, K}\ , \qquad (4.46c)$$

where $\mu = G + 9\alpha^2\, K$, we will satisfy the conditions of equation (4.45).

$W(\epsilon_{ij},\epsilon^{p}_{ij})$ is a continuous function, and it can easily be verified that

$$W(\epsilon_{ij},\epsilon^{p}_{ij}) \leq W^{e}(\epsilon_{ij},\epsilon^{p}_{ij}) \quad . \tag{4.47}$$

The solution algorithm is the same as the algorithm for the von Mises case. We want to minimise the functional

$$U_1 = \int W^{e}(\epsilon_{ij},\epsilon^{p}_{ij})\ dV - \int_{S_T} T_i\ u_i\ dS \tag{4.48}$$

for the first iteration. Minimisation yields a solution field ${}^{(1)}u_i$, and hence ${}^{(1)}\epsilon_{ij}$, ${}^{(1)}e_{ij}$, ${}^{(1)}\epsilon_{v}$, $e^{(1)}$, and $\epsilon^{(1)}$ (corresponding value of ϵ^{*}) can be computed. As in the case of the von Mises yield condition we want to fit a parabola $W_2(e^{*},\epsilon^{*})$ through the point $W(e^{(1)},\epsilon^{(1)})$ so that

$$\left.\frac{\partial W_2}{\partial e_{ij}}\right|_{(e^{(1)},\epsilon^{(1)})} = \left.\frac{\partial W}{\partial e_{ij}}\right|_{(e^{(1)},\epsilon^{(1)})} \tag{4.49}$$

and

$$\left.\frac{\partial W_2}{\partial \epsilon_{v}}\right|_{(e^{(1)},\epsilon^{(1)})} = \left.\frac{\partial W}{\partial \epsilon_{v}}\right|_{(e^{(1)},\epsilon^{(1)})} \quad . \tag{4.50}$$

A further condition that needs to be satisfied is that

$$W_2(e^{*},\epsilon^{*}) \geq W(e^{*},\epsilon^{*}) \quad \text{for all } (e^{*},\epsilon^{*}) \quad . \tag{4.51}$$

A function which satisfies the above condition is as follows :

$$W_2 = \frac{1}{\mu}\left[\frac{18\alpha^2 K e^{(1)} - 3\alpha K \epsilon^{(1)} + k}{2^{(1)}_e}\right] G(e^n_{ij} - e^{p(n-1)}_{ij})(e^n_{ij} - e^{p(n-1)}_{ij})$$

$$+ \frac{GK}{2\mu}\epsilon^{*2} - \frac{1}{\mu}\left[(6\alpha K G e^{(1)} - 3\alpha Kk)\epsilon^* + 3\alpha G K\epsilon^{(1)}e^{(1)} + k Ge^{(1)} - \frac{k^2}{2})\right] . \tag{4.52}$$

The quadratic potential function

$$U_2 = \int_V W_2(e^*, \epsilon^*)\, dV - \int_{S_T} T_i\, u_i\, dS \tag{4.53}$$

can thus be defined. Note that if we set $\alpha = 0$, the function U_2 defined in equation (4.14) is recovered.

Having defined these functions, the proof of convergence follows the same argument as for the von Mises case. For the (j+1)-th iteration we will have the shear modulus multiplier defined by

$$A^{(j)} = \left[\frac{18\alpha^2 K e^{(j)} - 3\alpha K \epsilon^{(j)} + k}{2\mu\, e^{(j)}}\right] , \tag{4.54a}$$

and an additional bulk modulus multiplier defined by

$$B^{(j)} = \frac{G}{\mu} . \tag{4.54b}$$

4.9 NUMERICAL EXAMPLE FOR THE DRUCKER-PRAGER YIELD CONDITION

The problem used in this example is a strip footing on an infinitely extending layer of overconsolidated clay. The shallow layer of clay is 12ft deep and extends infinitely in the horizontal direction, while the strip footing is 10ft wide. The problem is modelled in plane strain, and the symmetry about the vertical line through the centre of the footing is used. The finite element mesh is shown in Fig. 4.10, and the Drucker-Prager constants used are $k = 9.22$ psi and $\alpha = 0.112$. The elastic constants are Young's modulus $E = 30000$ psi and Poisson's ratio $\nu = 0.3$. The soil is assumed to be weightless, and a smooth and flexible footing is simulated by applying vertical pressure.

Resende et al [17] reported great difficulty in obtaining solutions to this problem when using a tangent predictor method with a subincrementation process for reducing the stress point onto the yield surface. The plot of load vs displacement at the centre of the footing appears in Fig. 4.11 . This plot was obtained using the secant method.

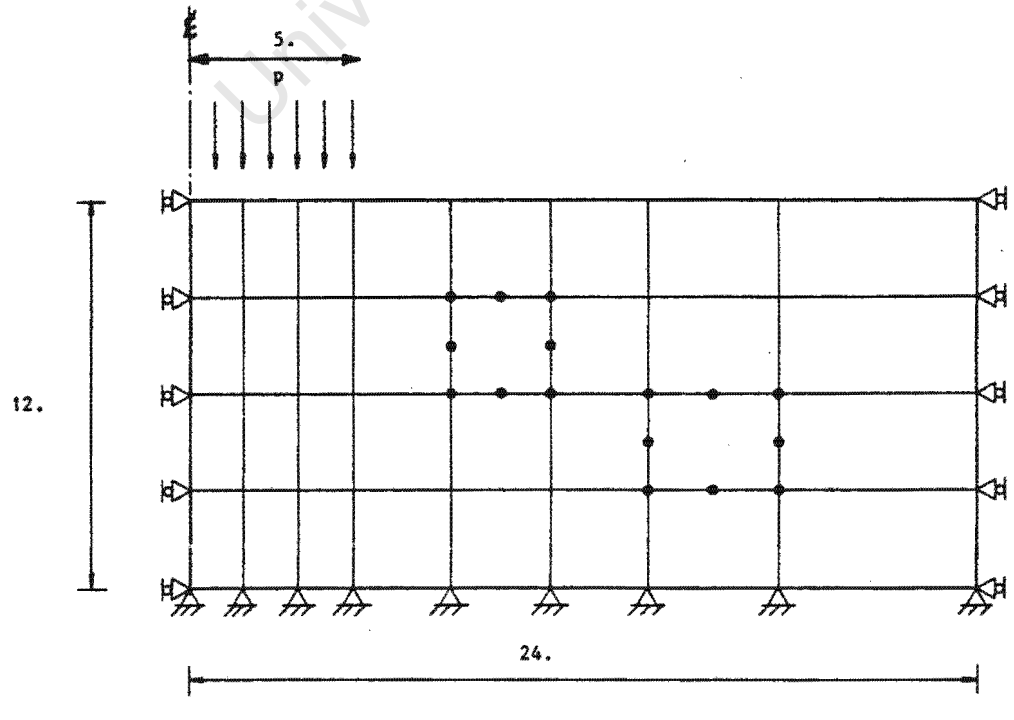

Figure 4.10 : Strip footing on an infinite layer of overconsolidated clay.

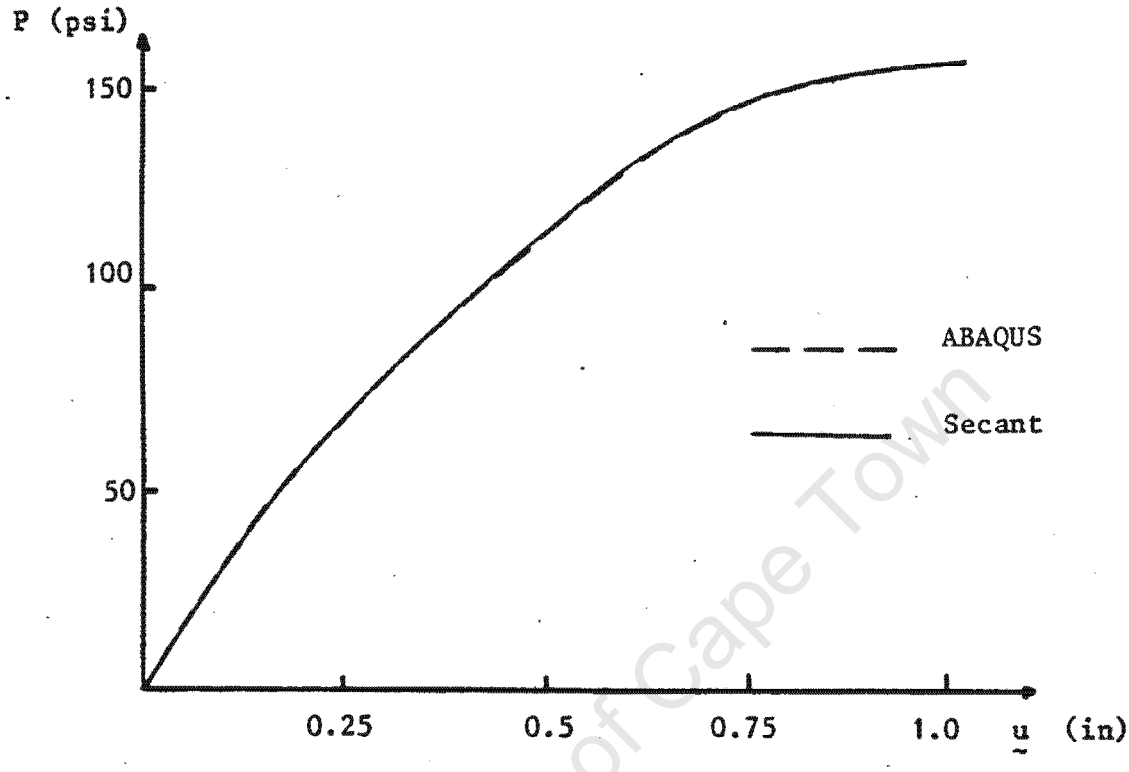

Figure 4.11 : Load vs displacement at the centre of footing.

The results are almost identical to results obtained with ABAQUS, and the limit load is between 155 psi and 160 psi which is in agreement with the value of 158 psi quoted by Mizuno and Chen [18].

The number of iterations for each time increment are tabulated in Table 4.1, and are compared with ABAQUS. The convergence checks are not the same for the two programs, but are close enough to show that the secant algorithm is relatively inefficient. Note that as the load approaches the limit load, the secant algorithm requires more iterations to converge.

LOAD (psi)	DISPLACEMENT at centre (in)	No. of iterations SECANT	No. of iterations ABAQUS
30	- 0.0963	1	1
40	- 0.1307	8	3
50	- 0.1718	8	3
60	- 0.2160	9	3
70	- 0.2629	12	3
80	- 0.3129	13	3
90	- 0.3651	14	3
100	- 0.4193	15	3
110	- 0.4753	16	3
120	- 0.5337	17	3
130	- 0.5966	19	3
140	- 0.6774	32	3
150	- 0.8175	81	3
155	- 0.9758	153	3
160	∞	no convergence	no convergence

Table 4.1

4.10 CONCLUSION

The secant algorithm, implemented as described, has several advantages. In general, it deals easily with complex load paths and with unloading. In addition, it always converges providing reliable results. The algorithm can easily be added to a code capable of linear analysis with imposed inelastic strains. The only changes which need to be made are to the shear and bulk moduli at each iteration.

One of the major disadvantages of the algorithm is the slow rate of convergence which is at its worst when a solution is sought for an applied load approaching the limit load. Since the convergence rate is monotonic a simple Aitken acceleration method may improve it, but it could possibly affect the robustness of the algorithm. A simple variation of an Aitken acceleration method has been tried, but with limited success only.

There appears to be little difficulty in defining potential functions for different yield surfaces, provided that the stresses at the end of the load increment can be written explicitly in terms of strain quantities. It appears that this algorithm is best suited to obtaining comparison solutions, and is also very helpful in understanding some of the minimum principles on which the Newton-Raphson methods are based.

CHAPTER 5

BACKWARD DIFFERENCE INTEGRATION WITH CONSISTENT TANGENT PREDICTORS

5.1 INTRODUCTION

In the preceding Chapters we have considered the Newton-Raphson and the secant approximation (essentially mathematical programming) methods for the solution of incremental elastic-plastic problems. The relationship between these two methods has been established, and it has been shown that when the secant predictor is used in the Newton-Raphson procedure (for an elastic, perfectly plastic material with a von Mises yield condition) the two are identical. We have assumed that the internal variables follow a straight line path in internal variable space. In the iterative procedure, the internal variables are only updated once convergence has been achieved, and this is essentially a backward difference scheme for the integration of the constitutive relations. The notion of consistency between the predictor and the integration algorithm, adopted in the incremental problem, plays a crucial role in the rate of convergence of the iterative scheme for the Newton-Raphson methods [19].

In this Chapter we will present the backward difference algorithm for a general yield condition, and then look at three yield surfaces in this general framework. They are the von Mises, the Drucker-Prager, and the Drucker-Prager cap with tension cut-off. The relationship between the consistent tangent predictor and some of the concepts in Chapters 3 and 4 is explored, and then the predictor for each of the yield conditions above is evaluated.

5.2 BACKWARD DIFFERENCE INTEGRATION OF THE CONSTITUTIVE RELATIONS

Let us start by assuming that the load path can be divided into m load steps. At the end of each step the total strain can be written as the sum of its elastic and plastic components

$$\epsilon_{ij} = \epsilon^{e}_{ij} + \epsilon^{p}_{ij} \quad . \tag{5.1}$$

The stress is related to the elastic part of the strain by means of the elastic stiffness modulus

$$\sigma_{ij} = D_{ijkl}(\epsilon_{ij} - \epsilon^{p}_{ij}) \quad . \tag{5.2}$$

The mean hydrostatic stress and volumetric strain respectively are

$$\sigma_{m} = \frac{1}{3}\,\sigma_{kk} \tag{5.3}$$

and

$$\epsilon_{v} = \epsilon_{kk} = \epsilon^{e}_{kk} + \epsilon^{p}_{kk} \quad . \tag{5.4}$$

The deviatoric stress and strain tensors were introduced in equations (3.32) as

$$s_{ij} = \sigma_{ij} - \frac{1}{3}\,\sigma_{kk}\,\delta_{ij} \tag{5.5}$$

and

$$e_{ij} = \epsilon_{ij} - \frac{1}{3}\,\epsilon_{kk}\,\delta_{ij} \quad , \tag{5.6}$$

where δ_{ij} is the Kronecker delta.

We define $\dot{\sigma}_{ij}$ and $\dot{\epsilon}_{ij}$ as the rate of stress and strain respectively. The components of plastic strain rate $\dot{\epsilon}^{p}_{ij}$ are given by classical plasticity for associated flow rule as

$$\dot{\epsilon}^{p} = \lambda_{\eta} \frac{\partial \phi_{\eta}}{\partial \sigma_{ij}} \quad , \quad \eta = 1, \ \ldots \ m \tag{5.7}$$

for a general multi-surface yield condition. ϕ_{η} are the individual yield surfaces, and λ_{η} are the non-negative multipliers associated with each surface.

We consider a generic time increment Δt , from t^{n-1} to t^{n} . We assume that we have the full solution at t^{n-1} and that holonomic behaviour takes place within each load step. We integrate equation (5.7) over the time interval to obtain

$$\Delta \epsilon^{p}_{ij} = \Lambda_{\eta} \left. \frac{\partial \phi_{\eta}}{\partial \sigma_{ij}} \right|_{\sigma^{n}_{ij}} \quad , \tag{5.8}$$

where $\Delta \epsilon^{p}_{ij}$ is the increment in plastic strain during the n-th load increment with

$$\epsilon^{pn}_{ij} = \epsilon^{p(n-1)}_{ij} + \Delta \epsilon^{p}_{ij} \quad ,$$

and where Λ_{η} are non-negative multipliers.

The strain increment can also be divided into deviatoric and volumetric components, and it can easily be verified that

$$\Delta e^{p}_{ij} = \Lambda_{\eta} \left. \frac{\partial \phi_{\eta}}{\partial s_{ij}} \right|_{s^{n}_{ij}}$$

$$\Delta \epsilon^{p}_{v} = \Lambda_{\eta} \left. \frac{\partial \phi_{\eta}}{\partial \sigma_{m}} \right|_{\sigma^{n}_{m}} \quad , \tag{5.9}$$

where $\Delta e^{p}_{ij} = e^{pn}_{ij} - e^{p(n-1)}_{ij}$

and $\Delta \epsilon^{p}_{v} = \epsilon^{pn}_{v} - \epsilon^{p(n-1)}_{v}$.

As in the previous chapters we define the quantities

$$e^{*} = \left[\tfrac{1}{2} \, (e^{n}_{ij} - e^{p(n-1)}_{ij})(e^{n}_{ij} - e^{p(n-1)}_{ij}) \right]^{\frac{1}{2}} \qquad (5.10)$$

$$\epsilon^{*} = \epsilon^{n}_{v} - \epsilon^{p(n-1)}_{v} \quad , \qquad (5.11)$$

and by assuming elastic behaviour in the n-th step, e^{*} is related to the second invariant of the stress tensor by

$$s = (\tfrac{1}{2} \, s_{ij} \, s_{ij})^{\frac{1}{2}} = \left[\tfrac{1}{2} \, . \, 2G(e^{n}_{ij} - e^{p(n-1)}_{ij}) \, . \, 2G \, (e^{n}_{ij} - e^{p(n-1)}_{ij}) \right]^{\frac{1}{2}}$$

$$= 2G \, e^{*} \quad . \qquad (5.12)$$

The relation between σ_{m} and ϵ^{*} is given in equation (4.44) for elastic behaviour as

$$\sigma_{m} = K \, \epsilon^{*} \quad . \qquad (5.13)$$

5.2.1 Von Mises and Drucker-Prager Yield Conditions

We need only consider the Drucker-Prager yield condition since the von Mises yield condition is essentially a special case of the Drucker-Prager yield conditon. The yield surface is identified by

$$\phi = [\tfrac{1}{2} \, s_{ij} \, s_{ij}]^{\frac{1}{2}} + 3\alpha\sigma_{m} - k \leq 0 \quad , \qquad (5.14)$$

which can be rewritten as

$$\phi^n = [\tfrac{1}{2}\, s_{ij}^n\, s_{ij}^n]^{\frac{1}{2}} + 3\alpha\sigma_m^n - k \leq 0 \qquad (5.15)$$

at the end of the n-th step. Where $\alpha=0$, the von Mises yield condition is recovered. The increment in plastic strain follows from equation (5.9) as

$$\Delta e_{ij}^p = \Lambda \frac{s_{ij}^n}{2s^n}$$

$$\Delta \epsilon_v^p = \Lambda\, 3\alpha \qquad . \qquad (5.16)$$

The stress at the end of the step is written as

$$s_{ij}^n = 2G(e_{ij}^n - e_{ij}^{p(n-1)} - \Delta e_{ij}^p) \qquad (5.17a)$$

$$\sigma_m^n = K(\epsilon_v^n - \epsilon_v^{p(n-1)} - \Delta\epsilon_v^p) \quad , \qquad (5.17b)$$

and substituting from equation (5.16)

$$s_{ij}^n = \left(\frac{s^n}{s^n + G\,\Lambda}\right) 2G\ (e_{ij}^n - e_{ij}^{p(n-1)}) \qquad (5.18a)$$

$$\sigma_m^n = K(\epsilon_v^n - \epsilon_v^{p(n-1)}) - 3\alpha\, K\, \Lambda \quad . \qquad (5.18b)$$

Multiplying both sides of equation (5.18a) by $\tfrac{1}{2}\, s_{ij}^n$ and extracting the square root yields the value

$$s^n = 2G\, e^* - G\,\Lambda \quad , \qquad (5.19)$$

and hence

$$s_{ij}^n = \left(\frac{2\, e^* - \Lambda}{2\, e^*}\right) 2G\ (e_{ij}^n - e_{ij}^{p(n-1)}) \quad . \qquad (5.20)$$

To complete these equations we need to evaluate Λ . In order to do this the following procedure is adopted : we assume the step to be elastic and evaluate

$$\hat{\phi}^n = 2G\, e^* + 3\alpha K \epsilon^* - k \quad . \tag{5.21}$$

If $\hat{\phi}^n \leq 0$, the linear elastic assumption holds and $\Lambda = 0$. This results in

$$s_{ij}^n = 2G(e_{ij}^n - e_{ij}^{p(n-1)}) \tag{5.22a}$$

$$\sigma_m^n = K(\epsilon_v^n - \epsilon_v^{p(n-1)}) \quad . \tag{5.22b}$$

If $\hat{\phi}^n > 0$, we use equations (5.18b), (5.19) and (5.20) to substitute into equation (5.15). Solving for Λ yields

$$\Lambda = \frac{3\alpha K}{G + 9\alpha^2 K} \epsilon^* + \frac{2G}{G + 9\alpha^2 K} e^* - \frac{k}{G + 9\alpha^2 K} \quad . \tag{5.23}$$

Substituting this expression for Λ into equations (5.20) and (5.18b) yields an explicit relation for stresses in terms of total strains :

$$s_{ij}^n = \frac{18\alpha^2 k\, e^* - 3\alpha K \epsilon^* + k}{(G + 9\alpha^2 K) e^*} G(e_{ij}^n - e_{ij}^{p(n-1)}) \tag{5.24a}$$

$$\sigma_m^n = \frac{G K \epsilon^* - 6G\alpha K e^* + 3\alpha K k}{(G + 9\alpha^2 K)} \quad . \tag{5.24b}$$

These relations were used as the starting point for constructing the potential functions in the previous Chapter.

5.2.2 Drucker-Prager Cap Model with Tension Cut-off

A full description of this model appears in a recent paper [20]. The model is made up of three distinct yield surfaces :

(i) Drucker-Prager yield condition,

(ii) a parabolic cap with a nonlinear hardening law,

and (iii) a tension cut-off surface.

We define

$$\phi_1 = s + 3\alpha\,\sigma_m - k \leq 0 \quad , \tag{5.25a}$$

$$\phi_2 = -\,3(\sigma_m - \sigma_m^c) + R^2\,s^2 \leq 0 \quad , \tag{5.25b}$$

$$\phi_3 = 3\sigma_m - T \leq 0 \quad , \tag{5.25c}$$

where

R is the parabolic cap shape factor,

T is the tension cut-off limit,

and σ_m^c is a hardening parameter which depends on the current plastic volume strain.

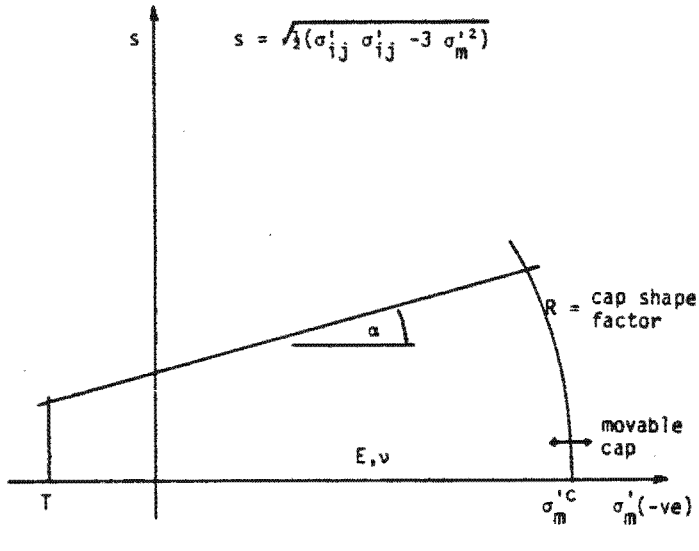

Figure 5.1 : Drucker-Prager cap yield with tension cut-off.

The hardening law on the cap is defined by

$$\bar{\epsilon}^p_v = \bar{\epsilon}^p_{v_o} + \epsilon^p_v = W(1 - e^{D\sigma^c_m}) \quad , \tag{5.26a}$$

where $\bar{\epsilon}^p_{v_o}$ is the initial plastic volume strain (degree of compaction) and W is a limiting value for the volumetric strain.

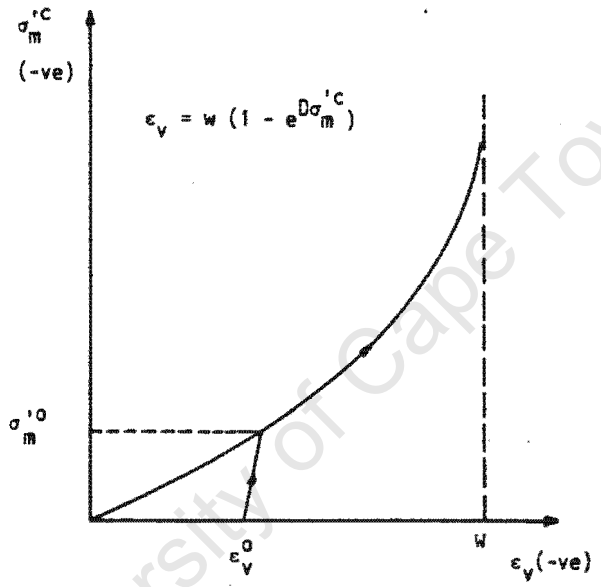

Figure 5.2 : Nonlinear hardening law on the cap.

This relation is represented diagrammatically in Fig. 5.2, and can be written as

$$\sigma^c_{kk} = 3\sigma^c_m = \frac{1}{D}\ln\left(1 - \frac{1}{w}(\bar{\epsilon}^p_{v_o} + \epsilon^p_v)\right) \quad . \tag{5.26b}$$

The increment in plastic strain can be obtained from equation (5.8) as

$$\Delta e^p_{ij} = \Lambda_1 \left.\frac{\partial \phi_1}{\partial s_{ij}}\right|_{s^n_{ij}} + \Lambda_2 \left.\frac{\partial \phi_2}{\partial s_{ij}}\right|_{s^n_{ij}} + \Lambda_3 \left.\frac{\partial \phi_3}{\partial s_{ij}}\right|_{s^n_{ij}} \tag{5.27a}$$

$$\Delta\epsilon_v^p = \Lambda_1 \left.\frac{\partial\phi_1}{\partial\sigma_m}\right|_{\sigma_m^n} + \Lambda_2 \left.\frac{\partial\phi_2}{\partial\sigma_m}\right|_{\sigma_m^n} + \Lambda_3 \left.\frac{\partial\phi_3}{\partial\sigma_m^n}\right|_{\sigma_m^n} , \qquad (5.27b)$$

and by evaluating the derivatives, these relations become

$$\Delta e_{ij}^p = \Lambda_1 \frac{s_{ij}^n}{2\, s^n} + \Lambda_2 R^2 s_{ij}^n \qquad (5.28a)$$

$$\Delta\epsilon_v^p = \Lambda_1 3\alpha - 3\Lambda_2 + 3\Lambda_3 \quad . \qquad (5.28b)$$

We assume that the behaviour in the step is linear elastic and evaluate

$$\hat{\phi}_1^n = 2G\, e^* + 3\alpha K \epsilon^* - k \quad , \qquad (5.29a)$$

$$\hat{\phi}_2^n = -3(K\epsilon^* - \sigma_m^c) + R^2(2G\, e^*)^2 \quad , \qquad (5.29b)$$

and

$$\hat{\phi}_3^n = 3K\epsilon^* - T \quad . \qquad (5.29c)$$

There are six modes of behaviour possible, and the initial choice of which mode is active will depend on equations (5.29).

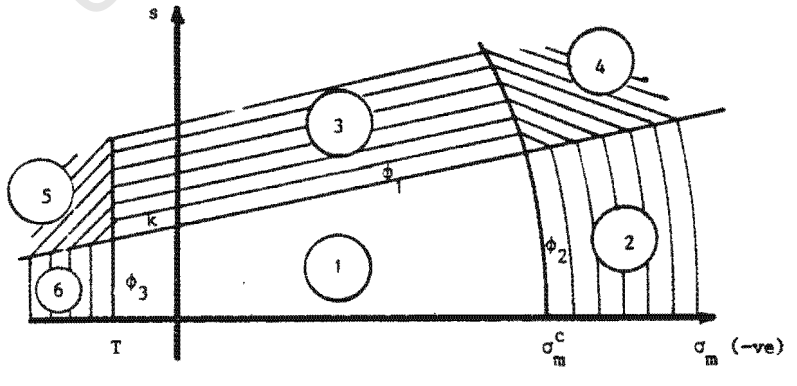

Figure 5.3 : Choice of mode active.

These modes, shown in Fig. 5.3, are identified as follows :

(i) Mode 1 the material behaves elastically ; in this case, $\hat{\phi}_1^n \leq 0$, $\hat{\phi}_2^n \leq 0$, and $\hat{\phi}_3^n \leq 0$ in equation (5.29)

(ii) Mode 2 the cap on the compression side is active. For this mode $\hat{\phi}_1^n \leq 0$, $\hat{\phi}_3^n \leq 0$, and $\hat{\phi}_2^n > 0$

(iii) Mode 3 only the Drucker-Prager yield surface is active and $\hat{\phi}_1^n > 0$, $\hat{\phi}_2^n \leq 0$, and $\hat{\phi}_3^n \leq 0$

(iv) Mode 4 the vertex between the Drucker-Prager yield surface and the cap is active and for this case, $\hat{\phi}_1^n > 0$, $\hat{\phi}_2^n > 0$, and $\hat{\phi}_3^n \leq 0$

(v) Mode 5 the vertex between the Drucker-Prager and tension cut-off is active and $\hat{\phi}_1^n > 0$, $\hat{\phi}_2^n \leq 0$, and $\hat{\phi}_3^n > 0$

(vi) Mode 6 the tension cut-off is active and here $\hat{\phi}_1^n \leq 0$, $\hat{\phi}_2^n \leq 0$, and $\hat{\phi}_3^n > 0$.

For each of these modes the plastic strain increment is given by equation (5.28), and the final state of stress by

$$s_{ij}^n = 2G(e_{ij}^n - e_{ij}^{p(n-1)} - \Delta e_{ij}^p) \qquad (5.30a)$$

$$\sigma_m^n = K(\epsilon_v^n - \epsilon_v^{p(n-1)} - \Delta\epsilon_v^p) \quad . \qquad (5.30b)$$

These equations can be written as

$$s_{ij}^n = \frac{2e^* - \Lambda_1}{2e^*(1 + 2G\,R^2\,\Lambda_2)}\, 2G(e_{ij}^n - e_{ij}^{p(n-1)}) \qquad (5.31a)$$

$$\sigma_m^n = 3K(\epsilon_v^n - \epsilon_v^{p(n-1)}) - 3K\alpha\Lambda_1 + 3K\,\Lambda_2 - 3K\,\Lambda_3 \quad , \qquad (5.31b)$$

and the values of Λ_1, Λ_2 , and Λ_3 will depend on which mode is active. We briefly deal with these individually.

5.2.2.1 Mode 1 active For this case the material behaves elastically and $\Lambda_1 = \Lambda_2 = \Lambda_3 = 0$. The stresses are

$$s_{ij}^n = 2G(e_{ij}^n - e_{ij}^{p(n-1)}) \tag{5.32a}$$

$$\sigma_m^n = K(\epsilon_v^n - \epsilon_v^{p(n-1)}) \quad , \tag{5.32b}$$

and all plastic strain increments are zero.

5.2.2.2 Mode 2 active Plastic strains take place starting from the cap. At the end of the step $\phi_2^n = 0$ (equations (5.25)). Since $\phi_1^n \leq 0$, $\Lambda_1 = 0$ and since $\phi_3^n \leq 0$, $\Lambda_3 = 0$. It is therefore follows that

$$s_{ij}^n = \frac{2G}{(1 + 2G\, R^2\, \Lambda_2)} (e_{ij}^n - e_{ij}^{p(n-1)}) \tag{5.33a}$$

$$\sigma_m^n = K(\epsilon_v^n - \epsilon_v^{p(n-1)}) + 3K\, \Lambda_2 \quad . \tag{5.33b}$$

We set $\phi_2^n = 0$ to evaluate Λ_2 , and hence we have

$$\phi_2^n = -\, 3K(\epsilon_v^n - \epsilon_v^{p(n-1)}) - 9K\, \Lambda_2 + \frac{1}{D} (\ln (1 - \frac{1}{W}(\bar{\epsilon}_v^p - 3\Lambda_2)))$$

$$+ \frac{2G^2\, R^2}{(1 + 2G\, R^2\, \Lambda_2)^2} (e_{ij}^n - e_{ij}^{p(n-1)})(e_{ij}^n - e_{ij}^{p(n-1)}) = 0 \quad . \tag{5.33c}$$

Since we cannot determine Λ_2 explicitly, we have to use some numerical. In this instance a Newton-Raphson method does not work effectively since the following limitation exists :

$$1 - \frac{1}{W}(\bar{\epsilon}_v^p - 3\Lambda_2) \geq 0 \quad . \tag{5.34}$$

We therefore make use of a bisection method, and while it may not be very efficient, it is robust.

5.2.2.3 Mode 3 active For this case, only the Drucker-Prager surface is active, and the explicit relations for stresses are determined in the same way as in Section 5.2.1. Since $\phi_2^n \leq 0$ and $\phi_3^n \leq 0$ it follows that $\Lambda_2 = \Lambda_3 = 0$, and hence the result

$$s_{ij}^n = \frac{18\alpha^2 K e^* - 3\alpha K \epsilon^* + k}{(G + 9\alpha^2 K)e^*} G(e_{ij}^n - e_{ij}^{p(n-1)}) \tag{5.35a}$$

$$\sigma_m^n = \frac{G K \epsilon^* - 6G\alpha K e^* + 3\alpha Kk}{(G + 9\alpha^2 K)} \quad . \tag{5.35b}$$

5.2.2.4 Mode 4 active $\phi_3 \leq 0$ and hence $\Lambda_3 = 0$, but both the Drucker-Prager yield surface and cap on the compression side are active. The stresses are

$$s_{ij}^n = \frac{2e^* - \Lambda_1}{2e^*(1 + 2G R^2 \Lambda_2)} 2G(e_{ij}^n - e_{ij}^{p(n-1)}) \tag{5.36a}$$

$$\sigma_m^n = K(\epsilon_v^n - \epsilon_v^{p(n-1)}) - 3K\alpha\Lambda_1 + 3K\Lambda_2 \quad , \tag{5.36b}$$

and the non-negative multipliers can be determined from

$$\phi_1^n = \frac{2e^* - \Lambda_1}{2e^*(1 + 2G R^2 \Lambda_2)} 2Ge^* + 3\alpha K \epsilon^* - 9\alpha^2 K \Lambda_1 + 9\alpha K \Lambda_2 - k = 0 \tag{5.37a}$$

$$\phi_2^n = -3(K\epsilon^* + 3K\alpha\Lambda_1 + 3K\Lambda_2) + \frac{1}{D}\ln\left(1 - \frac{1}{W}(\bar{\epsilon}_v^p - 3\Lambda_2 + 3\alpha\Lambda_1)\right)$$

$$+ R^2\left[\frac{2e^* - \Lambda_1}{2e^*(1 + 2G\,R^2\,\Lambda_2)}\right]^2 (2Ge^*)^2 = 0 \quad . \qquad (5.37b)$$

From equation (5.37a), Λ_1 can be written in terms of Λ_2 and the solution of the nonlinear equation is achieved in the same way as when mode 2 is active.

5.2.2.5 Mode 5 active This mode is active when $\phi_1^n > 0$ and $\phi_3^n > 0$. $\phi_2^n \leq 0$ and hence $\Lambda_2 = 0$

$$s_{ij}^n = \frac{2e^* - \Lambda_1}{2\,e^*} 2G(e_{ij}^n - e_{ij}^{p(n-1)}) \qquad (5.38a)$$

$$\sigma_m^n = K(\epsilon_v^n - \epsilon_v^{p(n-1)}) - 3K\alpha\Lambda_1 + 3K\Lambda_3 \quad , \qquad (5.38b)$$

where Λ_1 and Λ_3 can be determined explicitly from

$$\Lambda_1 = \frac{1}{G}(2Ge^* - k + \alpha T) \qquad (5.38c)$$

$$\Lambda_3 = \frac{1}{G}((G + 9\alpha^2 K)(3K\epsilon^* - T) - \alpha(2Ge^* + 3\alpha K\epsilon^* - k)) \quad . \qquad (5.38d)$$

5.2.2.6 Mode 6 active Plastic strains take place starting from the tension cut-off surface. In this case $\phi_1^n \leq 0$, $\phi_2^n \leq 0$, and $\phi_3^n > 0$. Since $\Lambda_1 = 0$ and $\Lambda_2 = 0$ the stresses can be written explicitly as

$$s_{ij}^n = 2G(e_{ij}^n - e_{ij}^{p(n-1)}) \qquad (5.39a)$$

$$\sigma_m^n = T/3 \quad . \qquad (5.39b)$$

Once the stresses have been evaluated, we substitute these values back into equation (5.25) to affirm that we have indeed assumed the correct mode to be active. If we have not chosen the correct mode, we base our next choice on the re-evaluated state until we have the correct mode and hence the correct state of stress.

5.3 A CONSISTENT TANGENT PREDICTOR

We define the tangent predictor which is consistent with the backward difference integration scheme as

$$D^{ep}_{ijkl} = \frac{\partial \sigma_{ij}}{\partial \epsilon_{kl}} \quad , \tag{5.40}$$

where the relationship between stress and strain is defined in the previous section.

5.3.1 The Drucker-Prager (von Mises) yield condition

For this yield condition we are minimising the potential energy functional (Section 4.7)

$$U^* = \int_V W(\epsilon_{ij})\, dV - \int_S T_i\, u_i\, dS \quad , \tag{5.41}$$

where

$$W = 2Ge^{*2} + \tfrac{1}{2} K\epsilon^{*2} \qquad \text{for } e^* \leq \frac{k - 3\alpha\, \sigma_m}{2G} \quad ,$$

$$W = \frac{1}{G + 9\alpha^2 k} (18\alpha^2\, K\, Ge^{*2} - 3\alpha\, K\, Ge^*\epsilon^* + 2k\, Ge^* + 3\alpha\, K\, k\epsilon^* + \frac{GK}{2}\epsilon^{*2} - \frac{k^2}{2}) \qquad \text{for } e^* > \frac{k - 3\alpha\, \sigma_m}{2G} \quad ,$$

and $$W = \frac{k}{3\alpha}\epsilon^* - \frac{1}{2K}\left[\frac{k}{3\alpha}\right]^2 \qquad \text{for } \epsilon^* - 6\alpha\, e^* \leq \frac{k}{3\alpha K} \quad .$$

Let us assume that we have a solution field $^{(j)}u_i$ and hence $^{(j)}\epsilon_{ij}$, $^{(j)}e_{ij}$ etc. at the end of the j-th iteration. Following the same argument as in Section 4.5, we can write

$$U^* = U_a^* + U_b^* + U_c^* + U_d^* \quad , \tag{5.42}$$

where

$$U_a^* = \int_V W(^{(j)}\epsilon_{ij})\, dV - \int_{S_T} T_i\, ^{(j)}u_i\, dS \quad ,$$

$$U_b^* = \int_V \Delta\epsilon_{ij} \left.\frac{\partial W(\epsilon_{ij})}{\partial \epsilon_{ij}}\right|_{(j)\epsilon_{ij}} dV - \int_{S_T} {}^{(j)}X_i\, \Delta u_i\, dS \quad ,$$

$$U_c^* = \int_V \tfrac{1}{2}\, \Delta\epsilon_{ij}\, \Delta\epsilon_{kl} \left.\frac{\partial^2 W(\epsilon_{ij})}{\partial \epsilon_{ij}\partial \epsilon_{kl}}\right|_{(j)\epsilon_{ij}} dV - \int_{S_T} {}^{(j)}r_i\, \Delta u_i\, dS \quad ,$$

and $$U_d^* = \int_V \sum_{m=3}^{\infty} \frac{1}{m!}\, \Delta\epsilon_{ij} \ldots \Delta\epsilon_{pq} \left.\frac{\partial^m W(\epsilon_{ij})}{\partial \epsilon_{ij} \ldots \partial \epsilon_{pq}}\right|_{(j)\epsilon_{ij}} dV \quad .$$

Minimisation of U^* is thus equivalent to the minimisation of

$$U^* = U_c^* + U_d^* \quad ,$$

since U_a is a constant, and by the principle of virtual work $U_b = 0$. If we disregard terms with $m \geq 3$, we are essentially minimising U_c^*

$$U^* = U_c^* = \int_V \tfrac{1}{2}\, \Delta\epsilon_{ij}\, \Delta\epsilon_{kl} \left.\frac{\partial^2 W(\epsilon_{ij})}{\partial \epsilon_{ij}\partial \epsilon_{kl}}\right|_{(j)\epsilon_{ij}} dV - \int_{S_T} {}^{(j)}r_i\, \Delta u_i\, dS \quad . \tag{5.43}$$

From the definition of $W(\epsilon_{ij})$, we know that

$$\frac{\partial W}{\partial \epsilon_{ij}} = \sigma_{ij} \quad , \tag{5.44}$$

and hence

$$U^* = \int_V \tfrac{1}{2}\, \Delta\epsilon_{ij}\, \Delta\epsilon_{kl} \left.\frac{\partial \sigma_{ij}}{\partial \epsilon_{kl}}\right|_{(j)_{\epsilon_{ij}}} dV - \int_{S_T} {}^{(j)}r_i\, \Delta u_i\, dS \quad . \tag{5.45}$$

In equation (5.45) it is evident that $\left.\frac{\partial \sigma_{ij}}{\partial \epsilon_{kl}}\right|_{(j)_{\epsilon_{ij}}}$ is the consistent predictor which is defined in equation (5.40).

In Section 3.8.3 we discussed various predictors for the von Mises yield condition. Among them was a consistent predictor defined in equation (3.67) as

$$\left[\underline{K} - \hat{\underline{L}}\left[\hat{H} + \frac{\partial}{\partial \Delta \underline{e}^p}\left(\frac{\partial D}{\partial \Delta \underline{e}^p}\right)\right]^{-1} \hat{\underline{L}}^T\right] \quad .$$

Evaluation of this predictor reveals that it is identical to the consistent predictor defined in equation (5.40).

5.3.2 The Drucker-Prager yield surface with a parabolic cap and Tension Cut-off

This multi-surface yield condition is the only one that we will consider, since it encompasses both the von Mises and Drucker-Prager yield conditions. We introduce certain values which will facilitate the calculation of the tangent operator.

We will consider only plane and axisymmetric problems, and write the stress and strain tensors in vector form as

$$\underset{\sim}{\sigma} = (\sigma_{11}, \sigma_{22}, \sigma_{12}, \sigma_{33})^T \tag{5.46a}$$

$$\underset{\sim}{\epsilon} = (\epsilon_{11}, \epsilon_{22}, \epsilon_{12}, \epsilon_{33})^T \quad . \tag{5.46b}$$

Similarly, we will write the deviator and hydrostatic stresses, and the deviator and volumetric strains in vector form

$$\underset{\sim}{s} = (s_{11}, s_{22}, s_{12}, s_{33}, \sigma_m) \tag{5.47a}$$

$$\underset{\sim}{e} = (e_{11}, e_{22}, e_{12}, e_{33}, \epsilon_v) \quad . \tag{5.47b}$$

Constraints imposed on the deviator stresses and strains are :

$$s_{11} + s_{22} + s_{33} = 0 \quad \text{and} \quad e_{11} + e_{22} + e_{33} = 0 \quad .$$

Simple transformations which relate the total stress and strain vectors to their deviatoric and hydrostatic/volumetric counterparts, and which satisfy the above constraints are defined by ;

$$\underset{\sim}{\sigma} = \left[T_s\right] \begin{Bmatrix} \underset{\sim}{s} \\ \sigma_m \end{Bmatrix} \quad , \tag{5.48}$$

where $$\left[T_s\right] = \begin{bmatrix} 1 & 0 & 0 & 0 & 1 \\ 0 & 1 & 0 & 0 & 1 \\ 0 & 0 & 1 & 0 & 0 \\ 0 & 0 & 0 & 1 & 1 \end{bmatrix} \quad ,$$

$$\text{and} \quad \begin{Bmatrix} \underset{\sim}{e} \\ \epsilon_v \end{Bmatrix} = \left[T_e\right] \underset{\sim}{\epsilon} \quad , \tag{5.49}$$

$$\text{where} \quad \left[T_e\right] = \frac{1}{3}\begin{bmatrix} 2 & -1 & 0 & -1 \\ -1 & 2 & 0 & -1 \\ 0 & 0 & 1 & 0 \\ -1 & -1 & 0 & 2 \\ 3 & 3 & 0 & 3 \end{bmatrix} .$$

We will rewrite equation (5.40) as

$$D^{ep}_{ijkl} = \frac{\partial \sigma_{ij}}{\partial s_{pq}} \frac{\partial s_{pq}}{\partial e_{rs}} \frac{\partial e_{rs}}{\partial \epsilon_{kl}} \tag{5.50}$$

$$= \left[T_s\right] \frac{\partial \underset{\sim}{s}}{\partial \underset{\sim}{e}} \left[T_e\right] \quad ,$$

and all that is necessary now is to evaluate $\dfrac{\partial \underset{\sim}{s}}{\partial \underset{\sim}{e}}$.

Let us define

$$E_{ij} = (e^n_{ij} - e^{p(n-1)}_{ij}) \quad , \tag{5.51a}$$

and hence

$$\frac{\partial e^*}{\partial e_{ij}} = \frac{E_{ij}}{2e^*} \quad . \tag{5.51b}$$

5.3.2.1 Mode 1 active The stresses are

$$s_{ij}^n = 2G(e_{ij}^n - e_{ij}^{p(n-1)})$$

$$\sigma_m^n = K(\epsilon_v^n - \epsilon_v^{p(n-1)}) \quad ,$$

and
$$\frac{\partial s_{ij}}{\partial e_{kl}} = 2G\ \delta_{ij}\delta_{kl} \tag{5.52a}$$

$$\frac{\partial \sigma_m}{\partial \epsilon_v} = K \quad ,$$

where

$$\delta_{ij} = 1 \quad \text{for} \quad i = j \tag{5.52b}$$
$$= 0 \quad \text{for} \quad i \neq j \quad .$$

In matrix form

$$\frac{\partial \underset{\sim}{\sigma}}{\partial \underset{\sim}{e}} = \begin{bmatrix} 2G & 0 & 0 & 0 & 0 \\ & 2G & 0 & 0 & 0 \\ & & 2G & 0 & 0 \\ & \text{sym} & & 2G & 0 \\ & & & & K \end{bmatrix} .$$

5.3.2.2 Mode 2 active The stresses are

$$s_{ij}^n = \frac{2G}{(1 + 2G\ R^2\ \Lambda_2)}(e_{ij}^n - e_{ij}^{p(n-1)})$$

$$\sigma_m^n = K(\epsilon_v^n - \epsilon_v^{p(n-1)}) + 3K\ \Lambda_2 \quad ,$$

where

$$\phi_2^n = -3K(\epsilon_v^n - \epsilon_v^{p(n-1)}) - 9K\ \Lambda_2 + \frac{1}{D}\ln\left(1 - \frac{1}{W}(\epsilon_v^p - 3\Lambda_2)\right)$$
$$+ \frac{2G^2\ R^2}{(1 + 2G\ R^2\ \Lambda_2)^2}(e_{ij}^n - e_{ij}^{p(n-1)})(e_{ij}^n - e_{ij}^{p(n-1)}) = 0 \quad .$$

Since ϕ_2^n includes a nonlinear hardening term, it is not possible to write Λ_2 explicitly in terms of the other variables. We will therefore adopt the following approach: at the end of the i-th iteration we have the solution fields $\epsilon_v^{n(i)}$, $e_{ij}^{n(i)}$, and $\Lambda_2^{(i)}$, which do not necessarily satisfy equilibrium, but which satisfy the equation

$$\phi_2^n(e_{ij}^{n(i)}, \epsilon_v^{n(i)}, \Lambda_2^{(i)}) = 0 \quad . \tag{5.53a}$$

We seek a solution at the (i+1)-th iteration such that

$$\phi_2^n(e_{ij}^{n(i+1)}, \epsilon_v^{n(i+1)}, \Lambda_2^{(i+1)}) = 0 \quad . \tag{5.53b}$$

Assuming that the difference between solutions of consecutive iterations is sufficiently small, it becomes possible to rewrite equation (5.53b) as a Taylor's series expansion about the solution at the i-th iteration. It follows that

$$\begin{aligned}\phi_2^n(e_{ij}^{n(i+1)}, \epsilon_v^{n(i+1)}, \Lambda_2^{(i+1)}) = \phi_2^n(e_{ij}^{n(i)}, \epsilon_v^{n(i)}, \Lambda_2^{(i)}) &- 3K\,\partial\epsilon_v - 9K\,\partial\Lambda_2 \\ &+ R^2\, s_{ij}^n \left[\frac{2G}{(1 + 2G\,R^2\,\Lambda_2)}\,\delta_{ij}\delta_{kl}\partial e_{kl} - \frac{2GR^2}{(1 + 2G\,R^2\,\Lambda_2)^2}\, s_{ij}^n\,\partial\Lambda_2\right] \\ &+ \frac{3}{DW}\left[\frac{1}{1 - \frac{1}{W}(\bar{\epsilon}_v^p - \Lambda_2)}\right]\partial\Lambda_2 + \text{higher order terms} \quad .\end{aligned} \tag{5.53c}$$

If we neglect the higher order terms, we are essentially linearising the hardening law at the beginning of the iteration. This leads to a predictor which is not consistent with the corrector algorithm, and thus results in a loss of the quadratic convergence rate. Inclusion of the higher order terms however, will require special numerical treatment which is not dealt with in this thesis.

Equation (5.53c) can now be rewritten as

$$-3K\,\partial\epsilon_v - 9K\,\partial\Lambda_2 + \frac{3}{DW}\left[\frac{1}{1 - \frac{1}{W}(\bar{\epsilon}^p_v - \Lambda_2)}\right]\partial\Lambda_2 + R^2\, s^n_{ij}\left[\frac{2G}{(1 + 2G\,R^2\,\Lambda_2)}\,\delta_{ij}\delta_{kl}\partial e_{kl} - \frac{2GR^2}{(1 + 2G\,R^2\,\Lambda_2)^2}\, s^n_{ij}\,\partial\Lambda_2\right] = 0. \tag{5.54a}$$

It follows from the stresses that the increments are

$$\partial s_{ij} = \left(\frac{2G}{(1 + 2G\,R^2\,\Lambda_2)}\right)\delta_{ij}\delta_{kl}\,\partial e_{kl} - \frac{2GR^2}{(1 + 2G\,R^2\,\Lambda_2)}\, s^n_{ij}\,\partial\Lambda_2 \tag{5.54b}$$

and

$$\partial\sigma_m = K\,\partial\epsilon_v + 3K\,\partial\Lambda_2 \quad . \tag{5.54c}$$

We write $\partial\Lambda_2$ in terms of ∂e_{kl} and $\partial\epsilon_v$ in equation (5.54a), and then substitute this expression into equations (5.54b) and (5.54c). The result is

$$\partial s_{ij} = \frac{2G}{(1 + 2G\,R^2\,\Lambda_2)}\,\delta_{ij}\delta_{kl}\,\partial e_{kl} - \frac{2GR^2}{(1 + 2G\,R^2\,\Lambda_2)}\, s^n_{ij}\left[\frac{-3K}{C}\,\partial\epsilon_v + \frac{R^2\,2G\,s^n_{kl}}{C(1 + 2GR^2\,\Lambda_2)}\,\partial e_{kl}\right] \tag{5.55a}$$

and

$$\partial\sigma_m = K\,\partial\epsilon_v + 3K\left[\frac{-3K}{C}\,\partial\epsilon_v + \frac{R^2\,2G}{C(1 + 2GR^2\,\Lambda_2)}\,\partial e_{ij}\right] \quad , \tag{5.55b}$$

where $$C = \left[9K + \frac{2GR^4\, s^n_{ij}\, s^n_{ij}}{1 + 2G\,R^2\,\Lambda_2} - \frac{3}{DW}\left(\frac{1}{1 - \frac{1}{W}(\bar{e}^p_v - 3\Lambda_2)}\right)\right] .$$

It follows that

$$\frac{\partial s_{ij}}{\partial e_{kl}} = M\,\delta_{ij}\delta_{kl} - \frac{R^4\,M^4}{C}\,E_{ij}\,E_{kl} \qquad (5.56a)$$

$$\frac{\partial s_{ij}}{\partial \epsilon_v} = \frac{3K\,R^2\,M^2}{C}\,E_{ij} \qquad (5.56b)$$

$$\frac{\partial \sigma_m}{\partial e_{kl}} = \frac{3K\,R^2\,M^2}{C}\,E_{ij} \qquad (5.56c)$$

$$\frac{\partial \sigma_m}{\partial \epsilon_v} = \left[K - \frac{9K^2}{C}\right] \quad , \qquad (5.56d)$$

where $M = \left(\frac{2G}{(1 + 2G\,R^2\,\Lambda_2)}\right)$. In matrix form this is

$$\frac{\partial \underset{\sim}{s}}{\partial \underset{\sim}{e}} = \begin{bmatrix} Q+SE_{11}E_{11} & SE_{11}E_{22} & SE_{11}E_{12} & SE_{11}E_{33} & PE_{11} \\ SE_{22}E_{11} & Q+SE_{22}E_{22} & SE_{22}E_{12} & SE_{22}E_{33} & PE_{22} \\ SE_{12}E_{11} & SE_{12}E_{22} & Q+SE_{12}E_{12} & SE_{12}E_{33} & PE_{12} \\ SE_{33}E_{11} & SE_{33}E_{22} & SE_{33}E_{12} & Q+SE_{33}E_{33} & PE_{33} \\ YE_{11} & YE_{22} & YE_{12} & YE_{33} & Z \end{bmatrix} , \qquad (5.57)$$

where $Q = M$

$$S = -\frac{R^4\,M^4}{C}$$

$$P = \frac{3K\,M^2R^2}{C}$$

$$Y = P$$

and $$Z = \left[K - \frac{9K^2}{C}\right] .$$

5.3.2.3 Mode 3 active The stresses at the end of the step are

$$s_{ij}^{n} = \frac{18\alpha^2 K\, e^{*} - 3\alpha\, K\, \epsilon^{*} + k}{(G + 9\alpha^2 K)e^{*}}\, G(e_{ij}^{n} - e_{ij}^{p(n-1)})$$

$$\sigma_{m}^{n} = \frac{G\, K\, \epsilon^{*} - 6G\alpha\, K\, e^{*} + 3\alpha\, Kk}{(G + 9\alpha^2 K)}$$

It can easily be verified that

$$\frac{\partial s_{ij}}{\partial e_{kl}} = \frac{(18\alpha^2 K\, e^{*} - 3\alpha\, K\, \epsilon^{*} + k)G}{(G + 9\alpha^2 K)e^{*}}\, \delta_{ij}\delta_{kl} + \frac{(3\alpha\, K\, \epsilon^{*} - k)G}{2(G + 9\alpha^2 K)e^{*3}}\, E_{ij}\, E_{kl} \qquad (5.58a)$$

$$\frac{\partial s_{ij}}{\partial \epsilon_{v}} = -\frac{3\alpha\, KG}{(G + 9\alpha^2 K)e^{*}}\, E_{ij} \qquad (5.58b)$$

$$\frac{\partial \sigma_{m}}{\partial e_{kl}} = -\frac{3\alpha\, KG}{(G + 9\alpha^2 K)e^{*}}\, E_{kl} \qquad (5.58c)$$

$$\frac{\partial \sigma_{m}}{\partial \epsilon_{v}} = -\frac{GK}{G + 9\alpha^2 K} \qquad (5.58d)$$

and the matrix of equation (5.57) is recovered with

$$Q = \frac{18\alpha^2 K\, e^{*} - 3\alpha\, K\, \epsilon^{*} + k}{(G + 9\alpha^2 K)e^{*}}$$

$$S = \frac{(3\alpha\, K\, \epsilon^{*} - k)G}{2(G + 9\alpha^2 K)e^{*3}}$$

$$P = -\frac{3\alpha\, KG}{(G + 9\alpha^2 K)e^{*}}$$

$$Y = P$$

and $$Z = \frac{GK}{G + 9\alpha^2 K}$$

5.3.2.4 Mode 4 active The stresses at the end of the step are

$$s^n_{ij} = \frac{2e^*(1 - \Lambda_1)}{2e^*(1 + 2G\,R^2\,\Lambda_2)}\,2G(e^n_{ij} - e^{p(n-1)}_{ij})$$

$$\sigma^n_m = K(\epsilon^n_v - \epsilon^{p(n-1)}_v) - 3K\alpha\Lambda_1 + 3K\,\Lambda_2 \quad ,$$

where

$$\phi^n_1 = 0 = \frac{(1 - \frac{\Lambda_1}{2e^*})}{(1 - 2G\,R^2\,\Lambda_2)}\,2Ge^* + 3\alpha(K\,\epsilon^* - 3\alpha\,K\,\Lambda_1 + 3K\,\Lambda_2) - k \tag{5.59a}$$

$$\phi^n_2 = 0 = -\,3(K\,\epsilon^* - 3\alpha\,K\,\Lambda_1 + 3K\,\Lambda_2) + R^2\left[\frac{(1 - \frac{\Lambda_1}{2e^*})2G}{(1 - 2G\,R^2\,\Lambda_2)}\right]^2 e^* + \frac{1}{D}\ln\,(1 - \frac{1}{W}(\dot{\epsilon}^p_v + 3\alpha\,\Lambda_1 - \Lambda_2)) \tag{5.59b}$$

Following the same argument used in the case of mode 2 when it is active, we write ϕ^n_1 and ϕ^n_2 as Taylor's series expansions about the solution field at the end of the previous iteration. Once again, by neglecting second and higher order terms, it follows that

$$\partial\phi_1 = 0 = b_{11}\,\partial e_{kl} + b_{12}\,\partial\epsilon_v - a_{11}\,\partial\Lambda_1 - a_{12}\,\partial\Lambda_2 \tag{5.60}$$

$$\partial\phi_2 = 0 = b_{21}\,\partial e_{kl} + b_{22}\,\partial\epsilon_v - a_{21}\,\partial\Lambda_1 - a_{22}\,\partial\Lambda_2 \quad , \tag{5.61}$$

where

$$b_{11} = \frac{M}{2e^*}\,E_{ij}$$

$$b_{12} = 3\alpha\,K$$

$$a_{11} = 9\alpha^2\,K + \frac{M}{2}$$

$$a_{12} = -\,9\alpha K + M^2 R^2\left(1 - \frac{\Lambda_1}{2e^*}\right)e^{*2}$$

$$b_{21} = R^2 M^2\left(1 - \frac{\Lambda_1}{2e^*}\right)(E_{ij})$$

$$b_{22} = -\,3K$$

$$a_{21} = a_{12} + \frac{3\alpha}{DW}\left[\frac{1}{1 - \frac{1}{W}(\dot{\epsilon}_v^p + 3\alpha\Lambda_1 - 3\Lambda_2)}\right]$$

$$a_{22} = 9K + 2R^4M^3\left(1 - \frac{\Lambda_1}{2e^*}\right)^2 e^{*2} - \frac{3}{DW}\left[\frac{1}{1 - \frac{1}{W}(\dot{\epsilon}_v^p + 3\alpha\Lambda_1 - 3\Lambda_2)}\right]$$

and $$M = \left[\frac{2G}{(1 + 2G\,R^2\,\Lambda_2)}\right] .$$

From the stresses we note that

$$\partial s_{ij} = M\,\delta_{ij}\delta_{kl}\,\partial e_{kl} - \frac{M}{2e^*}E_{ij}\,\partial\Lambda_1 - M^2R^2\left(1 - \frac{\Lambda_1}{2e^*}\right)E_{ij}\,\partial\Lambda_2 \qquad (5.62a)$$

$$\partial\sigma_m = K\,\partial\epsilon_v - 3\alpha K\,\partial\Lambda_1 + 3K\,\partial\Lambda_2 \quad . \qquad (5.62b)$$

From equations (5.60) and (5.61) we evaluate

$$\partial\Lambda_1 = \frac{a_{22}\,b_1 - a_{12}\,b_2}{a_{11}\,a_{22} - a_{12}\,a_{21}} \qquad (5.63a)$$

$$\partial\Lambda_2 = \frac{a_{11}\,b_2 - a_{21}\,b_1}{a_{11}\,a_{22} - a_{12}\,a_{21}} \quad , \qquad (5.63b)$$

where

$$b_1 = b_{11}\,\partial e_{kl} + b_{12}\,\partial\epsilon_v$$

$$b_2 = b_{21}\,\partial e_{kl} + b_{22}\,\partial\epsilon_v \quad ,$$

and then substitute these values into equation (5.62).

The matrix in equation (5.57) can be evaluated in the same way as before, and it is easily verified that

$$Q = M$$

$$S = -\frac{1}{d}\left\{\left(\frac{M}{2e^*} + \alpha M^2R^2L\right)\left[\frac{9\ K\ M}{2e^*} + 9\alpha\ K\ M^2R^2L - \frac{3M}{2e^*DW}\left(\frac{1}{1 - \frac{1}{W}(\bar{\epsilon}^p_v + 3\alpha\ \Lambda_1 - 3\Lambda_2)}\right)\right]\right\}$$

$$P = \frac{9\alpha\ K\ M}{dDW}\left(\frac{1}{2e^*} + \alpha MR^2L\right)\left(\frac{1}{1 - \frac{1}{W}(\bar{\epsilon}^p_v + 3\alpha\ \Lambda_1 - 3\Lambda_2)}\right)$$

$$Y = 0$$

$$Z = K - \frac{9\ K^2}{d}\ (\alpha^2 a_{22} + \alpha(a_{12} + a_{21}) + a_{11})$$

with

$$d = a_{11}a_{22} - a_{12}a_{21}$$

and

$$L = \left(1 - \frac{\Lambda_1}{2e^*}\right) .$$

5.3.2.5 Mode 5 active The stresses in this case are written explicity as

$$s^n_{ij} = \frac{2e^* - \Lambda_1}{2\ e^*}\ 2G(e^n_{ij} - e^{p(n-1)}_{ij})$$

$$\sigma^n_m = K(\epsilon^n_v - \epsilon^{p(n-1)}_v) - 3\alpha\ K\ \Lambda_1 + 3K\ \Lambda_3$$

with $\Lambda_1 = \frac{1}{G}\ (2G\ e^* - k + \alpha T)$

$$\Lambda_3 = \frac{1}{G}\ ((G + 9\alpha^2 K)(3\ K\ \epsilon^* - T) - \alpha(2G\ e^* + 3\alpha\ K\ \epsilon^* - k)) \quad ,$$

and hence

$$\frac{\partial s_{ij}}{\partial e_{kl}} = \frac{(k - \alpha T)}{e^*}\ \delta_{ij}\delta_{kl} - \frac{(k - \alpha T)}{2e^{*3}}\ E_{ij}\ E_{kl} \qquad (5.64a)$$

$$\frac{\partial s_{ij}}{\partial \epsilon_v} = 0 \qquad (5.64b)$$

$$\frac{\partial \sigma_m}{\partial e_{kl}} = 0 \qquad (5.64c)$$

$$\frac{\partial \sigma_m}{\partial \epsilon_v} = 0 \quad . \qquad (5.64d)$$

The matrix in equation (5.57) follows with

$$Q = \frac{k - \alpha T}{e^*}$$

$$S = - Q/2\ e^{*2}$$

$$P = 0$$

$$Y = 0$$

and $Z = 0$.

5.3.2.5 Mode 6 active The stresses are

$$s_{ij}^n = 2G(\epsilon_{ij}^n - \epsilon_{ij}^{p(n-1)})$$
$$\sigma_m^n = T/3 \quad ,$$

and hence

$$\frac{\partial s_{ij}}{\partial e_{kl}} = 2G\ \delta_{ij}\delta_{kl} \qquad (5.65a)$$

$$\frac{\partial s_{ij}}{\partial \epsilon_v} = 0 \qquad (5.65b)$$

$$\frac{\partial \sigma_m}{\partial e_{kl}} = 0 \qquad (5.65c)$$

$$\frac{\partial \sigma_m}{\partial \epsilon_v} = 0 \quad . \tag{5.65d}$$

The constants for the matrix in equation (5.57) are

$$Q = 2G$$

$$S = 0$$

$$P = 0$$

$$Y = 0$$

and $$Z = 0 \quad .$$

Note that when yielding occurs on the cap, the nonlinear hardening law is linearised. This linearisation essentially takes place at the beginning of the iteration, and the resulting predictor is therefore not truly consistent with the backward difference corrector algorithm.

5.3.2.7 Drucker-Prager yield condition The stresses are the same when mode 3 is active for the cap model. The constants for the matrix in equation (5.57) are the same as those described in Section (5.3.3.3), namely

$$Q = \frac{18\alpha^2 K\, e^* - 3\alpha\, K\, \epsilon^* + k}{(G + 9\alpha^2 K)e^*} G$$

$$S = \frac{(3\alpha\, K\, \epsilon^* - k)G}{2(G + 9\alpha^2 K)e^{*3}}$$

$$P = - \frac{3\alpha\, KG}{(G + 9\alpha^2 K)e^*}$$

$$Y = P$$

and $$Z = \left(\frac{GK}{G + 9\alpha^2 K}\right) \quad .$$

5.3.3.8 Von Mises Yield Condition (Elastic, Perfectly Plastic) Since this yield condition is effectively the Drucker-Prager yield condition with $\alpha = 0$, the constants are simply

$$Q = \frac{k}{e^*}$$

$$S = -\frac{k}{2e^{*3}}$$

$$P = 0$$

$$Y = 0$$

and $$Z = K \quad .$$

5.4 PLANE STRESS CONSIDERATIONS

We have presented the backward difference corrector in generalised three dimensional strain space. We have formulated the consistent tangent predictor by making the assumption that the out of plane shear terms

$$E_{23} = E_{32} = E_{13} = E_{31} = 0 \quad . \tag{5.66}$$

Using plane strain or axisymmetric considerations, the components of the matrix in equation (5.57) can easily be obtained. The predictor described can thus be applied without modification to the iterative process. In the case of plane stress however, the terms may not be easily obtained for certain yield criteria, and the predictor will then have to be modified to impose the zero condition for the out of plane stress.

5.4.1 Backward Difference Corrector for the von Mises yield condition

The stress at the end of the n-th step for an elastic perfectly plastic yield condition is given by

$$s_{ij}^{n} = \left(\frac{k}{2G\ e^{*}}\right) 2G\ (e_{ij}^{n} - e_{ij}^{p(n-1)}) \qquad (5.67a)$$

$$\sigma_{m}^{n} = K\ \epsilon_{v} \quad . \qquad (5.67b)$$

We enter the corrector phase without having a predicted value for the out of plane strain value $\epsilon_{33}^{e} = \epsilon_{33}^{n} - \epsilon_{33}^{p(n-1)}$, and hence the parameter $\frac{k}{2G\ e^{*}}$ cannot be determined exactly. We make use of the plane stress constraint that $\sigma_{33} = 0$ and employ an iterative scheme to evaluate $\frac{k}{2G\ e^{*}}$. This is described below, and for the first iteration it is assumed that the material point is elastic. We evaluate

$$\epsilon_{33}^{e} = -\frac{C_1}{C_2}(\epsilon_{11}^{e} + \epsilon_{22}^{e}) \quad , \qquad (5.68)$$

with $$C_1 = 4/3\ A^{(i)}\ G + K \quad , \qquad (5.69a)$$

$$C_2 = 2/3\ A^{(i)}\ G + K \quad , \qquad (5.69b)$$

where $A^{(i)} = \frac{k}{2G\ e^{*}}$, ($A^{(1)} = 1$ since it is assumed to be elastic)

in order to obtain an estimate ${}^{(1)}\epsilon_{33}$, which then enables us to evaluate ${}^{(1)}e^{*}$. The parameter

$$A^{(2)} = \frac{k}{2G\ e^{*(1)}}$$

can be computed in readiness for the second iteration. $A^{(i)}$ decreases monotonically, and we use the Aitken acceleration technique to speed up the convergence by taking three consecutive values of $A^{(i)}$ and predicting A^{*}, where

$$A^{*} = A^{(i)} - \frac{(A^{(i)} - A^{(i+1)})^2}{(A^{(i)} - 2A^{(i+1)} + A^{(i+2)})} \quad . \qquad (5.70)$$

The difference between two consecutive values of $A^{(i)}$ is used as a check on convergence. A series of Aitken accelerations can be performed, but generally, one or two should be sufficient for most cases.

5.4.2 Predictors for Plane stress

The elastic-plastic predictor is determined as in Section 5.3.3.8. In matrix form we have

$$\begin{Bmatrix} \sigma_{11} \\ \sigma_{22} \\ \sigma_{12} \\ \sigma_{33} \end{Bmatrix} = \begin{bmatrix} D_{11}^{ep} & D_{12}^{ep} & 0 & D_{14}^{ep} \\ D_{21}^{ep} & D_{22}^{ep} & 0 & D_{24}^{ep} \\ 0 & 0 & D_{33}^{ep} & 0 \\ D_{41}^{ep} & D_{42}^{ep} & 0 & D_{44}^{ep} \end{bmatrix} \begin{Bmatrix} \epsilon_{11} \\ \epsilon_{22} \\ \epsilon_{12} \\ \epsilon_{33} \end{Bmatrix} . \qquad (5.71)$$

By imposing the condition that $\sigma_{33} = 0$, we can write

$$D_{41}\epsilon_{11} + D_{42}\epsilon_{22} + D_{44}\epsilon_{33} = 0 \quad , \qquad (5.72a)$$

and hence it follows that

$$\epsilon_{33} = -\frac{1}{D_{44}} (D_{41}\epsilon_{11} + D_{42}\epsilon_{22}) \quad . \qquad (5.72b)$$

We can now rewrite equation (5.71) (leaving out the row and column involving out of plane stress and strain) as :

$$\begin{Bmatrix} \sigma_{11} \\ \sigma_{22} \\ \sigma_{12} \end{Bmatrix} = \begin{bmatrix} \left(D_{11} - \frac{D_{41}}{D_{44}}\right) & \left(D_{12} - \frac{D_{42}}{D_{44}}\right) & 0 \\ \left(D_{21} - \frac{D_{41}}{D_{44}}\right) & \left(D_{22} - \frac{D_{42}}{D_{44}}\right) & 0 \\ 0 & 0 & D_{33} \end{bmatrix} \begin{Bmatrix} \epsilon_{11} \\ \epsilon_{22} \\ \epsilon_{12} \end{Bmatrix} .$$

Note that this matrix is only symmetrical when $D_{41} = D_{42}$.

5.5 NUMERICAL EXAMPLES

We will consider a number of examples in this section to illustrate the effectiveness of the backward difference algorithm with a consistent predictor.

5.5.1 Thin Plate with Two Materials

Details of this problem are given in Section 3.8.4.1 , and the results obtained using the consistent predictor are reported there. It is evident from these results that this method is both efficient and stable for the case of a von Mises yield condition.

5.5.2 Strip Footing on a Layer of Overconsolidated Clay

The problem under discussion is described in detail in Section 4.8. At this point we will be considering two material models and the performance of each.

5.5.2.1 Drucker-Prager material The material parameters are the same as those used in the previous Chapter. The solutions obtained are also the same, but what does vary is the number of iterations required to reach convergence in each increment. For the consistent predictor algorithm implemented in NOSTRUM [14], four iterations are required per increment, as opposed to the three iterations per increment required by ABAQUS. The reason for this difference is that for the first iteration of each increment in NOSTRUM the material behaviour is assumed to be elastic. The benefit of this feature would become evident in the case where cyclic loading is applied. The results for this problem are plotted below in Fig. 5.4 .

5.5.2.2 Drucker-Prager with Cap The Drucker-Prager constants are the same as those described above. The parameters required to define the cap are the cap shape factor R = 0 (vertical cap), the initial cap position σ^c_{kk} = - 46.53 psi, the limiting volumetric plastic strain W = - 0.003, the "rate" of plastic compaction D = $0.0087(\frac{1}{psi})$, and the tension cut-off value T = 82.00 psi. The convergence rate in this case is not quadratic as it generally is for consistent predictors. The reason for this is that the hardening law has been linearised at the beginning of the iteration. In this example the algorithm does not reach the limit load because numerical problems are encountered at 125 psi. The results obtained for the displacement at the centre of the footing are shown in Fig. 5.4 below.

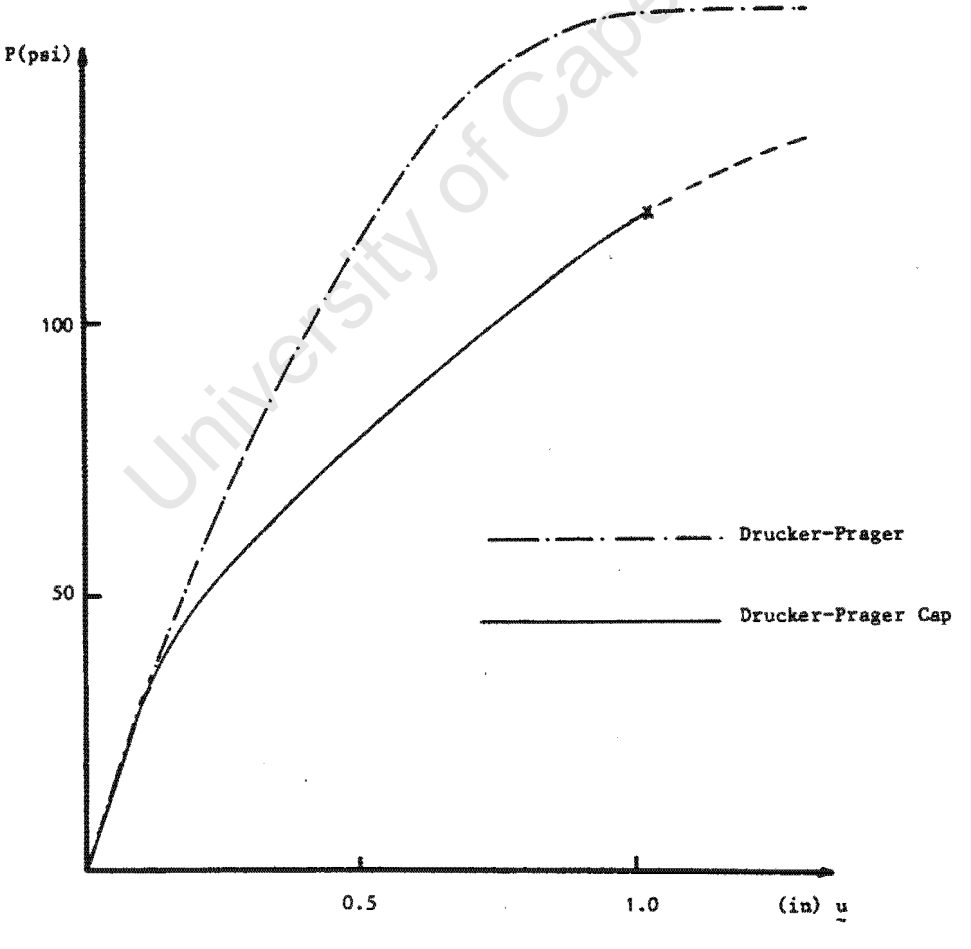

Figure 5.4 : Load vs displacement.

5.6 CONCLUSION

In this Chapter we have formally presented the backward difference corrector algorithm which is essentially used throughout this thesis. In the case of the von Mises yield condition, the backward difference method is simply the radial return algorithm. A consistent predictor has been derived for the backward difference algorithm, and three yield conditions in particular, have been discussed. They are the von Mises, Drucker-Prager, and Drucker-Prager cap yield conditions. The numerical examples which are solved reveal that the rate of convergence for this combination of predictor and corrector is in general quadratic. The cap model however, proves to be an exception when yielding occurs on the nonlinear hardening cap since the predictor in this case is not consistent.

CHAPTER 6

A FINITE ELEMENT FORMULATION FOR THE CONSOLIDATION OF POROUS MEDIA

6.1 BRIEF LITERATURE REVIEW AND OUTLINE OF FORMULATION

In this survey we discuss the development of consolidation theory in the finite element context. The three dimensional theory of Biot [21] can be regarded as the common starting point for all the early finite element formulations for consolidation.

There are essentially two methods of approach. The first is to consider and solve the mechanical and seepage problems separately. This is the method adopted by Christian and Boehmer [22] who used finite elements for the solution of the mechanical problem, a finite difference method for the solution of the seepage problem, and an Euler forward integration scheme to map the transient response. The second was suggested by Sandhu and Wilson [23]. They included the continuity of the pore fluid together with the equilibrium and compatibility for the mechanical problem in a single functional. Many researchers essentially use the basic formulation proposed by Sandhu and Wilson and then make minor adaptions in order to suit individual needs [24-29].

Most researchers assumed the material behaviour to be linear elastic [24-26] until the beginning of the decade . In recent years the thrust has been to include both material and geometric nonlinearities [27-29]. The most recent work in this field has been the development of special purpose elements to cope with rapidly changing pore pressures at free boundaries [30].

In this chapter we are concerned with the development of a formulation for consolidation which can be easily implemented in a finite element code. The emphasis in particular is on making the formulation compatible with the Drucker-Prager cap model discussed in the previous chapter since this model represents the behaviour of a consolidating soil very well. The approach is similar to that of Christian and Boehmer where the mechanical response and fluid flow are considered separately. At any instant in time, as discussed in Chapter 2, the mechanical problem is essentially quasi-static with an imposed volumetric (migration) strain measuring the amount of pore fluid that has migrated to or from an element of soil. The pore pressures evaluated in the mechanical problem are substituted into the seepage equation yielding flow rates. These equations are coupled by means of a backward difference integration scheme to map the transient response.

6.2 FORMULATION OF THE MECHANICAL PROBLEM

For this formulation it is assumed that the soil is saturated and that the pore fluid is incompressible. We have previously defined the migration water strain as

$$\epsilon_w = \frac{dV_w}{V_o} \qquad (6.1)$$

Since the fluid phase of the soil is capable of transmitting hydrostatic stresses only, it will be necessary to consider the fluid phase and the soil skeleton separately. This is achieved by the definition of the effective stress,

$$\sigma_{ij} = \sigma'_{ij} + p\,\delta_{ij} \qquad (6.2)$$

where σ_{ij} is the total stress tensor,

σ'_{ij} is the effective stress tensor,

δ_{ij} is the Kronecker delta,

and p is the hydrostatic pressure in the pore fluid.

This definition holds true in incremental terms, and equation (6.2) can be rewritten as

$$\Delta\sigma_{ij} = \Delta\sigma'_{ij} + \Delta p\ \delta_{ij} \quad . \tag{6.3}$$

The elastic-plastic constitutive equations of the soil skeleton involve the effective stress tensor, and the contribution of stress from the pore fluid can be considered to overlay the hydrostatic stress in the soil skeleton. The effective stress increment can be related to the strain increment by means of a tangent stiffness modulus,

$$\Delta\sigma'_{ij} = D^{ep}_{ijkl}\Delta\epsilon_{kl} \quad , \tag{6.4}$$

where D^{ep}_{ijkl} depends on the current state of the material.

Incremental equilibrium and compatibility conditions, in terms of total stress increments must also be observed:

$$\frac{\partial\Delta\sigma_{ij}}{\partial x_j} + \Delta F_i = 0 \qquad \text{on } V \ , \tag{6.5a}$$

$$\Delta\sigma_{ij}\ \nu_i = \Delta T_j \qquad \text{on part of the boundary } S_T \ , \tag{6.5b}$$

$$\Delta\epsilon_{ij} = \frac{1}{2}\left(\frac{\partial\Delta u_i}{\partial x_j} + \frac{\partial\Delta u_j}{\partial x_i}\right) \ , \tag{6.5c}$$

$$\Delta u_i = \Delta\bar{u}_i \quad \text{on the remainder of the boundary } S_u \ , \tag{6.5d}$$

where x_i is the position vector,

ν_i is the outward normal to the surface,

T_j is the surface traction,

F_i is the body force,

u_i is the displacement vector,

$\bar{u}_i$ is the prescribed displacement,

and V is the volume of the body.

It follows from the incompressibility of the pore fluid that the volumetric strain is constrained to be ϵ_w, and hence

$$\Delta u_{i,i} = \Delta \epsilon_w \tag{6.6}$$

for the porous medium. A solution to the incremental problem which satisfies equations (6.4),(6.5), and (6.6) can be obtained by minimising the augmented potential energy functional

$$U_p^A = \frac{1}{2}\int_V \Delta\sigma'_{ij}\Delta\epsilon_{ij}dV + \int_{S_T}\Delta T_i\Delta u_i dS + \int_V \Delta F_i \Delta u_i dV + \int_V \zeta(\Delta u_{i,i} - \Delta\epsilon_w)dV \quad , \tag{6.7}$$

where ζ is a Lagrange multiplier which, upon evaluation, turns out to be the increment in pore pressure Δp [1]. Equation (6.7) can thus be written as

$$U_p^A = \frac{1}{2}\int_V \Delta\sigma'_{ij}\Delta\epsilon_{ij}dV + \int_{S_T}\Delta T_i\Delta u_i dS + \int_V \Delta F_i \Delta u_i dV + \int_V \Delta p(\Delta u_{i,i} - \Delta\epsilon_w)dV \quad . \tag{6.8}$$

In the finite element formulation, Δu_i, $\Delta\epsilon_w$, and Δp are discretised and we define

$$p = [N^p]\ \underset{\sim}{p} \quad , \tag{6.9a}$$

$$\epsilon_w = [N^p]\ \underset{\sim}{\epsilon}_w \quad , \tag{6.9b}$$

and $$u_i = [N]\ \underset{\sim}{u} \quad , \tag{6.9c}$$

where $[N]$ and $[N^p]$ are shape functions over the elements, and $\underset{\sim}{p}$, $\underset{\sim}{\epsilon}_w$, and $\underset{\sim}{u}$ are vectors of the nodal values of the respective variables. Since $\underset{\sim}{p}$ and $\underset{\sim}{\epsilon}_w$ are associated with the derivatives of displacement $\underset{\sim}{u}$, $[N^p]$ is an order lower than $[N]$.

We can denote the relation between strain and displacements as

$$\underset{\sim}{\epsilon} = [B]\ \underset{\sim}{u} \quad , \tag{6.10}$$

and $$\epsilon_w = [B_v]\ \underset{\sim}{u} \quad , \tag{6.11}$$

where the coefficients of the matrices $[B]$ and $[B_v]$ derived from $[N]$ are dependent on whether we are considering plane strain or axial symmetry [1-3]. With the stress increments related to strain increments by equation (6.4), the augmented potential energy functional in terms of discrete nodal values can be written as

$$U_p^A = \frac{1}{2}\int_V \Delta\underset{\sim}{u}^T[B]^T[D^{ep}][B]\Delta\underset{\sim}{u}\ dV + \int_{S_T} \Delta\underset{\sim}{T}^T\Delta\underset{\sim}{u}\ dS + \int_V \Delta\underset{\sim}{F}^T\Delta\underset{\sim}{u}\ dV$$
$$+ \int_V \Delta\underset{\sim}{u}^T[B_v]^T[N^p]\ \Delta\underset{\sim}{p}\ dV - \int_V \Delta\underset{\sim}{\epsilon}_w\ [N^p]^T[N^p]\ \Delta\underset{\sim}{p}\ dV \tag{6.12}$$

in terms of discrete nodal values, where $[D^{ep}]$ is the tangent stiffness matrix derived from the tangent stiffness modulus which is defined in equation (6.4).

Minimizing the above equation with respect to $\Delta\underset{\sim}{u}$ and $\Delta\underset{\sim}{p}$, we obtain the following system of equations :

$$\begin{bmatrix} K^s & H \\ H^T & 0 \end{bmatrix} \begin{Bmatrix} \Delta\underset{\sim}{u} \\ \Delta\underset{\sim}{p} \end{Bmatrix} = \begin{Bmatrix} \Delta\underset{\sim}{P} \\ \Delta\underset{\sim}{g} \end{Bmatrix} \quad , \tag{6.13}$$

where

$$[K^s] = \int_V [B]^T [D^{ep}][B]\, dV \quad ,$$

$$[H] = \int_V [B_v]^T [N^p]\, dV \quad ,$$

$$\Delta\underset{\sim}{P} = \int_{S_T} \Delta\underset{\sim}{T}\, dS + \int_V \Delta\underset{\sim}{F}\, dV \quad ,$$

$$\Delta\underset{\sim}{g} = \int_V [N^p]^T [N^p]\, dV\, \Delta\underset{\sim}{\epsilon}_w \quad ,$$

$$= [L]\, \Delta\underset{\sim}{\epsilon}_w \quad .$$

6.3 FORMULATION OF THE SEEPAGE PROBLEM

Equilibrium of forces acting on the pore fluid (Darcy's law), continuity, and incompressibility of the fluid phase lead to the governing differential equation [31],

$$k_{ij} \frac{\partial^2 p}{\partial x_i \partial x_j} = -\gamma_w \dot{\epsilon}_w \quad , \tag{6.14}$$

where k_{ij} is the permeability tensor

and γ_w is the specific weight of the pore fluid.

This is the classical statement of the seepage problem which has the boundary conditions

$$p = p_s \text{ on part of the boundary } S_p \ , \tag{6.15a}$$

$$\text{and} \quad \underset{\sim}{\nu}.\underset{\sim}{v} = \psi \text{ on the remainder of the boundary } S_v \ , \tag{6.15b}$$

where p_s is the prescribed pore pressure on the boundary,

$\underset{\sim}{v}$ is the velocity of the fluid at the boundary,

and ψ is the specified fluid flow across the boundary.

A weak statement of this problem is given by

$$\int_V q(k_{ij} \frac{\partial^2 p}{\partial x_i \partial x_j}) \, dV = - \int_V q(\gamma_w \dot{\epsilon}_w) \, dV \tag{6.16}$$

where q is some arbitrary test function which satisfies the boundary conditions. Applying Green's theorem, this equation can be rewritten as

$$\int_V [\frac{\partial q}{\partial x_i} k_{ij} \frac{\partial p}{\partial x_j}] dV + \int_{S_v} q(v_j \nu_j) dS + \int_{S_p} q(k_{ij} \frac{\partial p}{\partial x_i}) \nu_j dS = \int_V q(\gamma_w \dot{\epsilon}_w) dV \ . \tag{6.17}$$

In the finite element formulation we consider the same elements as in the mechanical problem, and we approximate p,q, and $\dot{\epsilon}_w$ by

$$\begin{aligned} p &= [N^p] \, \underset{\sim}{p} \ , \\ q &= [N^p] \, \underset{\sim}{q} \ , \\ \text{and} \quad \dot{\epsilon}_w &= [N^p] \, \underset{\sim}{\dot{\epsilon}}_w \ . \end{aligned} \tag{6.18}$$

By summing over all of the J elements in the domain, equation (6.17) can be written as

$$\underset{\sim}{q}^T \sum_{e=1}^{J} \left[\int_{V_e} \left(\left[\frac{\partial N^p}{\partial x_i}\right]^T k_{ij} \left[\frac{\partial N^p}{\partial x_j}\right] \right) dV_e + \int_{S_e - S_{ve}} [N^p]^T \left(k_{ij} \left[\frac{\partial N^p}{\partial x_i}\right] \nu_j \right) dS_e \right] \underset{\sim}{p}$$

$$= \underset{\sim}{q}^T \sum_{e=1}^{J} \left[\int_{V_e} \gamma_w [N^p]^T [N^p] \, dV_e \, \dot{\underset{\sim}{\epsilon}}_w - \int_{S_{ve}} [N^p]^T v_j \nu_j dS_e \right] \qquad (6.19)$$

where V_e is the volume of the element, S_e the surface of the element, and S_{ve} the part of S_e which coincides with S_v. Since q is arbitrary, the equation reduces to

$$\sum_{e=1}^{J} \left[[K_e] + [P_e] \right] \underset{\sim}{p} + \sum_{e=1}^{J} \underset{\sim}{f}_e = \gamma_w \sum_{e=1}^{J} \left[[L_e] \right] \dot{\epsilon}_w , \qquad (6.20)$$

where

$$[K_e] = \int_{V_e} \left[\frac{\partial N^p}{\partial x_i}\right]^T k_{ij} \left[\frac{\partial N^p}{\partial x_j}\right] dV_e ,$$

$$\underset{\sim}{f}_e = \int_{S_{ve}} [N^p]^T v_j \nu_j dS_e ,$$

$$[P_e] = \int_{S_e - S_{v_e}} [N^p]^T \left(k_{ij} \left[\frac{\partial N^p}{\partial x_i}\right] \nu_j \right) dS_e ,$$

and $$[L_e] = \int_{V_e} [N^p]^T [N^p] \, dV_e .$$

It follows from continuity considerations that $\sum_{e=1}^{J} [P_e] \underset{\sim}{p} = 0$ at interelement boundaries [32] and there is therefore no need to evaluate these zero contributions. The matrix $[P_e]$ is only evaluated if pore pressure is specified on the element boundary, and thus the global equation follows:

$$[K^w] \underset{\sim}{p} + \underset{\sim}{f} = \gamma_w [L] \dot{\epsilon}_w \qquad (6.21)$$

where $$[K^w] = \sum_{e=1}^{J} \left[[K_e] + [P_e] \right] ,$$

$$\underset{\sim}{f} = \sum_{e=1}^{J} \underset{\sim}{f}_e \quad ,$$

and $$[L] = \sum_{e=1}^{J} [L_e] \quad .$$

6.4 COUPLING THE MECHANICAL AND SEEPAGE PROBLEMS

It is necessary to introduce a time integration scheme to couple equations (6.13) and (6.21) . Using the relation $\Delta \underset{\sim}{g} = [L]\Delta \underset{\sim}{\epsilon}_w$ we can write

$$\Delta \underset{\sim}{\epsilon}_w = \int_{t_{n-1}}^{t_n} \dot{\underset{\sim}{\epsilon}}_w \, dt \quad . \tag{6.22}$$

This can be approximated as

$$\Delta \underset{\sim}{\epsilon}_w = \Delta t \, \dot{\underset{\sim}{\epsilon}}_{(n-1+\beta)} \quad , \tag{6.23}$$

where

$$\dot{\underset{\sim}{\epsilon}}_{w(n-1+\beta)} = (1-\beta) \, \dot{\underset{\sim}{\epsilon}}_{w(n-1)} + \beta \, \dot{\underset{\sim}{\epsilon}}_{w(n)} \quad , \tag{6.24}$$

with $\dot{\underset{\sim}{\epsilon}}_{w(n-1)}$ and $\dot{\underset{\sim}{\epsilon}}_{w(n)}$ being the discrete values of $\dot{\underset{\sim}{\epsilon}}_w$ at times t_{n-1} and t_n respectively. In order to be compatible with the integration of the constitutive equations, β is set to be unity and this choice is defined as the Euler backward integration scheme [2]. Rewriting equation (6.21) as

$$\dot{\underset{\sim}{\epsilon}}_w = \frac{1}{\gamma_w} [L]^{-1} \left[[K^w] \underset{\sim}{p} + \underset{\sim}{f} \right] \quad ,$$

and substituting in equation (6.24), $\Delta \underset{\sim}{g}$ becomes

$$\Delta \underset{\sim}{g} = \frac{\Delta t}{\gamma_w} \left[[K^w] (\underset{\sim}{p}_{(n-1)} + \Delta \underset{\sim}{p}) + \underset{\sim}{f} \right] \quad . \tag{6.25}$$

Substituting equation (6.25) into equation (6.13), we obtain the global set of equations

$$\begin{bmatrix} K^s & H \\ H^T & -\frac{\Delta t}{\gamma_w}[K^w] \end{bmatrix} \begin{Bmatrix} \Delta \underset{\sim}{u} \\ \Delta \underset{\sim}{p} \end{Bmatrix} = \begin{Bmatrix} \Delta \underset{\sim}{P} \\ \Delta \underset{\sim}{g}' \end{Bmatrix} , \tag{6.26a}$$

where

$$\Delta \underset{\sim}{g}' = \frac{\Delta t}{\gamma_w} [K^w] \underset{\sim}{p}_{(n-1)} + \underset{\sim}{f}_n \quad . \tag{6.26b}$$

6.5 INCREMENTAL SOLUTION PROCEDURE

The process starts off with an initial water strain field $\underset{\sim}{\epsilon}^o_w$ which will normally be zero at $t_o = 0$. The solution algorithm is then summarised as follows:

1. Time increment n - 1 → n

   1.1 Set i = 0

   1.2 Evaluate $\Delta \underset{\sim}{P}$ from the applied loads data.

   1.3 Iteration loop i = i + 1

      1.3.1 If (i = 1 and (n-1) = 0) then

      solve equation (6.13) with $\Delta \underset{\sim}{g} = [L]\ \underset{\sim}{\epsilon}^o_w$.

      Evaluate the residual forces and set $\Delta \underset{\sim}{P}$ equal to the out of balance forces.

      Go to 1.3

      1.3.2 If (i = 2 and (n-1) = 0) or (i = 1 and (n-1) ≥ 1) then

      solve equation (6.26) with $\Delta \underset{\sim}{g}' = \frac{\Delta t}{\gamma_w}[K^w]\underset{\sim}{p}_{n-1} + \underset{\sim}{f}_n$.

      Evaluate the residual forces and set $\Delta \underset{\sim}{P}$ equal to the out of balance forces.

      Check for convergence.

      If no, go to 1.3

      If yes, go to 1.4

1.3.3 If ($i \geq 3$ and $(n-1) = 0$) or ($i \geq 2$ and $(n-1) \geq 1$) then solve equation (6.26) with $\Delta \underset{\sim}{g}' = 0$.

Evaluate the residual forces, and set $\Delta \underset{\sim}{P}$ equal to the out of balance forces.

Check for convergence.

If no, go to 1.3

If yes, go to 1.4

1.4 If t_n is the last time value go to 2.

Set $n = n + 1$, go to 1.

2. Exit the increment loop.

6.6 NUMERICAL IMPLEMENTATION

The formulation presented here has been implemented in NOSTRUM to solve plane strain and axisymmetric problems. For [N] to be an order higher than $[N^p]$, nine-noded Lagrangian elements are used to approximate the displacements, and 4-noded bilinear elements approximate the pore pressure field for elements containing pore fluid. It is assumed that the soil is orthotropic with respect to its permeability, and hence we set $k_{ij} = 0$ for $i \neq j$.

For the purpose of modelling the response of the soil skeleton, the linear model or any of the plasticity models described in the previous Chapters are available. The Drucker-Prager cap model best represents the volumetric behaviour of the consolidating soil [20], and its relevance to this formulation can be appreciated.

A simple dynamic time-stepping algorithm which increases the time step length Δt during the solution procedure has been included. Each time increment is set to

$$\Delta t_n = \theta \, \Delta t_{n-1} \quad , \tag{6.27}$$

where θ is the time increment multiplier. The choice of Δt_o and θ will determine the discrete time values of the solution procedure.

6.7 NUMERICAL EXAMPLES

In order to illustrate the effectiveness of the algorithm, a series of examples is presented. The results are compared with available closed form solutions, examples drawn from literature, and the numerical results obtained using ABAQUS [8].

6.7.1 One dimensional consolidation

The simplest case of consolidation is the one dimensional problem in which the total stress is constant with time, and drainage occurs at the top of the consolidating stratum of depth H. Under these conditions a closed form solution, which is used for comparison with the numerical solutions, can be obtained [33]. This problem can be modelled by using a vertical strip of plane strain elements which are restrained horizontally. The drainage is effected by setting the pore pressure to zero at the top of the strip where a uniform pressure is applied. This pressure P_o is applied instantaneously at t=0 and kept constant throughout the analysis. The finite element mesh and the boundary conditions are shown in Fig. 6.1(a) . The load and material parameters used in the linear analysis are as follows:

$P_o = 47997,$

$E = 287400,$

$\nu = 0.4,$

and $k_{11} = k_{22} = 1.22 \times 10^{-4}.$

We define the dimensionless time factor

$$T_{v1} = \frac{C_{v1}}{H^2} \times t \quad -,$$

where

$$C_{v1} = \frac{E(1-\nu)}{(1+\nu)(1-2\nu)} \frac{k_{11}}{\gamma_w}$$

is the coefficient of consolidation. The numerical subscript refers to the dimension of the coefficient.

Additional parameters required for the cap model are as follows :

$k = 12000,$

$\alpha = 0.11,$

$R = 0.0,$

$\sigma_m'^o = -30000,$

$W = -0.07,$

and $D = -3 \times 10\text{-}5.$

Fig. 6.1(b) shows the pore pressure profiles for the analytical and numerical solutions at discrete time intervals. In Figs. 6.1(c) and 6.1(d) the pore pressures are plotted against time, and in Fig. 6.1(e) displacements at the surface and in the centre of the layer are plotted against T_v.

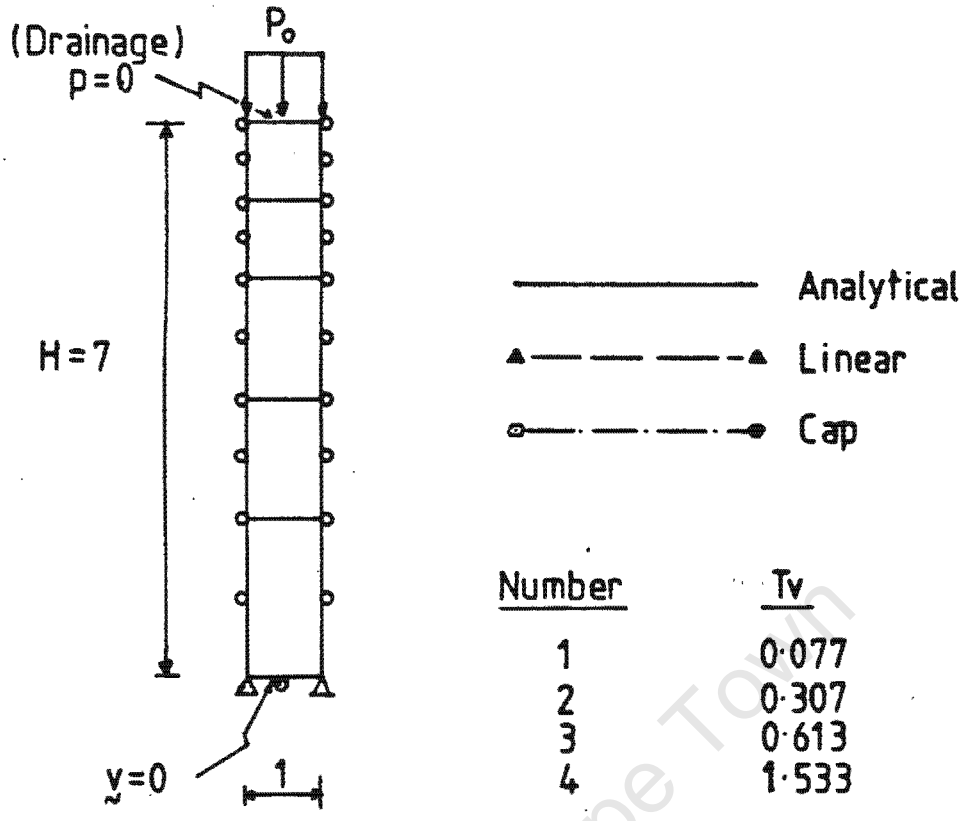

Figure 6.1(a) : One-dimensional consolidation.

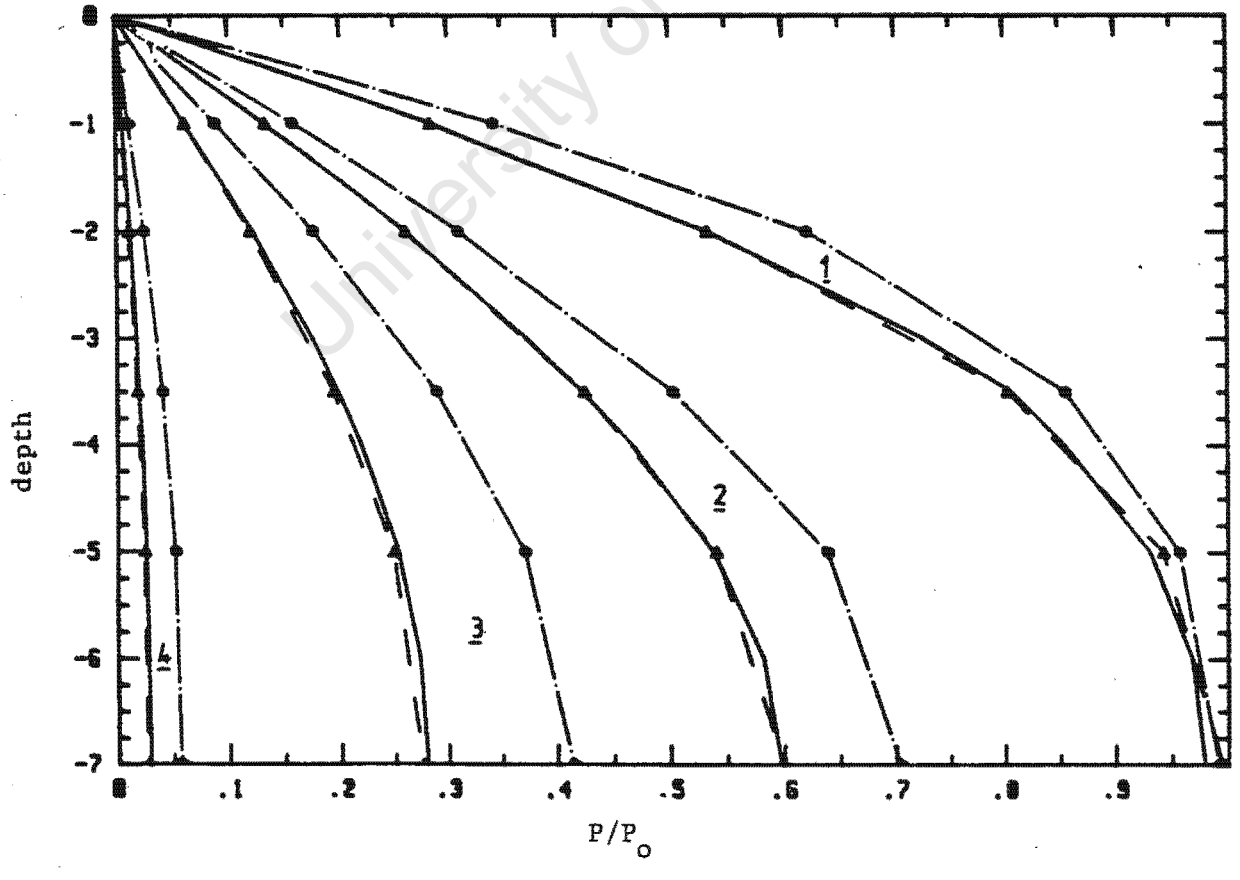

Figure 6.1(b) : Pore pressure vs depth.

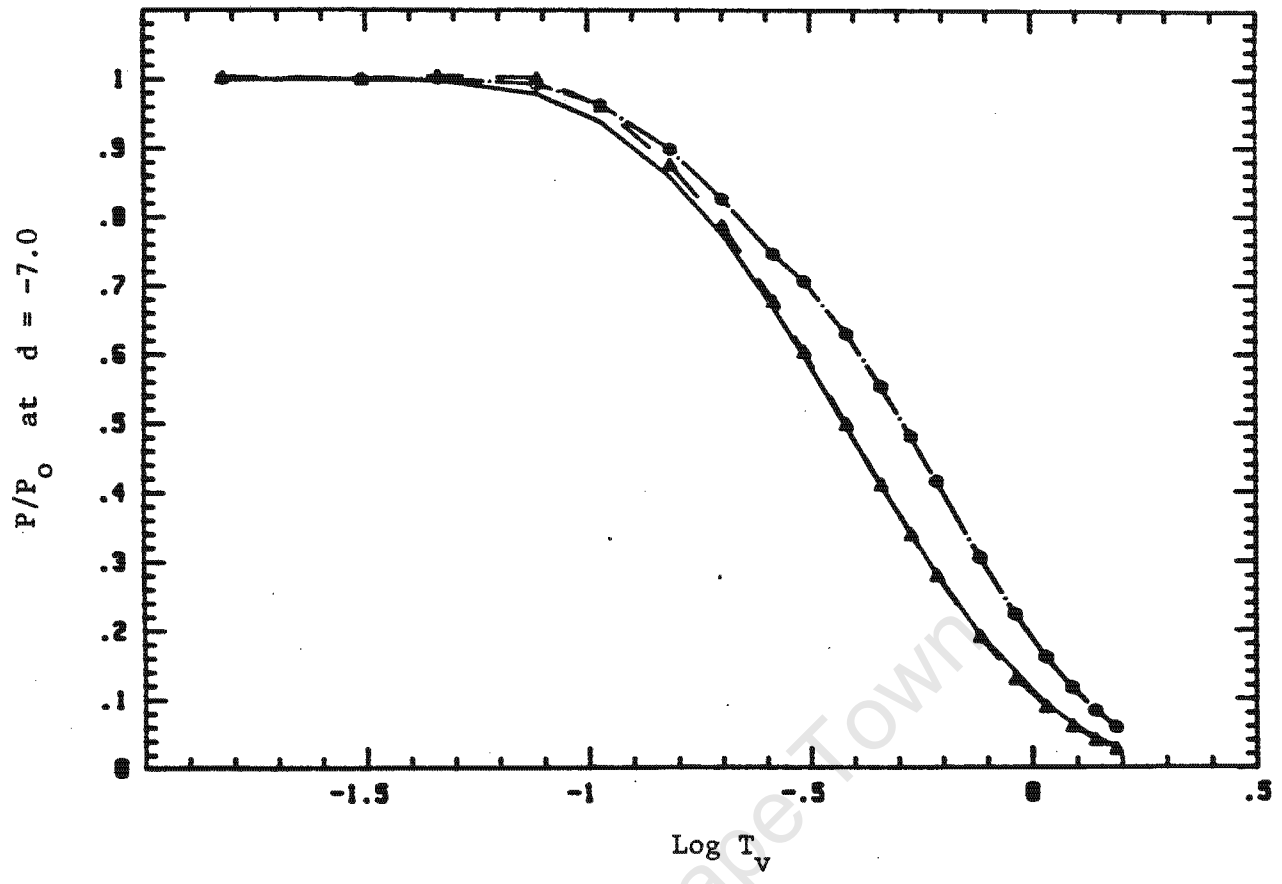

Figure 6.1(c) : Pore pressure vs time.

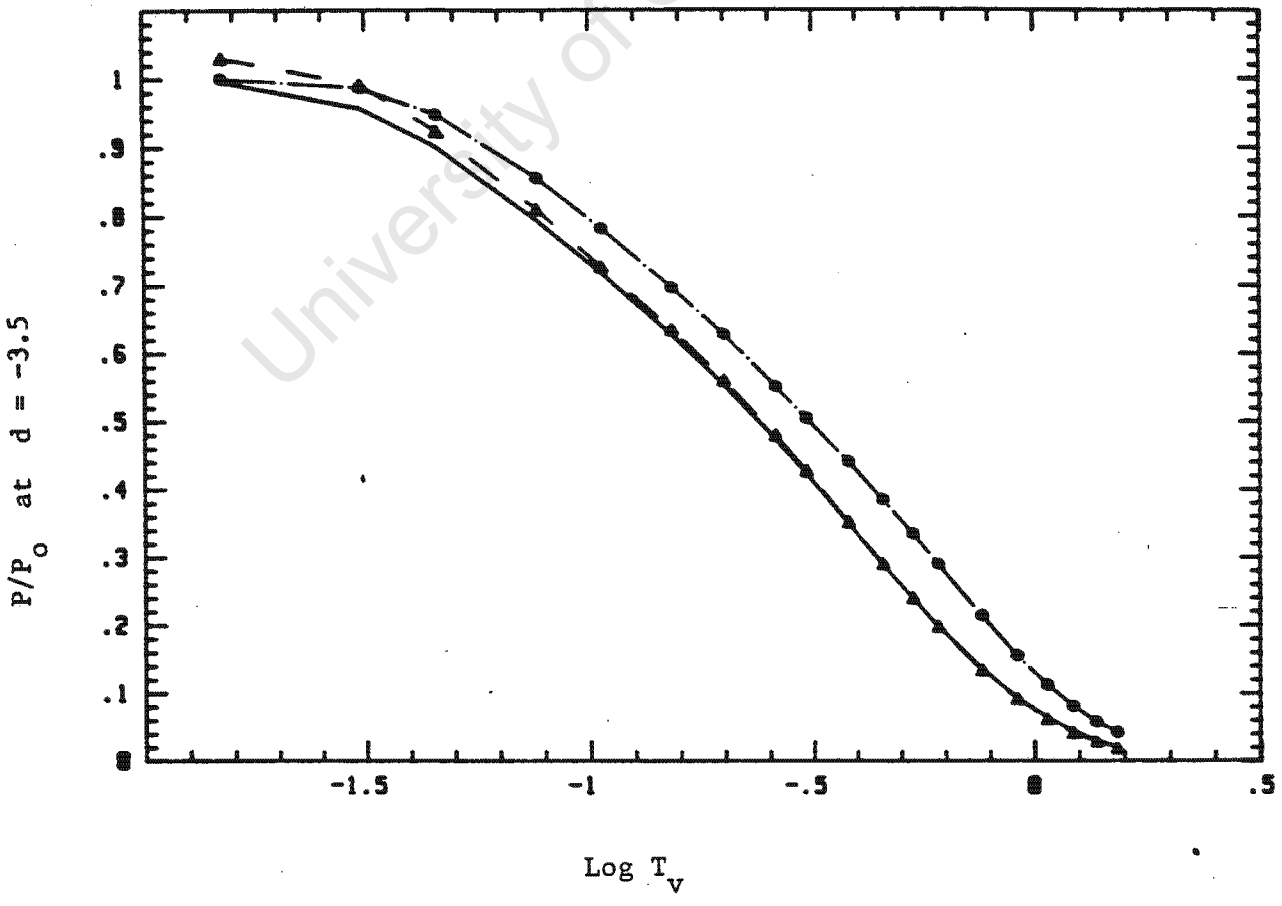

Figure 6.1(d) : Pore pressure vs time.

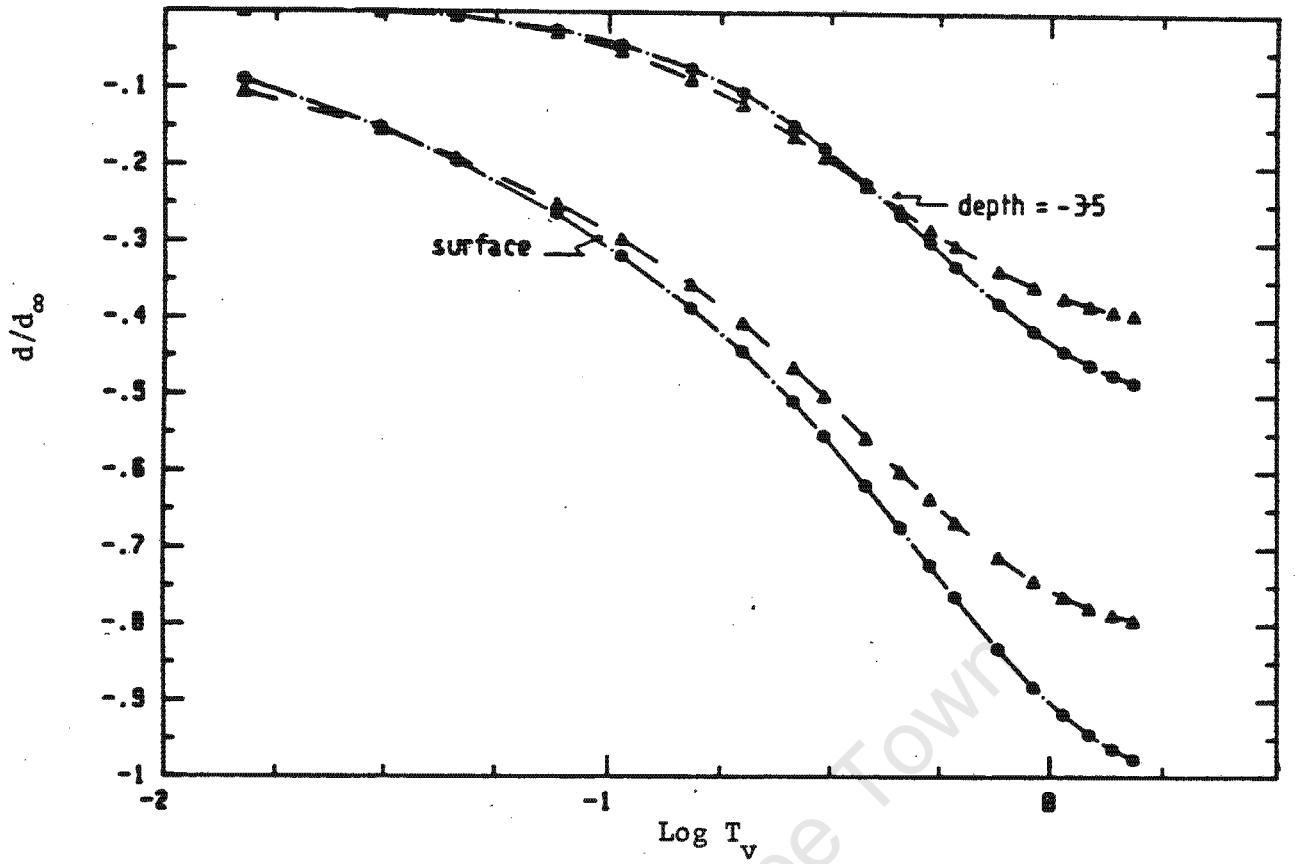

Note: d_∞ = drained displacement at the surface (Cap model)

Figure 6.1(e) : Displacement vs time.

In general, the numerical solutions compare very favourably with the analytical solution. By comparing the results obtained with the cap model to those quoted by Siriwardane and Desai [27], (where a Cam Clay model was used for the soil behaviour), we see that our results follow the same trends.

6.7.2 Triaxial sample

The problem of the radial consolidation of a triaxial sample is modelled using axisymmetric elements. Since no displacement occurs in the direction of the axis, we need only consider a thin disc with the top and bottom restrained. The finite element mesh and corresponding boundary conditions are shown in Fig. 6.2(a) . We assume linear behaviour for the soil skeleton, and the numerical results obtained are compared with analytical solutions quoted by Christian and Boehmer [22] who present a detailed discussion of the problem. A uniform radial pressure P_o is applied instantaneously around the circumference of the sample at $t = 0$, and the pore pressure is set to zero for drainage to occur.

The load and material parameters used in this example are as follows:

$$P_o = 1 ,$$

$$E = 1 ,$$

$$\nu = 0.33 \text{ or } \nu = 0.0 ,$$

$$k_{11} = k_{22} = 1 ,$$

$$T_{v1} = \frac{C_{v1}}{R^2} \times t \quad ,$$

and $T_{v2} = \frac{C_{v2}}{R^2} \times t$ with $C_{v2} = \frac{E}{2(1+\nu)(1-2\nu)} \frac{k_{11}}{\gamma_w}$.

At discrete time intervals for which analytical solutions are available, pore pressures vs radius of the sample are plotted in Fig. 6.2(b) . The pressure at the centre of the sample is plotted against time in Fig. 6.2(c) . In both cases $\nu = 0.33$ and the numerical results compare well with the analytical solution.

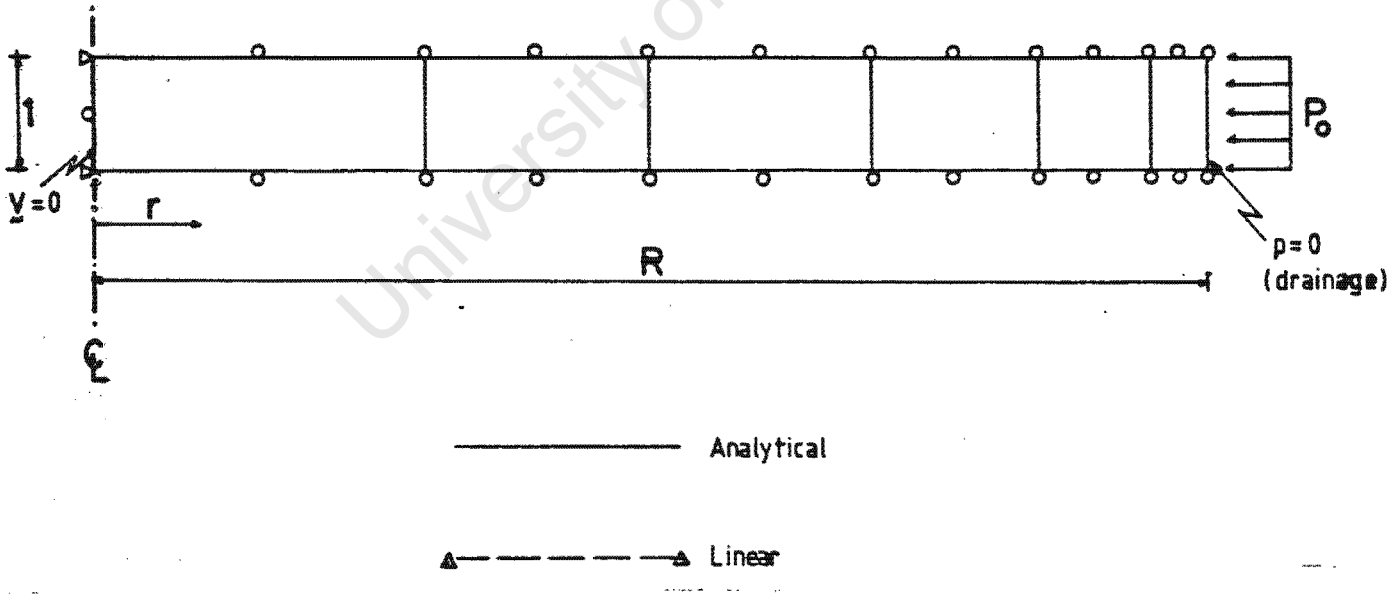

Figure 6.2(a) : Triaxial sample problem description.

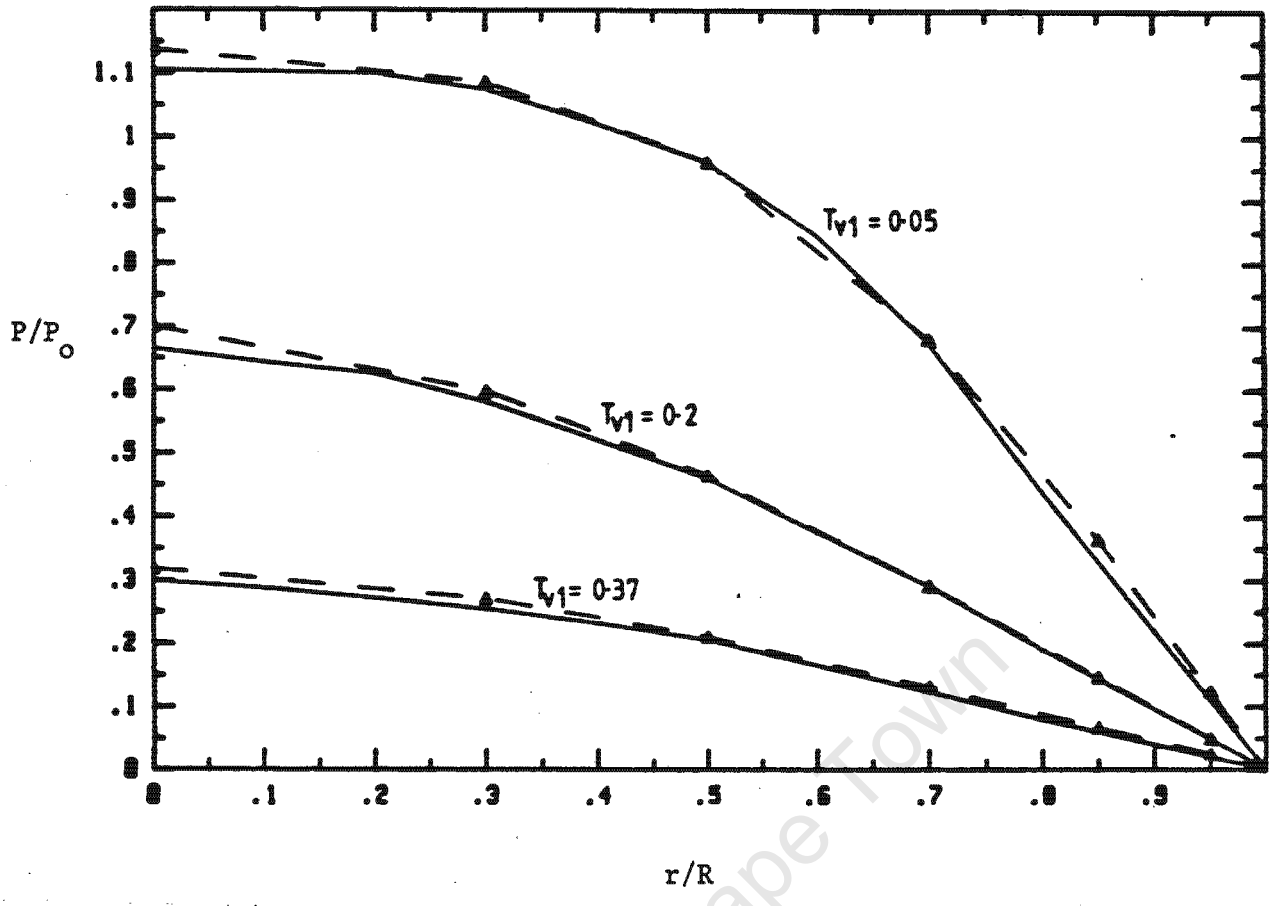

Figure 6.2(b) : Pore pressure vs radius.

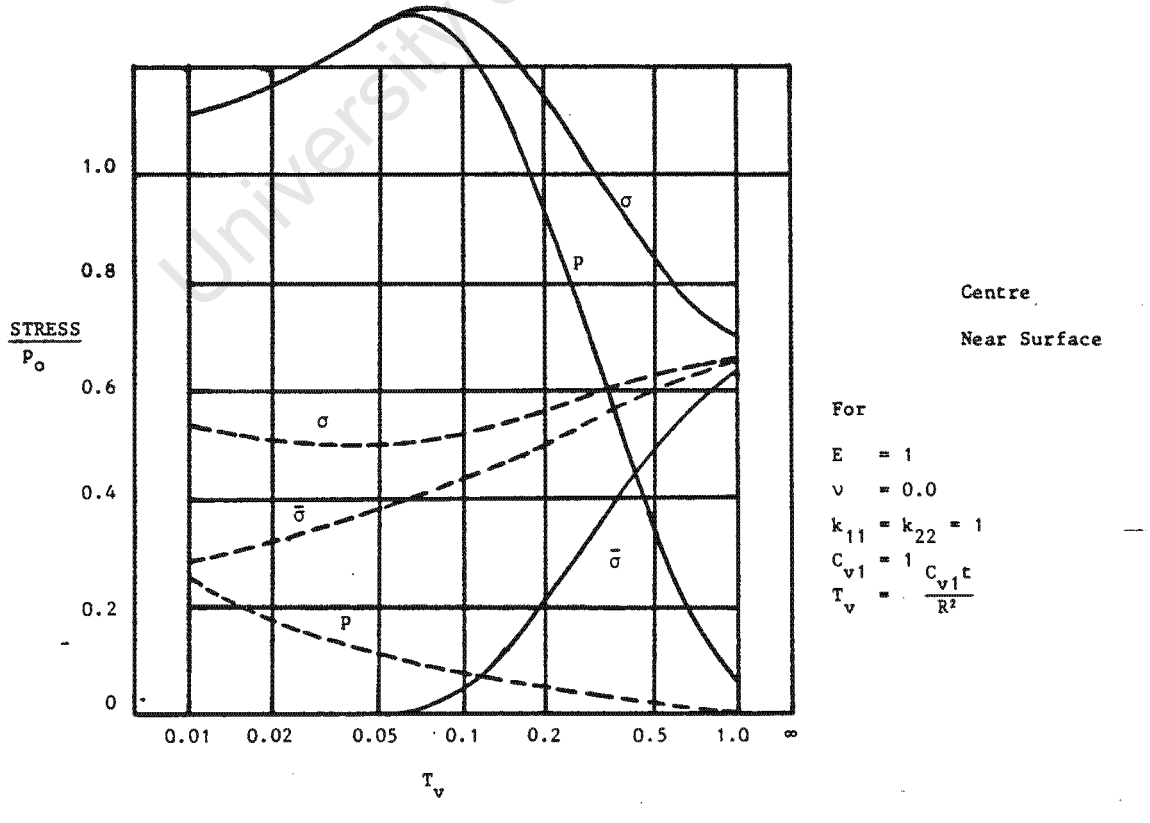

Figure 6.2(c) : Stresses vs time.

Fig. 6.2(d) shows the total volumetric stress, the effective volumetric stress and the pore pressure both near the surface and near the edge of the sample for $\nu = 0.0$. The results near the centre are identical to those obtained by Boehmer and Christian. The results near the surface follow the same trend as those of Boehmer and Christian, but differ numerically as they are not at the same distance from the surface. The phenomenon of redistribution (total stresses nearly constant with changing effective stress) and the Mandel-Cryer effect (effective stresses nearly constant with changing total stresses) are illustrated in this example, and are discussed in some detail in Boehmer and Christian's paper.

6.7.3 Mesh size and time incrementation analysis

In this example we illustrate an important issue in consolidation problems, namely the dependence choice of initial time step on the mesh size. For this purpose we consider Terzaghi's one dimensional consolidation and model it as before. The generic layout of the meshes used is depicted in Fig. 6.3(a) . The element at the free surface has the dimension ℓ .

The following load and material parameters are used :

$$E = 1.0 \ ,$$

$$\nu = 0.3 \ ,$$

$$k_{11} = k_{22} = 1.0 \ ,$$

$$\gamma_w = 1.34615 \ ,$$

$$P_o = 1.0 \ ,$$

and $$T_v = \frac{C_v}{H^2} \times t \quad \text{with} \quad C_v = \frac{E(1-\nu)}{(1+\nu)(1-2\nu)} \frac{k_{11}}{\gamma_w} = 1.0 \ .$$

For the case where $\ell = 1$, the form of solutions at three time steps is sketched in Fig. 6.3(b). The parameter t_c, referred to in the sketches, is defined by

$$t_c = \frac{\gamma_w \ell^2}{6Ek_{22}} \quad . \tag{6.28}$$

The significance of this parameter is discussed in [34]. Because the governing equations are parabolic, the initial solution is a local "skin effect" solution. With the progression of time this "skin effect" reduces as can be seen in Fig. 6.3(b).

Fig. 6.3(c) shows the time at which the numerical solutions differ by less than 0.05 P_o from the analytical solutions for the first time. These are plotted for different values of ℓ and are close to the locus of t_c .

Finally we consider the effect of the time step multiplier θ in equation (6.27). Using an initial time step Δt_o of 1.0 with $\theta = 1.1$, $\theta = 1.5$, and $\theta = 2.5$, full consolidation is achieved in respectively 36, 14, and 9 steps. The results obtained using the mesh with $\ell = 1$ are compared to the analytical solution in Fig. 6.3(d). It is seen that as θ decreases the solution improves, but more steps are required to reach full consolidation.

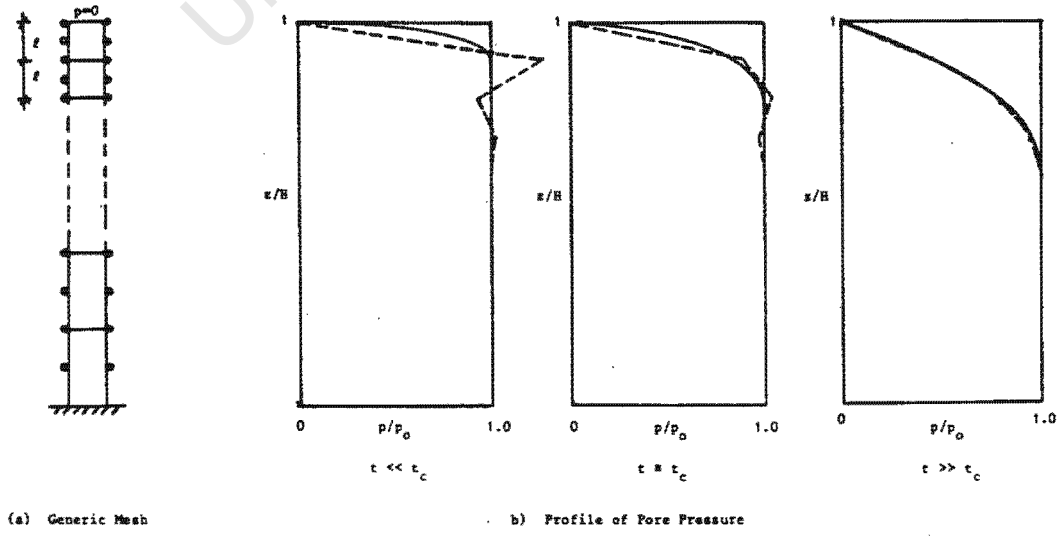

Figure 6.3

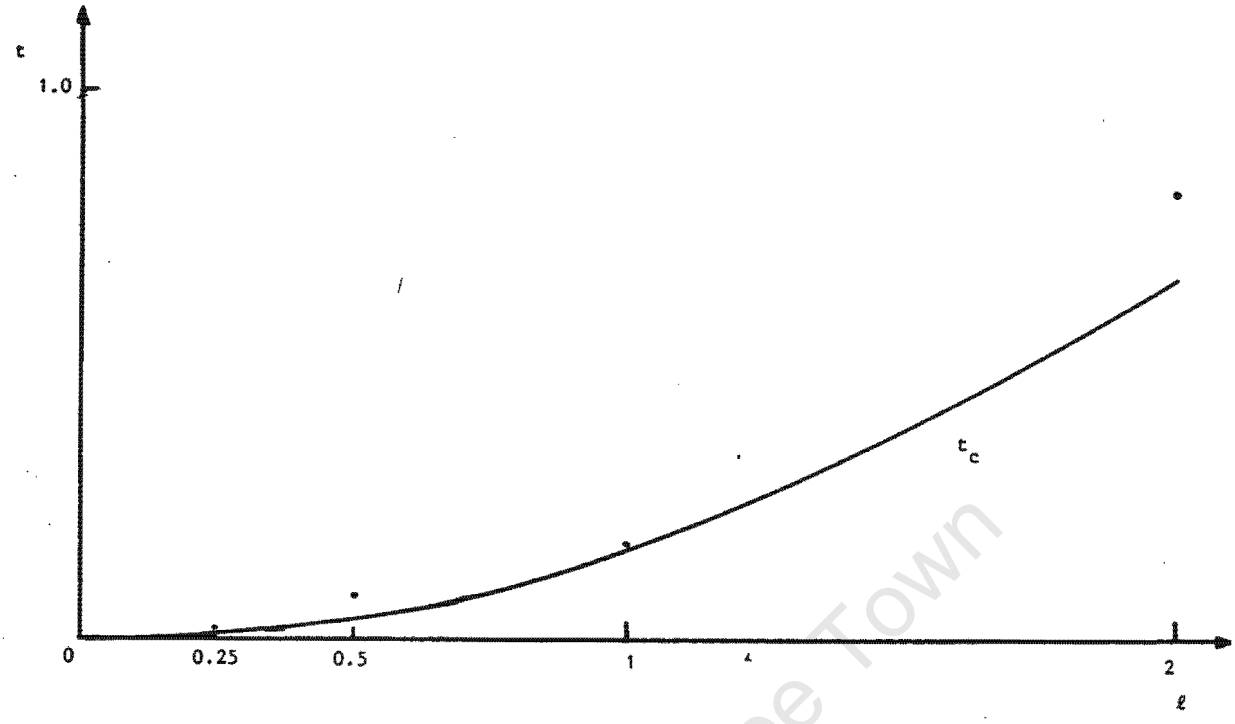

Figure 6.3(c) : Time to stabilise vs element dimension.

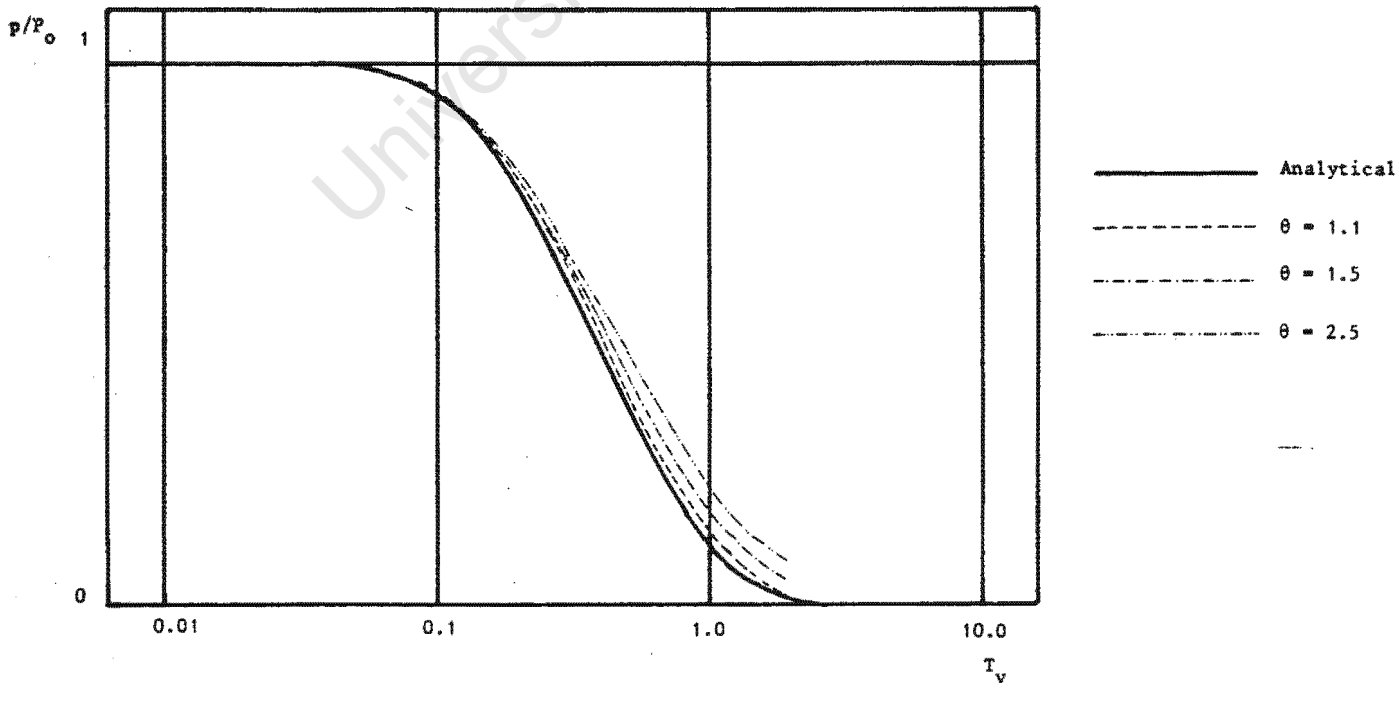

Figure 6.3(d) : Effect of θ.

6.7.4 Two dimensional analysis

In this example we consider a footing of width 2B on a soil layer of thickness 4B. Drainage occurs at both the top and the bottom of the layer. Plane strain elements are used, and the finite element model is shown in Fig. 6.4(a). The load on the footing is increased linearly to reach full value at 25 days. The surface displacements at different time intervals are plotted in Fig. 6.4(b) for both linear and nonlinear solutions.

The material parameters for the linear part of the example are:

$E = 622700,$

$\nu = 0.4,$

$k_{11} = k_{22} = 1.22 \times 10^{-5},$

and $T_v = \frac{C_{v1}}{H^2} \times t$.

Additional parameters required for the cap model are:

$k = 12000.0$,

$\alpha = 0.11$,

$R = 0.0$,

$\sigma_m^o = -10000.0$,

$W = -0.10$,

$D = 7 \times 10^{-6}$,

and $T = 70000$.

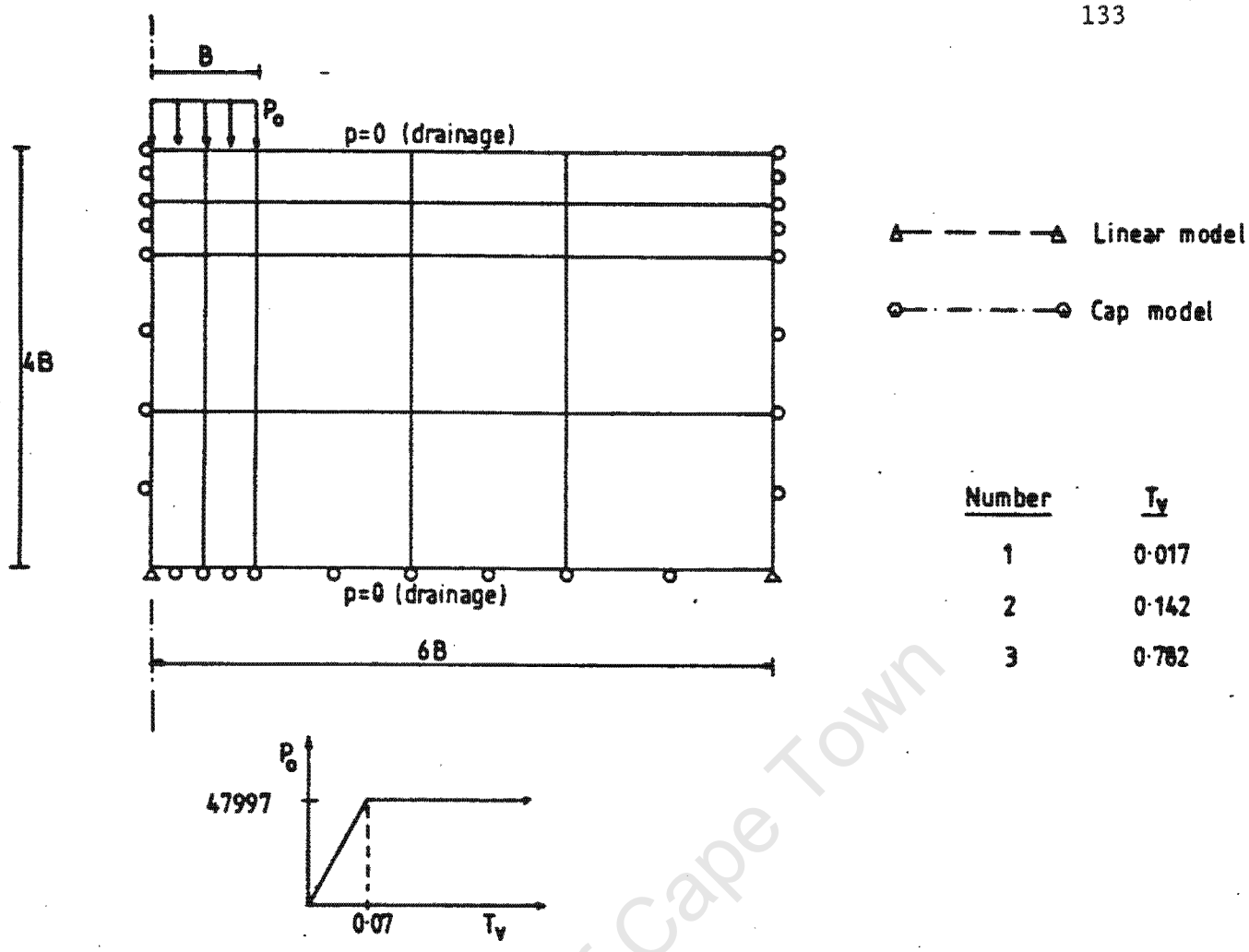

Figure 6.4(a) : 2-D consolidation problem description.

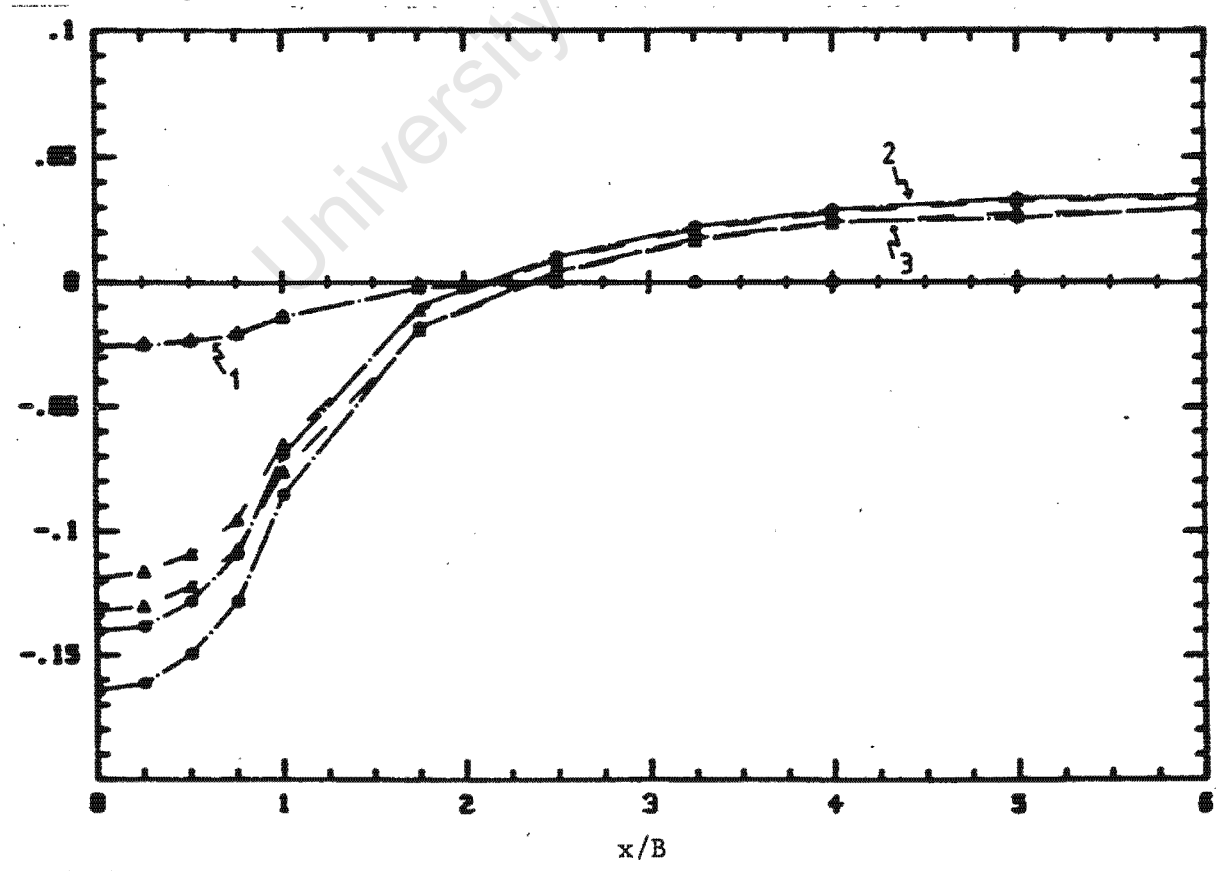

Figure 6.4(b) : Surface displacement.

The results for the elastic case are in exact agreement with the numerical results obtained with ABAQUS. When comparing the nonlinear case to similar examples in the literature [27], we see that our solution follows the same trends.

6.8 CONCLUSION

The consolidation formulation described in this chapter provides results which are consistent with closed form solutions, and with results obtained by other authors, as well as results obtained with ABAQUS. The main objective here has been to develop a formulation which would fit into the framework of the incremental procedures described in the previous chapters, and more specifically, one that would complement the Drucker-Prager cap model. It has been shown that this can be effected by the defined migration water strain which couples the mechanical and seepage problems. The water strain is equivalent to the volumetric strain of the soil. Since the cap parameters depend on the volumetric strain, this formulation is especially suited to the cap model.

CHAPTER 7

CONCLUSION

The formulations of the incremental problem for elastic-plastic materials presented in this thesis have provided valuable insights into how existing numerical techniques are linked to the governing variational principles. The use of imposed inelastic strains in particular has facilitated the formulation and implementation of both the secant approximation algorithm and the consolidation algorithm. In addition to this, the inelastic strains have been helpful in understanding the mechanics of the physical problems. A summary will be presented of the conclusions drawn at the end of Chapters 3 to 6.

The application of mathematical programming techniques to incremental elastic-plastic analysis has revealed that certain Newton-Raphson methods do in fact have a parallel in mathematical programming. It has been shown that the secant approximation algorithm which involves the successive minimisation of quadratic potential functionals can be formulated as a Newton-Raphson method. This secant algorithm is guaranteed to converge, but since it is not very efficient the applicability is limited to comparison solutions. A Newton-Raphson technique which utilises both a backward difference scheme for the integration of the plastic constitutive equations as well as a tangent predictor which is consistent with the corrector algorithm has provided numerical solutions which exhibit a quadratic rate of convergence. This is true for most of the yield conditions considered, except in the case of the Drucker-Prager cap model when yielding takes place on the nonlinear hardening cap.

In general, the numerical results obtained with the algorithms presented compare well with available analytical solutions and with results obtained with other finite element packages. In a case where a forward difference scheme is used for the integration of the constitutive equations, great difficulty is encountered in obtaining solutions to a particular problem. The solution to the same problem however, can be easily calculated using the backward difference approach with either the secant approximation for a predictor, or the consistent tangent predictor. The convergence rate of the consistent tangent algorithm is far superior to the other predictor algorithms considered, and would therefore be recommended for use in commercial packages.

REFERENCES

1. K-J.Bathe, Finite Element Procedures in Engineering Analysis, Prentice Hall, 1982.

2. O.C.Zienkiewicz, The Finite Element Method, McGraw-Hill, 1977.

3. D.R.J.Owen and E.Hinton, Finite Elements in Plasticity : Theory and Practice, Pineridge Press, 1980.

4. C.S.Desai and J.F.Abel, An Introduction to the Finite Element Method, Van Nostrand Reinhold, 1972.

5. G.Maier and J.Munro, "Mathematical programming application to engineering plastic analysis", Applied Mechanics Reviews, 35, 1631-1643, 1982.

6. U.Perego, "Backward difference operators and consistent predictors for linear hardening elastic-plastic constitutive laws", Technical Report No 91, Applied Mechanics Research Unit, University of Cape Town, to appear.

7. G.Maier and A.Nappi, "On the unified framework provided by mathematical programming to plasticity", Mechanics of Material Behaviour (edited by G.J.Dvorak and R.T.Shield), Elsevier, 253-273, 1983.

8. Hibbitt, Karlsson and Sorensen, Inc. ABAQUS User's Manual Version 4.5, Providence, Rhode Island, 1984.

9. J.B.Martin, "An internal variable approach to the formulation of finite element problems in plasticity", Physical Nonlinearities in Structural Analysis (edited by J.Holt and J.LeMaitre), Springer-Verlag, 165-176, 1981.

10. J.M.M.C.Marques, "Stress computations in elastoplasticity", Engineering Computations, 1, 42-51, 1984.

11. A.R.S.Ponter and J.B.Martin, "Some extremal properties and energy theorems for inelastic materials and their relationship to the deformation theory of plasticity",J. Mech. Phys. Sol., 20, 281-300, 1972.

12. P.Carter and J.B.Martin, "Work bounding functions for plastic materials",J. Appl. Mech., 43, 434-438, 1976.

13. J.B.Martin, "Convergence and shakedown for dicrete load steps in statically loaded elastic-plastic bodies", Technical Report No 69, Applied Mechanics Research Unit, University of Cape Town, January 1986.

14. G.A.Duffett, T.B.Griffin, J.B.Martin, C.D.Mercer, B.D.Reddy and L.Resende, "NOSTRUM - A Finite Element Program for Nonlinear Structural Mechanics", Technical Report No 18a, Applied Mechanics Research Unit, University of Cape Town, November 1983.

15. R.D.Krieg and D.B.Krieg, "Accuracies of numerical solution methods for the elastic, perfectly plastic model", J. Pressure Vessel Technol., ASME, 99, 510-515, 1977.

16. A.R.S.Ponter, Private Communication, November 1984.

17. L.N.Resende, W.W.Bird, N.J.Marais and B.K.R.Wiswe, "Application of Elastic-Plastic and Elastic-Viscoplastic Models to Geotechnical Engineering", Technical Report No 40, Applied Mechanics Research Unit, University of Cape Town, November 1983.

18. E.Muzino and W.F.Chen, "Cap Models for Clay Strata to Footing Loads", Computers and Structures, 17 (4), 511-528,1983.

19. J.C.Simo and R.L.Taylor, "Consistent tangent operators for rate-independent elastoplasticity", Comput. Meth. Appl. Mech. Eng., 48, 101-118, 1985.

20. L.Resende and J.B.Martin, "Formulation of Drucker-Prager Cap Model", J. Eng. Mech. Div., ASCE, 111, (EM7), 855-881, 1985.

21. M.A.Biot,General theory of three-dimensional consolidation", J. Applied Physics, 12, 155-164, 1941.

22. J.T.Christian and J.W.Boehmer, "Plane strain consolidation by finite elements", J. Soil Mech. Found. Div., ASCE, 96, (SM4), 1453-1457, 1970.

23. R.S.Sandhu and E.L.Wilson, "Finite element analysis of seepage in elastic media", J. Eng. Mech. Div., ASCE, 95, (EM3), 641-652, 1969.

24. J.R.Booker and J.C.Small, "An investigation of the stability of numerical Solutions of Biot's equations of consolidation", Int. J. Solids Structures, 11, 907-917, 1975.

25. C.S.Desai and J.T.Christian, Numerical Methods in Geotechnical Engineering, McGraw-Hill, New York, 1977.

26. G.Krause, "Finite element schemes for porous elastic media", J. Eng. Mech. Div., ASCE, 104, (EM3), 605-620, 1978.

27. H.J.Siriwardane and C.S.Desai, "Two numerical schemes for nonlinear consolidation", Int. J. Num. Meth. Eng., 17, 405-426, 1981.

28. J.H.Prevost, "Consolidation of anelastic porous media", J. Eng. Mech. Div., ASCE, 107, (EM1), 169-186, 1981.

29. K.L.Meijer, "Comparison of finite and infinitesimal strain consolidation by numerical experiments", Int. J. Numer. Anal. Methods Geomech., 8, 531-548 1984.

30. R.S.Sandhu, Shyan Chyun Lee and Hwie-ing The, "Special Finite Elements for Analysis of Soil Consolidation", Int. J. Num. Anal. Meth. Geomech., 9, 125-147, 1985.

31. Y.K.Zaretski, Theory of Soil Consolidation, IPST, Jerusalem, 1972.

32. E.B.Becker, G.F.Carey and J.T.Oden, Finite Elements An Introduction, Vol I, Prentice-Hall, 1981.

33. T.W.Lambe and R.V.Whitman, Soil Mechanics, Wiley, 1969.

34. Hibbitt, Karlsson and Sorensen, Inc. ABAQUS Example Problems Manual Version 4.5, Providence, Rhode Island, 1984.

APPENDIX A

Published work

The following papers , of which I am a co-author, have been accepted for publication :

1. W.W.Bird and J.B.Martin, "A secant approximation for holonomic elastic-plastic incremental analysis with a von Mises yield condition", Eng. Comput., 3, 192-201, 1986

2. J.B.Martin, B.D.Reddy, T.B.Griffin and W.W.Bird, "Applications of mathematical programming concepts to incremental elastic-plastic analysis", to appear in Engineering Structures.